BROAD-SPECTRUM ELECTROMAGNETIC BACKSCATTER

by

William P. Waite

CRES Technical Report No. 133-17

Sponsored and Monitored by:

Department of the Army
U.S. Army Topographic Command
Corps of Engineers
Engineer Topographic Laboratories
Fort Belvoir, Virginia

Contract No. DAAK 02-68-C-0089

Partially supported by NASA Contract NAS9-10261

CRES

THE UNIVERSITY OF KANSAS • CENTER FOR RESEARCH INC
ENGINEERING SCIENCE DIVISION • LAWRENCE, KANSAS

BROAD-SPECTRUM ELECTROMAGNETIC BACKSCATTER

Technical Report 133-17

William P. Waite

August, 1970

Sponsored and Monitored by:

Department of the Army
U. S. Army Topographic Command
Corps of Engineers
Engineer Topographic Laboratories
Fort Belvoir, Virginia

Contract No. DAAK02-68-C-0089

Partially supported by NASA Contract NAS9-10261

BROAD-SPECTRUM ELECTROMAGNETIC BACKSCATTER

ABSTRACT

An experimental investigation of broad-spectrum electromagnetic backscatter was performed. Continuous spectral responses of natural and manmade targets and surfaces were measured to examine the fine grain and gross variations with frequency of the backscattered return. Averaging in frequency, or effective panchromatic illumination, was investigated as a means of reducing the variance of the fine grain or fading variations. In addition, the use of multiple panchromatic bands, or polypanchromatic illumination, was investigated as a recognition means for the underlying spectral response remaining after fading effects were removed.

The frequency variation of a discrete scatterer model was examined for a variety of illuminating conditions ranging from monochromatic through bandwidths far in excess of resolution requirements. The theoretical reduction in return variance was shown to be a function of the resolution bandwidth and illumination bandwidth ratio.

Experimental measurements of return variance for several effective bandwidths were compared with the predictions of the theoretical model. The general behavior of decreasing variance with increasing illumination bandwidth agreed reasonably well; however, in all cases the experimental figures were larger than predicted. This effect was attributed to resonance variations underlying the fading distribution. The use of an approximate regression analysis for calculation of the experimental fading variance produced substatially better agreement.

The spectral response variations remaining after the removal of fading affects were normalized and compared with similar response characteristics from the visual and infrared regions. Resonance effects on at least two frequency scales were noted and were observed to produce variations comparable to those measured in the visual and infrared regions.

Monochromatic and panchromatic images were produced to illustrate the improvement obtainable with frequency averaging. The decreased scintillation of the panchromatic imagery was observed to materially aid the recognition of target tone and shape. Multiple panchromatic images were combined into a color display to illustrate the potential of poly-panchromatic illumination as a means of identifying spectral response characteristics.

The results of this experiment graphically illustrate the improvement in return variance possible with panchromatic illumination. In addition, the spectral response variations remaining after the removal of fading effects were shown to be comparable to the variations encountered in the visual and infrared regions.

ACKNOWLEDGEMENTS

To acknowledge merely the advice and guidance of my advisor, Professor R. K. Moore, is inadequate. He not only suggested the topic for this study, but provided the facility which supported this endeavor and an atmosphere that stimulated and encouraged the accomplishment of research.

The financial support of Project THEMIS under Department of the Army, Corps of Engineers, Engineer Topographic Laboratories Contract No. DAAK02-68-C-0089 and the National Aeronautics and Space Administration under Contract No. NAS9-10261 is gratefully acknowledged. The support and understanding of the U. S. Army Engineer Topographic Laboratories as contract monitor of Project THEMIS was particularly appreciated.

The efforts of the Remote Sensing Laboratory staff were essential to the completion of this work, especially the photographic assistance of Mr. Dwight Egbert and the patience of Miss Donna Opperman, Mrs. Kay Nugent, and Mrs. Mary Ann Bernier while typing the many revisions of the manuscript.

To my wife and four children I owe a special debt, for without their encouragement and understanding the completion of this study would have been impossible.

TABLE OF CONTENTS

Chapter Page

ABSTRACT ii
ACKNOWLEDGMENT iv
TABLE OF CONTENTS v
LIST OF FIGURES vii
LIST OF ILLUSTRATIONS xii
LIST OF TABLES xiii

1. INTRODUCTION 1
2. BACKGROUND. 5
    2.1 Theoretical Analyses 8
    2.2 Experimental Analyses 24
3. VARIANCE REDUCTION OF RADAR BACKSCATTER WITH BROAD-SPECTRUM ILLUMINATION 38
    3.1 Target Model 38
    3.2 Monochromatic Illumination 48
    3.3 Broad-Spectrum Illumination 50
    3.4 Postdetection Averaging of Independent Resolution Cells 60
    3.5 Comparison of Averaging Methods 62
4. EXPERIMENTAL INSTRUMENTATION 68
    4.1 System Function 70
    4.2 System Description 70
    4.3 System Calibration 93
5. SCATTERING EXPERIMENT 101
    5.1 Description of Targets 101
    5.2 Measurement Results 105
    5.3 Discussion of Results 112
6. IMAGING EXPERIMENT 133
    6.1 Measurement Technique 134
    6.2 Measurement Results 135
    6.3 Discussion of Results 144

Chapter Page

7. CONCLUSIONS 145

APPENDIX A DERIVATION OF AN IDENTITY 147

APPENDIX B EVALUATION OF AN INTEGRAL 150

BIBLIOGRAPHY 154

LIST OF FIGURES

Figure		Page
Figure 2.1	Line target model (from Birkemeir and Wallace, 1963)	9
Figure 2.2	Wavelength dependence of normalized radar cross section (random scatterer model) from Spetner and Katz, 1960	22
Figure 2.3	Wavelength dependence of normalized radar cross section (specular point model) from Spetner and Katz, 1960	22
Figure 2.4	Effect of illuminating bandwidth in the visible region of the spectrum. (a) Coherent (6328A, laser) light. (b) Incoherent (3200° Kelvin, incandescent) light.	25
Figure 2.5	Results of experimental determination of blip-to-scan ratio versus range for air targets, and comparison with theoretical results. R = radar range giving 50% blip-to-scan ratio on fixed frequency. Curves 1 give the result of the measurements with a jet plane (a small fighter), curves 2 with a small one-engine propeller aircraft and curves 3 with a medium-sized twin-engined propeller aircraft (from Gustafson and As, 1964).	27
Figure 2.6	Reduction of glint using jumping-frequency radar to track sea targets, as compared with fixed-frequency radar. Relative distribution of target positions, recorded with a 16 mm film camera and measured at intervals of 0.5 milliradians, is shown together with the silhouettes of the targets, which are reproduced in their apparent actual size in milliradians (from Gustafson and As, 1964).	27
Figure 2.7	Scintillation spectra (tree covered terrain, slight wind). (a) No frequency shift. (b) Frequency shift 5 Mc at 60 cps rate (from Kosowsky et al., 1963).	28
Figure 2.8	Effect of frequency average on image of sphere targets. (a) Monochromatic image of two spheres (f = 1.5 MHz). (b) Swept frequency image of two spheres (f = 1.5 MHz ± 10%) (from Rouse, 1965).	29

Figure Page

Figure 2.9 Naval Research Laboratory airborne backscatter measurements. (a) City of Chicago. (b) New Jersey woods 31

Figure 2.10 Naval Research Laboratory ground-based back-scatter measurements. (a) Tree-covered terrain. (b) Terrain covered with tall dry weeds. (c) Terrain covered with tall green weeds or flags. (d) Terrain partially covered with short dry grass (after Grant and Yaplee, 1957). 33

Figure 2.11 Sandia Corporation airborne backscatter measurements. (a) Farmland near Cameron, Mo. (b) Area of apartment buildings in Kansas City, Mo. (after Edison et al., 1960). . . 34

Figure 2.12 Ohio State University ground-based back-scatter measurements. (a) Asphalt road. (b) Concrete road. (c) Disked ground. (d) Three-foot green oats (June), (after Cosgriff et al., 1960). 35

Figure 2.13 Waterways Experiment Station ground-based backscatter measurements. (a) Wheat sample 3-1/2 inch vegetation height. (b) Wheat sample 29 inch vegetation height (after Lundien, 1966). 37

Figure 3.1 Discrete scatterer model of target area. 39

Figure 3.2 Rectangular frequency spectrum 50

Figure 3.3 Rectangular spectrum. (a) Energy spectral density. (b) Autocorrelation function of energy spectral density 51

Figure 3.4 Variance reduction with rectangular spectrum panchromatic illumination 54

Figure 3.5 $\frac{\sin x}{x}$ frequency spectrum 55

Figure 3.6 $\frac{\sin x}{x}$ spectrum. (a) Time domain function (b) Time domain autocorrelation function. (c) Square of autocorrelation function 57

Figure 3.7 Variance reduction with $\frac{\sin x}{x}$ spectrum panchromatic illumination. 59

Figure 3.8 Variance reduction through postdetection averaging of independent resolution cells 62

Figure Page

Figure 3.9 Comparison of averaging methods 63

Figure 3.10 Comparison of averaging methods 66

Figure 4.1 Slow-sweep method of obtaining broad-bandwidth. (a) Sweep modulation. (b) Pulse modulation. (c) Spectrum of single pulse. (d) Overlapping spectra due to slow change of carrier frequency 71

Figure 4.2 System block diagram 72

Figure 4.3 Driver circuit for grounded cathode microwave PIN diode switch 75

Figure 4.4 Driver circuit for grounded anode microwave PIN diode switch 75

Figure 4.5 Duplexing arrangement and timing sequence. . . 78

Figure 4.6 E-plane patterns for 3-foot reflector. (a) Frequency 4 GHz. (b) Frequency 8 GHz. 79

Figure 4.7 E-plane patterns for 6-foot reflector. (a) Frequency 4 GHz. (b) Frequency 8 GHz 80

Figure 4.8 Block diagram of digital control system 86

Figure 4.9 Circuit diagram of pulse forming network 88

Figure 4.10 Block diagram of scattering coefficient signal processor 89

Figure 4.11 Signal process timing sequence. (a) Sampling sequence. (b) Integration and read sequence. 89

Figure 4.12 Circuit diagram of integrator. 91

Figure 4.13 Component arrangement and timing sequence for imaging operation 94

Figure 4.14 Backscatter cross section of an infinitely conducting sphere (after Rheinstein, 1968). . . . 95

Figure 4.15 Sweep frequency return from 12-inch diameter calibration sphere 100

Figure Page

Figure 5.1 Probability density functions of frequency fading distributions for targets 1-4 107

Figure 5.2 Probability density functions of frequency fading distributions for targets 5-7 108

Figure 5.3 Spectral response curves for two different effective bandwidths 110

Figure 5.4 Spectral response curves for two different effective bandwidths 111

Figure 5.5 Spectral response of target 1 113

Figure 5.6 Spectral response of target 2 114

Figure 5.7 Spectral response of target 3 115

Figure 5.8 Spectral response of target 4 116

Figure 5.9 Spectral response of target 5 117

Figure 5.10 Spectral response of target 6 118

Figure 5.11 Spectral response of target 7 119

Figure 5.12 Spectral response with 1 GHz effective bandwidth 125

Figure 5.13 Spectral response with 1 GHz effective bandwidth 126

Figure 5.14 Color film dye layer sensitivity ranges (from Sorem, 1967) 128

Figure 5.15 Spectral response variations in the visual region. (a) Spectral reflectance of seven species of plants representing diverse groups. (b) Spectral reflectance of bark from two species of trees and parts of several animals (from Gates, 1970) 129

Figure Page

Figure 5.16 Relative spectral radiance spectra for agricultural scenes in the range of 0.4-1.05u, August 30, 1966, 11:50-11:56 a.m. Curves should be compared in functional form only; gain settings were changed between spectra (from Holmes, 1970). 130

Figure 5.17 Normalized spectral response curves 131

Figure 5.18 Normalized spectral response curves 132

Figure 6.1 Successive monochromatic images made with no change in system parameters 137

Figure 6.2 Monochromatic images taken at slightly different frequencies 138

Figure 6.3 Comparison of monochromatic and panchromatic images 139

Figure 6.4 Comparison of monochromatic and panchromatic images 140

Figure 6.5 Comparison of monochromatic and panchromatic images 141

Figure 6.6 Polypanchromatic images 142

Figure 6.7 Relative target locations on B-scan imagery.
(a) Undistorted sketch of target area.
(b) Sketch of target area in B-scan geometry 143

LIST OF ILLUSTRATIONS

Illustration		Page
Illustration 4.1	Broad-bandwidth radar measurement system . . .	69
Illustration 5.1	Roof-top installation of measurement system . .	102
Illustration 5.2	Field of view from dormitory showing target locations	103

LIST OF TABLES

Table		Page
Table 2.1	Possible combinations for wavelength dependence of radar backscattering cross-section (from Spetner and Katz, 1960).	22
Table 5.1	Experimental values of return mean and variance	109
Table 5.2	Experimental mean and variance of fading distribution	122
Table 5.3	Measured and predicted improvement in variance as a function of illumination bandwidth	122

CHAPTER 1

INTRODUCTION

An experimental investigation was made of broad-spectrum electromagnetic backscatter. Continuous spectral signatures of natural and man-made objects and surfaces were obtained to examine the fine grain and gross variation with frequency of the backscattered return. Averaging in frequency was used to reduce the variance of the fine grain or fading signal and to produce panchromatic imagery. The use of multiple panchromatic bands separated in frequency was investigated as a means of identifying spectral signatures. In addition, multiple panchromatic images were combined into a color or polypanchromatic display.

The statistical nature of radar return from complex targets or surfaces has long been recognized (Swerling, 1960). Only recently, however, has any attempt been made to utilize frequency diversity as a means of decreasing the variance of the return signal distribution. Although so-called "frequency agile" radar systems were developed some years ago, the frequency diversity of these systems was added principally as an anti-jamming feature. It was soon recognized that the frequency shift served to decorrelate the pulse-to-pulse returns and, in many cases, improve both detection and tracking capabilities (Birkemeier and Wallace, 1963; Kosowsky et al., 1963; Gustafson and Ås, 1964; Lind, 1968). Most analyses still considered the measure of improvement to be a determination of the frequency shift required to effectively obtain independent pulse-to-pulse samples for various targets (Ray, 1966; Beasley and Ward, 1968).

Moore, Waite, and Rouse (1969) first suggested the use of continuous broad-spectrum illumination with a bandwidth substantially in excess of that required for system resolution. Operation in this fashion gives signal decorrelation within the resolution cell thus enabling one to obtain additional samples of the distribution. Moore and Waite (1969) in a study of Doppler scatterometer systems showed the difference in variance reduction between predetection and postdetection frequency integration. The only experimental results available for verifying the improvement in return distribution variance with frequency averaging are those of Rouse (1968), and these show only the qualitative improvement of image quality for an acoustic modeling system.

In Chapter 2 the improvement in return variance with frequency averaging predicted by the referenced methods is examined. The spectral response data with variable bandwidths presented in Chapter 5, and the monochromatic and panchromatic imagery shown in Chapter 6 serve to illustrate and verify the predicted improvement with frequency averaging.

Most of the work with "frequency agile" systems considers the limit of improvement to be reached when successive pulses are independent samples of the return distribution. Continuous broad-spectrum or panchromatic illumination can provide additional independent samples of the distribution within each pulse. This is particularly important for systems already operating at the maximum pulse sample rate (PRF) consistent with range ambiguity, such as side-looking imaging radars. Imaging systems must provide not merely signal detection, but a reasonable measure of the differential scattering cross-section of each resolvable element. If averaging is insufficient to reduce the fading or scintillation of the return, the image has a speckled or grainy appearance. In Chapter 3 a unified theory of broad-spectrum backscatter from complex targets is developed with relates resolution, system bandwidth and return variance or measurement reliability.

The development of side-looking imaging radar has aroused interest in the potential of radar as a tool for geoscience applications (Pierson et al., 1965; Moore, 1966; Rouse et al., 1969). This interest was part of the overall interest in remote sensing capabilities stimulated by NASA and by the potential offered by orbital platforms. Much of the conjecture concerning the geoscience applications of remote sensing assumes that a unique spectral signature can be defined for any target or surface of interest (Parker and Wolff, 1965; Lyon and Vickers, 1966; Pardoe, 1969). This assumption has not been verified even for much more limited objectives.

The investigation of spectral signatures is somewhat easier in shorter wavelength regions of the spectrum than microwave, for here the measurement and use of spectral response information has been a standard technique for some time. The users of the microwave or radar region of the spectrum have long been content with definition of returns from a few isolated frequencies usually identified merely with band designations. While a number of investigators have attempted theoretical descriptions of the frequency dependence of radar backscatter, virtually none of these has received adequate experimental verification (Spetner and Katz, 1960; Fung and Leovaris, 1968; Rouse, 1968).

Polychromatic systems for measurements of scattering at multiple discrete frequencies have been used for some time (Grant and Yaplee, 1957; Wiltse et al., 1957; Ament et al., 1959; Ohio State University, 1963). However, the fundamental purpose of these systems has been to provide appropriate design information for particular monochromatic radar systems. With such a limited amount of spectral information, the question of signature content within the microwave region may hardly be approached. It is apparent that continuous spectral signatures over the microwave region are required both for verifying existing theory and for investigating possible resonance phenomena contributing to signature information.

The experimental portion of this study provides the first known continuous spectral response measurements over a one-octave frequency range. In addition, the use of a color display for possible signature identification is illustrated by the polypanchromatic imagery presented in Chapter 6.

The design and construction of a system providing controlled broad-spectrum illumination was a substantial portion of the total effort. The system is capable of providing spectral response curves over a one-octave frequency range and with a variety of sampling bandwidths and incidence angles. In addition, capability for the production of monochromatic and variable bandwidth panchromatic imagery is incorporated. A thorough knowledge of the system, calibration method and data processing is required for interpretation of the experimental results. A complete description of the system is provided in Chapter 4.

The measurement program is divided into two sections: 1) scattering experiment, and 2) imaging experiment. The scattering experiment consisted of the measurement of spectral response curves for natural and cultural targets and surfaces. These measurements were performed over a range of effective bandwidths and across a frequency range of 4 GHz to 8 GHz. The reduction in return distribution variance with increased effective bandwidth was compared with the theory developed in Chapter 3. The coarse structure (structure remaining after fading and scintillation effects were averaged out) of the spectral response curves across the full range was examined for comparative signature content. The scattering experiment procedure and results are presented in Chapter 5.

The imaging experiment consisted of recording B-scan imagery of area extensive targets, including those targets measured in more detail in the scattering experiment. Monochromatic images showed the complex lobing or scintillation normally expected. Panchromatic images with sufficient bandwidth in excess of resolution requirements illustrated the predicted improvement. Multiple panchromatic images from widely different portions of the operating range were combined in a color display to illustrate the polypanchromatic method of spectral signature recognition. The imaging experiment procedure and results are presented in Chapter 6.

CHAPTER 2

BACKGROUND

The study of broad-spectrum radar is basically the study of the frequency dependence of electromagnetic backscatter. Studies of this dependence have proceeded along two widely separated lines of investigation that might well be termed macroscopic and microscopic approaches. Macroscopic studies concerned with the variation of average backscatter power over a wide frequency range have been performed by both radar design engineers and scattering theorists. Most of these studies have been conducted to provide specific design information for monochromatic radar systems (Goldstein, 1946; Kerr, 1951; Wiltse et al., 1957; Grant and Yaplee, 1957; Ament et al., 1959; Edison et al., 1960; Cosgriff et al., 1960).

The advent of lunar radar stirred considerable interest in the frequency dependence of the backscattered return as a means of estimating the surface statistics from multifrequency data. Most of the lunar studies have used a Kirchhoff or physical optics theory to obtain an expression for the mean return involving the correlation distance and standard deviation of the surface. Curve fitting the resultant equations to the backscattered data at different frequencies and incidence angles yields differing values for the surface statistics (Evans, 1957; Hayre, 1964). While this may indicate that frequency does have a "size filtering" effect, little can be said regarding the uniqueness of solutions obtained in this fashion (Fung, 1965).

More recently the use of radar as a sensor for geoscience investigations has received considerable attention (Pierson et al., 1965). Such applications require that the radar return be correlated with the characteristics of the illuminated surface. The instrument parameters that may be varied in such an investigation are the incidence angle, frequency and polarization of the radar sensor (Rouse et al., 1969).

Surface identification, therefore, requires a knowledge of the return amplitude dependence upon each of these parameters.

The theoretical description of radar ground return depends upon the mathematical model used to describe the surface (Moore, 1969). The description of such a relatively simple surface as the sea is extremely difficult, even though it has relatively modest slopes and may be considered homogeneous (Chia, 1968). To adequately describe land surfaces with their greatly increased variability appears almost hopeless. It appears, then, that determination of radar return dependence for natural surfaces must depend upon empirical measurements. Theoretical description of the return will serve principally as an aid in interpretation and extrapolation of the measurements.

The study of fine grain variations with frequency (or the microscopic approach) has been concentrated primarily in the area of tracking and search radar applications (Birkemeier and Wallace, 1963; Ray, 1966; Hansen, 1968). The received signal from any complex target or surface is subject to unwanted variations due to the structure of the target. The most common model used to describe such complex targets is one composed of a large number of independent point scatterers randomly distributed in amplitude and phase. The radar return is the phasor summation of contributions from each scattering center within the resolvable element. The variation of the received signal is normally termed "fading", although in some cases this term is reserved for variations in signal amplitude alone. The term "glint" denotes the wander of the apparent center of reflectivity as measured by a tracking radar.

The random scintillation or fading of the radar return described above leads to errors in detection or tracking performance dependent upon the probability distribution of the return. It has long been recognized that improved performance may be realized by the integration or averaging of several return pulses, each a sample of the return distribution (Marcum, 1960; Swerling, 1960). As might be expected, the improvement in performance is related to the estimation of the distribution mean and thus to the effective number of independent samples averaged. If the pulse-to-pulse samples of the distribution are correlated, the effective number of independent samples may be significantly less than the number of pulses. Several authors have shown the improvement that may be obtained through the use of frequency diversity on the pulse-to-pulse basis to decorrelate successive pulses and increase the effective number of independent samples (Kosowsky et al., 1963; Gustafson and Ås, 1964; Beasley and Ward, 1968; Lind, 1968).

The estimation of the distribution mean, even with the use of frequency agility, is still limited by the sample rate or pulse repetition frequency (PRF) of the system. The PRF of most systems is not determined by these considerations but by the unambiguous range requirement (Skolnik, 1962; Barton, 1964). The possible use of frequency diversity or broad-spectrum illumination to provide independent samples of the target distribution within a single pulse period has been suggested (Moore et al., 1969). This technique in essence trades bandwidth for a better estimate of the distribution mean. A more detailed analysis of the relationships between bandwidth, resolution and variance of the sample mean is presented in Chapter 3.

The use of the imaging radar for geoscience applications offers an interesting combination of user requirements. The coverage or swath width usually should be relatively broad, but this limits the pulse sample rate due to the unambiguous range requirement. At the same time, the geoscientist desires resolution compatible with the smallest features to be discriminated and a high confidence level that the return amplitude represents the differential scattering cross-section for each resolution cell. These requirements aid both detection and delineation of homogeneous areas. Since coverage and delineation of homogeneous areas are at least as important as resolution in this application, the use of panchromatic or broad-spectrum illumination offers an additional degree of freedom to the system designer. The ultimate aim of the geoscientist is not merely delineation of differences, but actual recognition. To achieve this end the addition of multiple panchromatic bands or polypanchromatic illumination to determine spectral signature information may well be desirable.

In the remainder of this chapter we shall examine the theoretical and experimental background of panchromatic and polypanchromatic illumination. While the emphasis of this study is on the application of these techniques to imaging radar systems, virtually all of the background material is drawn from studies conducted with other goals in mind. The chapter sections are further divided into panchromatic analyses wherein the broad-spectrum illumination is used to reduce the scintillation effects, and polypanchromatic analyses to investigate the possible information content of spectral signatures.

2.1 Theoretical Analyses

2.1.1 Panchromatic Illumination

Numerous articles dealing with the performance of frequency agile radars are applicable here. The basic concept in each remains that of achieving pulse-to-pulse decorrelation through the use of frequency diversity. A sample of these papers is examined along with the panchromatic analysis of Moore, Waite and Rouse (1969).

2.1.1.1 Birkemeier and Wallace Model

Birkemeier and Wallace (1963) examine the improvement in tracking performance of monopulse and conical scan systems afforded by pulse-to-pulse frequency modulation. The frequency shift is obtained by a linear frequency modulation with a period much longer than the pulse repetition period. The target model is one investigated earlier by Delano (1953) and Muchmore (1960) and is shown in Figure 2.1.

The elements of the target are considered to be uniformly distributed along the strip, each with an independent random phase angle uniformly distributed from zero to 2π. The critical frequency shift, Δf_c, necessary to consider samples of the return signal essentially uncorrelated is calculated for the above model.

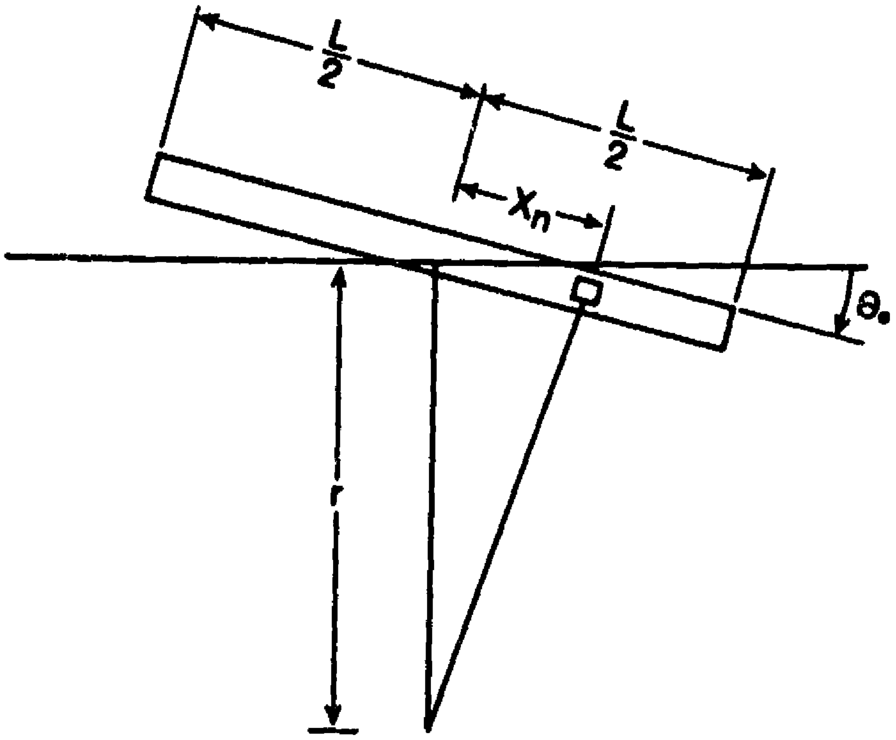

Figure 2.1 Line target model (from Birkemeier and Wallace, 1963).

The voltage return from the target as a function of frequency is given by

$$V(f) = \sum_{n} a_n \cos\left(\frac{4\pi r_n f}{c} + \varphi_n\right) \tag{2.1}$$

where a_n = amplitude of the return from the nth reflecting element

r_n = distance in the range dimension from the nth reflecting element to a plane perpendicular to a line connecting the radar with the mean center of reflectivity of the target

φ_n = independent random phase angle uniformly distributed from zero to 2π.

The autocorrelation function of the fading as a function of frequency is then

$$R_v(\Delta f) = E\left[\sum_n a_n \cos\left(\frac{4\pi r_n f}{c} + \varphi_n\right) \sum_m a_m \cos\left(\frac{4\pi r_m f'}{c} + \varphi_m\right)\right. \quad (2.2)$$

where $f' = f + \Delta f$

Since the φ_n's are independent

$$E\left[\cos\varphi_n \cos\varphi_m\right] = \frac{1}{2}\delta_m^n , \qquad E\left[\sin\varphi_n \sin\varphi_m\right] = \frac{1}{2}\delta_m^n$$

$$\text{and} \quad E\left[\cos\varphi_n \sin\varphi_m\right] = 0$$

where $\delta_m^n = 1$ if $m = n$, $\delta_m^n = 0$ if $m \neq n$.

Using the above, equation (2.2) reduces to

$$R_v(\Delta f) = E\left[\frac{1}{4}\sum_n a_n^2 \cos \frac{4\pi r_n}{c}(f - f')\right] \quad (2.3)$$

If the frequency sweep is symmetrical such that the probability is 1/2 that Δf is positive and 1/2 that Δf is negative, then

$$E\left[\cos\left(\frac{4\pi r_n \Delta f}{c}\right)\right] = \frac{1}{2}\cos\left(\frac{4\pi r_n \Delta f}{c}\right) + \frac{1}{2}\cos\left(\frac{4\pi r_n \Delta f}{c}\right)$$

$$= \cos\left(\frac{4\pi r_n \Delta f}{c}\right)$$

The summation of equation (2.3) may be approximated by an integral over the target length L noting that $r_n = x_n \sin \Theta_o$, and that the integral is an even function of x,

$$R_v(\Delta f) = \frac{E[a_n^2]}{2} \int_0^{L/2} \cos\left(\frac{4\pi \sin \Theta_o \Delta f x}{c}\right) dx$$

$$= \frac{E[a_n^2]}{2} \frac{\sin(\alpha \Delta f)}{\alpha \Delta f} \tag{2.4}$$

where $\alpha = \frac{2\pi L \sin \Theta_o}{c}$

Let E(f) be the voltage as a function of frequency after square law envelope detection of the signal. Since the spectrum of E(f) is given by the convolution of the spectrum of V(f) on itself, the autocorrelation coefficient of E(f) is given by the square of the autocorrelation coefficient of V(f). This yields

$$\rho_E(\Delta f) = \frac{R_E(\Delta f)}{R_E(0)} = \frac{\sin^2(\alpha \Delta f)}{(\alpha \Delta f)^2} \tag{2.5}$$

The decision as to how much decorrelation is required to produce essentially independent samples is somewhat arbitrary, however, Birkemeir and Wallace define the critical frequency as the first zero of the autocorrelation coefficient. Thus,

$$\Delta f_c = \frac{c}{2L \sin \Theta_o} = \frac{150}{L \sin \Theta_o} \text{ MHz} \tag{2.6}$$

As might be expected the critical frequency change is that required to change by 180 degrees the phase at the target extreme and the phase at the reference point at the center of the target.

2.1.1.2. Ray Model

Ray (1966) uses a slightly different model to calculate the frequency change required to produce essentially uncorrelated samples.

Assume a target with a maximum dimension D', measured along a radius from the radar. The maximum dimension may be determined by either the physical size of the target itself or the range resolution of the system. Let x be the radial distance from the nearest portion of the target complex to an arbitrary element of the complex, f the frequency transmitted by the system, and Δf a small change in f.

For a CW transmitted signal, the phase of the echo from any element referred to the phase of the element nearest the radar is

$$\theta = \frac{4\pi x f}{c} \qquad (2.7)$$

where c is the velocity of light. The derivative of θ with respect to f is

$$\frac{d\theta}{df} = \frac{4\pi x}{c} \qquad (2.8)$$

and forms a spectrum for rate of change of phase with respect to transmitted frequency. Since the target complex is assumed to be randomly located scatterers with a range of x = 0 to x = D', the result is a power spectrum of width $4\pi D'/c$.

In analogy with the autocorrelation function for noise with a bandwidth of W given by

$$\theta(\tau) = \frac{\sin 2\pi W\tau}{2\pi W\tau} \qquad (2.9)$$

Ray expresses the autocorrelation function with respect to frequency as

$$\Theta(\Delta f) = \frac{\sin 4\pi D'\Delta f/c}{4\pi D'\Delta f/c} \tag{2.10}$$

Ray assumes sufficient decorrelation to be achieved when the autocorrelation function falls to 0.5 which yields a required frequency change of

$$\Delta f = \frac{0.15\, c}{D'} = \frac{45}{D'} \text{ MHz} \tag{2.11}$$

If the decorrelation required is extended to the first zero of the autocorrelation function as done by Birkemeier and Wallace, the result is

$$\Delta f_c = \frac{c}{4D'} = \frac{75}{D'} \text{ MHz} \tag{2.12}$$

This value is seen to be exactly one-half that obtained in the analysis by Birkemeier and Wallace. This difference is not due to the fact that Birkemeier and Wallace use the energy autocorrelation function while Ray uses the signal or voltage autocorrelation function since both should yield the same result when assuming the first zero of the autocorrelation function constitutes independence. The difference is due to an error by Ray in equation (2.10) in which the image or negative frequency portion of the power spectral density is neglected. For a real spectrum of width, $4\pi D'/c$, the autocorrelation function with respect to frequency should be

$$\Theta(\Delta f) = \frac{\sin 2\pi D'\Delta f/c}{2\pi D'\Delta f/c} \tag{2.13}$$

This yields for assumed independence at 0.5 a value of

$$\Delta f = \frac{0.3\,c}{D'} = \frac{90}{D'}\ MHz \tag{2.14}$$

If the decorrelation required is extended to the first zero of the autocorrelation function, Ray's result now agrees with that of Birkemeier and Wallace.

$$\Delta f_c = \frac{c}{2D'} = \frac{150}{D'}\ MHz \tag{2.15}$$

2.1.1.3 Moore, Waite and Rouse Model

Moore et al. (1969) propose a system with panchromatic illumination where the bandwidth of the illuminating signal is in excess of that required for system range resolution. The excess bandwidth (that above the resolution requirement) can be used to frequency average the return and reduce amplitude (fading) and angle-of-arrival (glint) fluctuations due to phase interference effects. The effect of this averaging is identical to that produced by averaging independent samples of the return obtained by pulse-to-pulse decorrelation with frequency shift. The significant point is that this technique produces averaging within a single pulse period and hence may be used where the PRF is dictated by other constraints.

Scatter from a rough surface like the ground may be expressed by the integral (Beckmann and Spizzichino, 1963)

$$E(k) = \frac{e^{-j2kR_0}}{R_0}\int_S f\, e^{j\bar{k}\cdot\bar{r}}\, dS \tag{2.16}$$

where E = the backscattered field

$\bar{k}$ = $\frac{2\pi}{\lambda}$ the wave number expressed as a vector from dS toward the radar

R_o = the distance from the radar to a reference point on the target

$\bar{r}$ = a vector from the reference point to the area element dS

f = a function of polarization, incident angle, wave number, and local reflection coefficient.

Although the general character of the field is set partly by f, the detailed structure is almost entirely due to wave interference effects expressed by the phase factor.

$$\bar{k} \cdot \bar{r} = kr \cos \theta$$

With broad-band illumination, the field observed at any point in space is frequency-averaged so that the fine structure of equation (2.16) is not present.

$$\langle E(k) \rangle_k = \frac{1}{\Delta k} \int_{k_o - \Delta k/2}^{k_o + \Delta k/2} \frac{e^{-j2kR_o}}{R_o} \int_S f \, e^{j \bar{k} \cdot \bar{r}} \, dS \, dk \tag{2.17}$$

The bandwidth over which a radar must transmit to achieve the kind of averaging indicated by equation (2.17) depends on the fine structure in the pattern of frequency variation of the field of equation (2.13). The concept of required bandwidth may be illustrated by calculating it for the special case of a slightly rough one-dimensional surface for which shows (Rice, 1951)

$$E(q) = A k^2 \int_{-\infty}^{\infty} e^{jqx} Z(x) \, dx \tag{2.18}$$

where $q = 2k \sin \Theta$ (Θ is the incident angle)

A = a function of distance and radar parameters

Z = the height of the rough-surface point at location x.

The field E is seen to be the Fourier transform in q of the surface height function. A power pattern may be defined as

$$W(q) = \frac{|E(q)|^2}{A^2 K^2} = |\mathfrak{F}(z)|^2 \tag{2.19}$$

where $\mathfrak{F}$ means "Fourier transform of". The power pattern is therefore the power spectrum of $z(x)$. The power spectrum of a function is the Fourier cosine transform of its autocorrelation function, so

$$W(q) = \mathfrak{F}_c\left[\rho_z(x)\right] \tag{2.20}$$

where $\mathfrak{F}_C$ is the Fourier cosine transform symbol. Thus, the power patterning is related to the surface-height autocorrelation function by a simple transform.

The spacing in q (and therefore in frequency) of independent samples can be determined from the autocorrelation function of W, which is

$$C(\Delta q) = \frac{\int_{-\infty}^{\infty} W(q)\, W(q+\Delta q)\, dq}{\int_{-\infty}^{\infty} W^2(q)\, dq} = \frac{\mathfrak{F}_c\left[\rho_z^2(x)\right]}{\int_{0}^{\infty} \rho_z^2(x)\, dx} \tag{2.21}$$

As an example, consider an autocorrelation function exp [-x/L], which has been shown to describe surface configuration at contour map scale in several areas (Hayre and Moore, 1961). The expression for $C(\Delta q)$ is

$$C(\Delta q) = e^{-(L\Delta q/2)^2} \tag{2.22}$$

If we consider independence essentially achieved for $C(\Delta q) = e^{-2}$, the resulting expression for frequency spacing of independent samples is

$$\Delta f = \frac{c\sqrt{2}}{\pi L \sin\theta} = \frac{135}{L \sin\theta}\ \mathrm{MHz} \tag{2.23}$$

which is in close agreement with the value predicted by both Birkemeier and Wallace and Ray.

2.1.2 Polypanchromatic Illumination

Polypanchromatic is used here only to designate that the frequency dependence of interest is that exclusive of phase interference effects.

2.1.2.1 Kirchhoff Model

The method of physical optics, or the Kirchhoff method, assumes that the field incident on an irregular surface is locally reflected with the Fresnel reflection coefficient. Stated in another way, the reflection from each point on the surface is considered to be identical to that which would be reflected by an infinite plane tangent to the surface at the point of observation. While this assumption does not restrict one to any particular range of roughness relative to the incident wavelength, it does restrict one to "locally flat" surfaces where the radius of curvature of the surface is large with respect to the incident wavelength. The most commonly used criterion for applicability is due to Brekhovskikh (1952) and is given by

$$4 \pi \rho \cos \theta >> \lambda$$

where ρ is the radius of curvature of the surface at the point of incidence and θ is the local angle of incidence between the incident energy vector and the unit normal to the surface at the point of incidence.

For a plane wave incident upon a random surface, the more or less standard Kirchhoff method predicts an average far-zone backscatter power of the form (Hagfors, 1966).

$$P(\theta) = \frac{1}{(\lambda \cos \theta)^2} \int J_0(2k \sin \theta \, \tau) \, \chi(2k \sin \theta, -2k \sin \theta) \, \tau \, d\tau \qquad (2.24)$$

where k = $2\pi/\lambda$ the wave number
θ = the incident angle
τ = the distance along the surface
J_o = the zero order Bessel function
χ = the characteristic function associated with the surface height distribution

and the integration is over the illuminated area. A proportionality constant unimportant to our discussion has been omitted from the above expression.

Most theories assume a gaussian surface height distribution which gives

$$P(\theta) = \frac{1}{(\lambda \cos \theta)^2} \int J_0(2k \sin \theta \, \tau) \, e^{-K(1-r(\tau))} \, \tau \, d\tau \qquad (2.25)$$

where $K = 16\ ^2(\sigma/\lambda)^2\cos^2\Theta$
σ = the standard deviation of the surface
$r(\tau)$ = the surface autocorrelation function

The frequency dependence of equation (2.25) is determined by the argument of the zero-order Bessel function and the constant K. The contribution to the integral of the Bessel function decreases with increases in either incidence angle or frequency. The factor K incorporates the dependence of the integral upon the relative roughness of the surface with respect to wavelength through the ratio $(\sigma/\lambda)^2$. As K becomes much larger than one, the contribution of the exponential becomes negligible except near the region of zero lag ($r(\tau)$ close to one). The region of $r(\tau)$ that contributes to the value of the integral is therefore wavelength dependent.

The description of the wavelength dependence of the surface may be seen to be intimately tied to the description of the surface through the autocorrelation function. The most commonly assumed autocorrelation functions are the gaussian and exponential, although composite functions with wavelength dependence have likewise been used (Davies, 1954; Hayre and Moore, 1961; Fung and Moore, 1966).

The various types of autocorrelation functions used to evaluate the integral of equation (2.22) predict a wavelength variation of λ^0 to λ^{-6}. No attempt is made to justify any one of these choices since none of them may serve as more than a guide to the type variation expected from natural targets.

2.1.2.2 Spetner and Katz Random Scatterer Model

Spetner and Katz (1960) consider the radar return from a surface assumed to be composed of a large number of incoherent independent scatterers. The normalized radar cross-section is the product of the density of scatterers per unit area, and the average cross-section of a single scatterer. At sufficiently short wavelengths, the effective scatterers are distinct and may be identified with the real or physical scatterer.

As wavelength increases, adjacent scatterers tend to merge and the effective density of scatterers decreases. The density of effective scatterers is given by

$$\rho_s = \begin{cases} \rho_o & \lambda < (C_1/\rho_o)^{1/2} \\ C_1/\lambda^2 & \lambda > (C_1/\rho_o)^{1/2} \end{cases} \qquad (2.26)$$

where p_S = density of effective scatterers per unit area

p_O = density of real scatterers per unit area

λ = incident wavelength

C_1 = constant

The average scatterer cross section, for wavelengths small compared to the dimensions of the scatterer, is

$$\sigma_1 = \rho \frac{4\pi A^2}{\lambda^2}, \qquad \lambda \text{ small} \qquad (2.27)$$

where ρ = power reflection coefficient

A = effective area of the scatterer

For wavelengths large compared to the scatter dimensions, Rayleigh-type scattering is assumed and the scattering cross section is given by

$$\sigma_1 = \frac{C_2 v^2}{\lambda^4}, \qquad \lambda \text{ large} \qquad (2.28)$$

where v = volume of the scatterer

C_2 = constant

The transition wavelength between the application of equation (2.24) and (2.25) is denoted λ_o. Thus

$$\sigma_1 = \begin{cases} \rho \dfrac{4\pi A^2}{\lambda^2}, & \lambda < \lambda_o \\ \dfrac{C_2 v^2}{\lambda^4}, & \lambda > \lambda_o \end{cases} \qquad (2.29)$$

Combining equation (2.26) and (2.27) gives four possible combinations for radar backscattering cross section, $\sigma°$. These are summarized in Table 2.1. Figure 2.2 shows in graphic form the wavelength dependence of $\sigma°$ in the various regions.

2.1.2.3 Spetner and Katz Specular Point Model

For this model the surface is assumed to be reflective, of irregular shape, but continuous and with continuous derivatives. The contributions to the radar return are assumed to come predominately from two sources: the energy which is reflected from large facets of the surface oriented perpendicular to the line-of-sight, and the energy which is scattered isotropically by the small scatterers.

The scattering coefficient is assumed to have the form

$$\sigma^o = \rho_{ss}\,\sigma_{1s} + \rho_{sL}\,\sigma_{1L} \qquad (2.30)$$

where p_{ss}, p_{sL} = scatterer densities for small and large scatterers respectively

σ_{1s}, σ_{1L} = scattering cross sections for small and large scatterers respectively

The dependence of p_{ss} is the same as shown in equation (2.26) but here it is valid only for large λ. The average number of facet-type scatterers per unit area, p_{sL}, is the average density of points on the surface

TABLE 2.1

	$\lambda < \lambda_o$	$\lambda > \lambda_o$
$\lambda < (C_1/p_o)^{1/2}$	$\sigma^o = \frac{4\pi p_o \rho A^2 s}{\lambda^2}$	$\sigma^o = \frac{C_2 p_o v^2}{\lambda^4}$
$\lambda > (C_1/p_o)^{1/2}$	$\sigma^o = \frac{4\pi C_1 \rho A^2 s}{\lambda^4}$	$\sigma^o = \frac{C_1 C_2 v^2}{\lambda^6}$

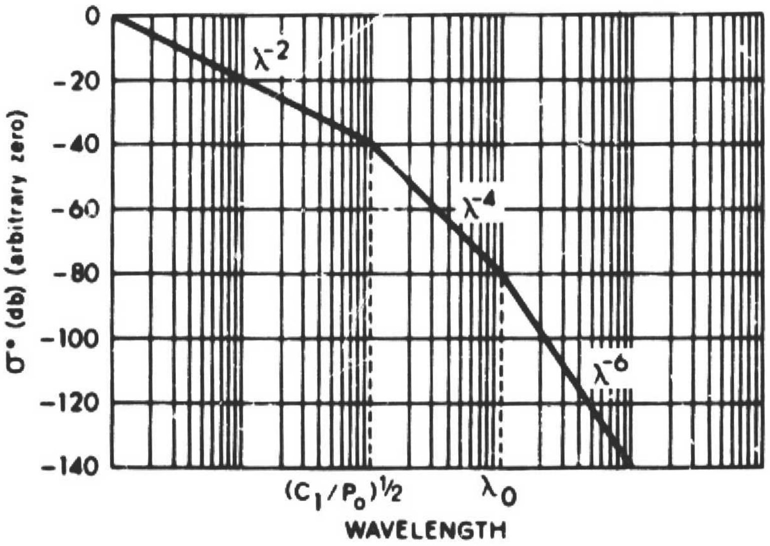

Figure 2.2 Wavelength dependence of normalized radar cross section (random scatterer model) from Spetner and Katz, 1960.

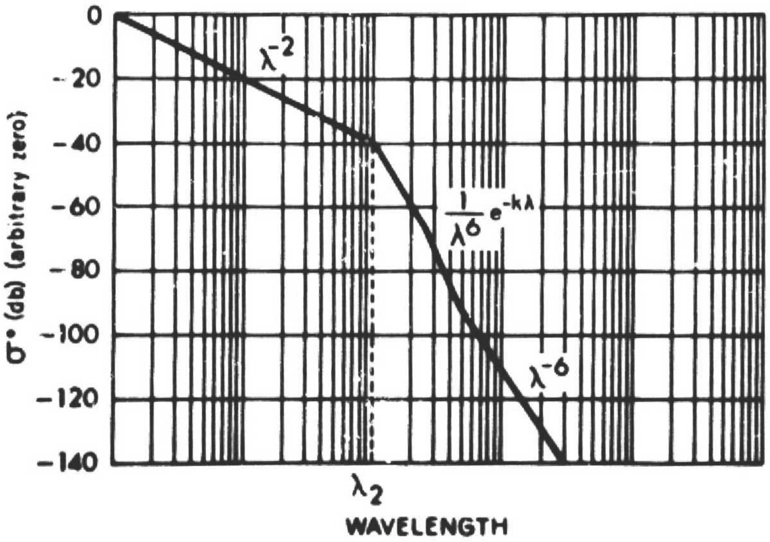

Figure 2.3 Wavelength dependence of normalized radar cross section (specular point model) from Spetner and Katz, 1960.

oriented normal to the incident energy. p_{sL} is, therefore, dependent upon the slope spectrum of the surface, and in particular upon the variance of the surface slope, S_o^2. Assuming a flat-slope spectrum with a cutoff at λ^{-1}, define a wavelength dependent effective slope variance, S^2, related to the measured variance, S_o^2, by

$$S^2 = \begin{cases} S_o^2 , & \lambda < \lambda_2 \\ S_o^2 \, \lambda_2/\lambda , & \lambda > \lambda_2 \end{cases} \tag{2.31}$$

The density of horizontal facets is then

$$\rho_{sL}(90°) = \begin{cases} C_3/\lambda_2^2 , & \lambda < \lambda_2 \\ C_3/\lambda^2 , & \lambda > \lambda_2 \end{cases} \tag{2.32}$$

The scattering cross sections for large and small scatterers are

$$\sigma_{1L} = \rho \frac{4\pi A^2}{\lambda^2} \qquad \text{(flat plate)} \tag{2.33}$$

and

$$\sigma_{1S} = \rho \frac{C_4}{\lambda^4} \qquad \text{(Rayleigh scatter)} \tag{2.34}$$

The transition region between the applicability of equation (2.33) and (2.34) will be denoted by λ_2 as in equation (2.31). Thus

$$\sigma_1 = \begin{cases} \rho \dfrac{4\pi A^2}{\lambda^2} , & \lambda < \lambda_2 \\ \rho \dfrac{C_4}{\lambda^4} , & \lambda > \lambda_2 \end{cases} \tag{2.35}$$

The final expression for the normalized radar cross-section of an irregular reflecting surface having a gaussian slope distribution and a flat slope spectrum sharply cut off at $\nu = \lambda_2^{-1}$ is given by

$$\sigma^\circ = \begin{cases} \rho \dfrac{4\pi A^2 C_3}{\lambda^2 \lambda_2^2} \; e^{(-\cot^2\theta/2S_o^2)} , & \lambda < \lambda_2 \\[2ex] \dfrac{C_3 C_4}{\lambda^6} \; e^{(-\cot^2\theta)\lambda/2S_o^2\lambda_2} + \dfrac{C_5}{\lambda^6} , & \lambda > \lambda_2 \end{cases} \qquad (2.36)$$

The results for $C_5 < C_3C_4$ are shown in Figure 2.3.

2.2 Experimental Analyses

2.2.1 Panchromatic Illumination

While considerable has been written regarding the improvement in fading and glint statistics to be expected with frequency diversity, remarkable few measurement data have been published.

2.2.1.1. Visible Light Analogy

Perhaps the most striking illustration of the averaging of fading with bandwidth may be seen in the visible region. Figure 2.4 shows photographs of a target illuminated first with monochromatic laser light and then with normal panchromatic or broad-band incoherent light. The scintillation or grainy appearance of the laser illuminated photograph well illustrates the problem of phase interference effects, while the smooth tones of the panchromatic photograph show the effect possible with frequency averaging.

2.2.1.2 Philips Teleindustri Experiments

Gustafson and Ås (1964) measured the comparative performance of a fixed-frequency radar and a so-called jumping-frequency system.

DE/CRES/Univ. of Kansas/1970

transparency size 5mm 10mm

Speckle effect illustrated by illuminating a photographic transparency with:

A) Coherent (6328 Å, laser) light.
B) Incoherent (3200° Kelvin, incandescent) light.

Figure 2.4 Effect of illuminating bandwidth in the visible region of the spectrum.

The jumping-frequency system employed frequency shifting on a pulse-to-pulse basis. Measurements were conducted in both search and tracking systems.

The experimental results for the search mode of operation are summarized in Figure 2.5. The abbreviations FF and JF refer to fixed-frequency and jumping-frequency operation, respectively. The theoretical curves shown are calculated on the assumption that the fixed-frequency returns are completely correlated within a single scan, but totally uncorrelated scan-to-scan while the jumping-frequency returns are assumed pulse-to-pulse independent (Marcum, 1960; Swerling, 1960).

Tracking measurements on aircraft with both modes of operation indicated roughly a 20% increase in range to the first drop-out of tracking when jumping-frequency operation was used. Figure 2.6 shows the reduction of glint obtained when using jumping-frequency radar to track sea targets.

2.2.1.3 Norden Experiments

Kosowsky, et al. (1963) conducted angle-of-arrival and scintillation measurements for natural terrain using fixed-frequency and pulse-to-pulse frequency shifting. The redistribution of the scintillation energy obtained by frequency-shifting is shown in Figure 2.7. The low frequency spectrum is substantially reduced over that obtained without frequency shifting, and after filtering leads to an improved estimate of the true angle-of-arrival in a finite observation time.

2.2.1.4 University of Kansas Acoustic Experiments

Rouse (1968) conducted acoustic imaging experiments of complex targets both with fixed-frequency and with a linear FM sweep. Post-detection integration was used to obtain large effective bandwidths. While no measurements of variance reduction were made, the resulting images illustrate the improvement obtainable with panchromatic illumination; the images of Figure 2.8 clearly show the improvement in image quality much

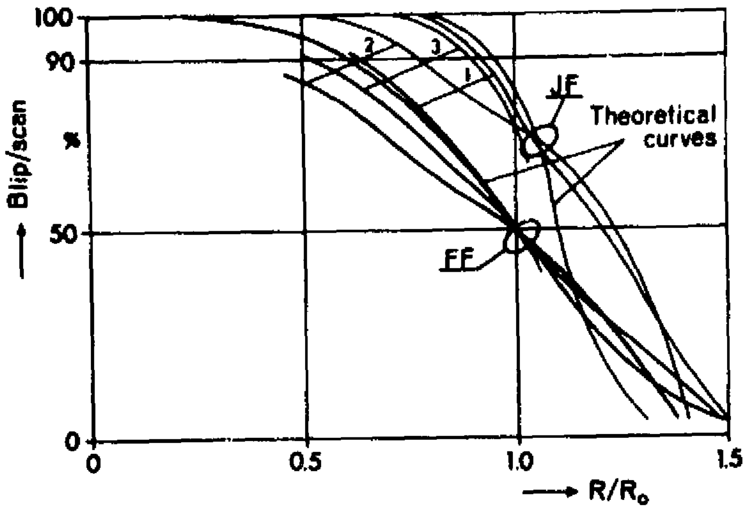

Figure 2.5 Results of experimental determination of blip-to-scan ratio versus range for air targets, and comparison with theoretical results. R = radar range; R_O = radar range giving 50% blip-to-scan ratio on fixed frequency. Curves 1 give the result of the measurements with a jet plane (a small fighter), curves 2 with a small one-engined propeller aircraft and curves 3 with a medium-sized twin-engined propeller aircraft (from Gustafson and Ås, 1964).

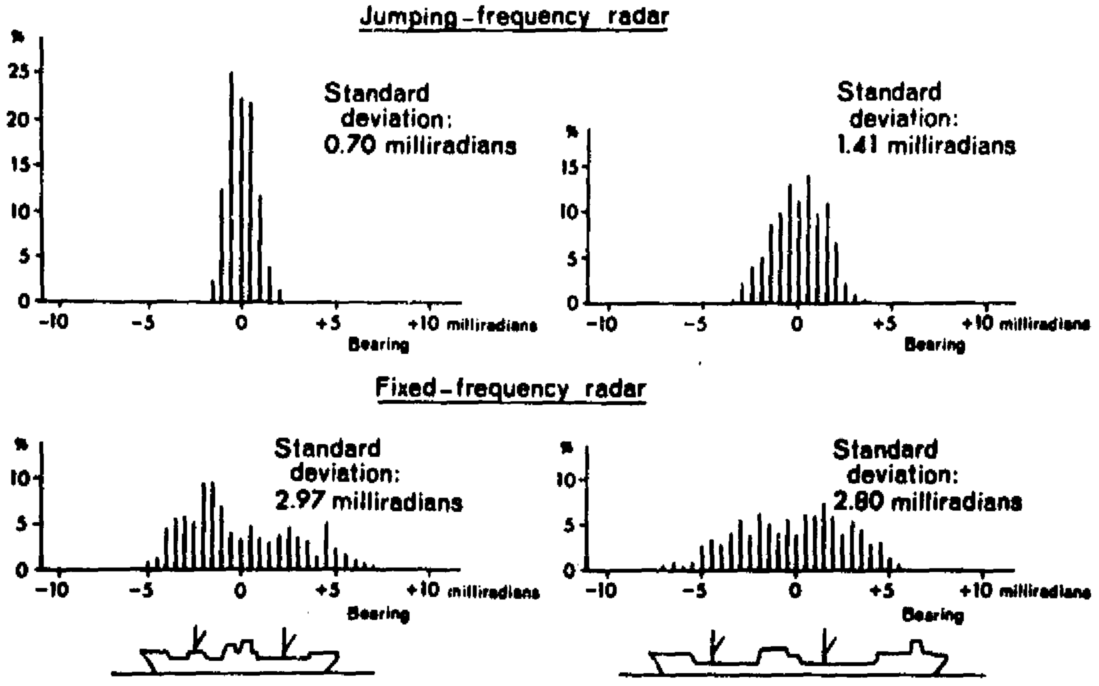

Figure 2.6 Reduction of glint using jumping-frequency radar to track sea targets, as compared with fixed-frequency radar. Relative distribution of target positions, recorded with a 16 mm film camera and measured at intervals of 0.5 milliradians, is shown together with the silhouettes of the targets, which are reproduced in their apparent actual size in milliradians (from Gustafson and Ås, 1964).

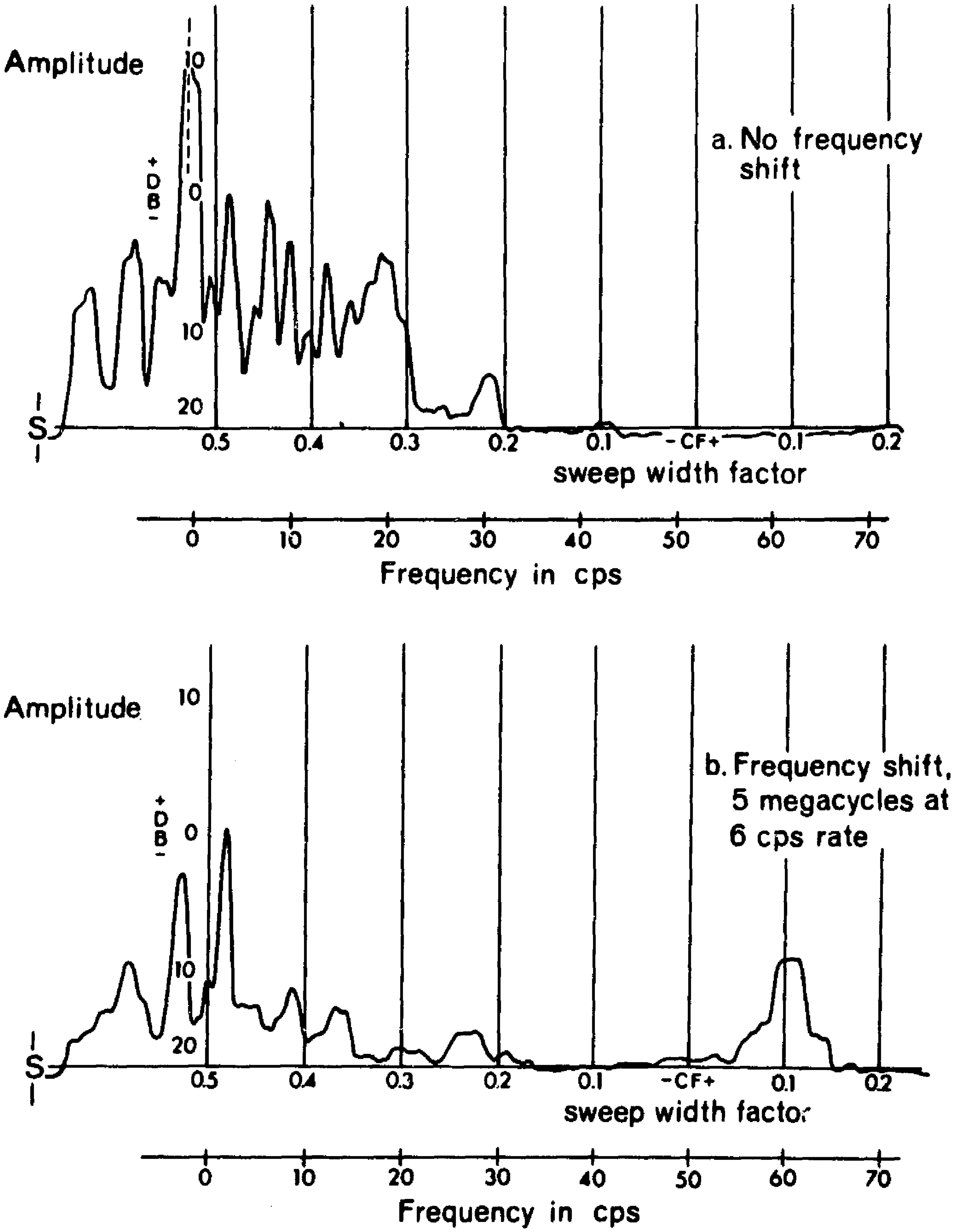

Figure 2.7 Scintillation spectra (tree covered terrain, slight wind) from Kosowski et al., 1963.

(a) Monochromatic image of two spheres
(f = 1.5 MHz)

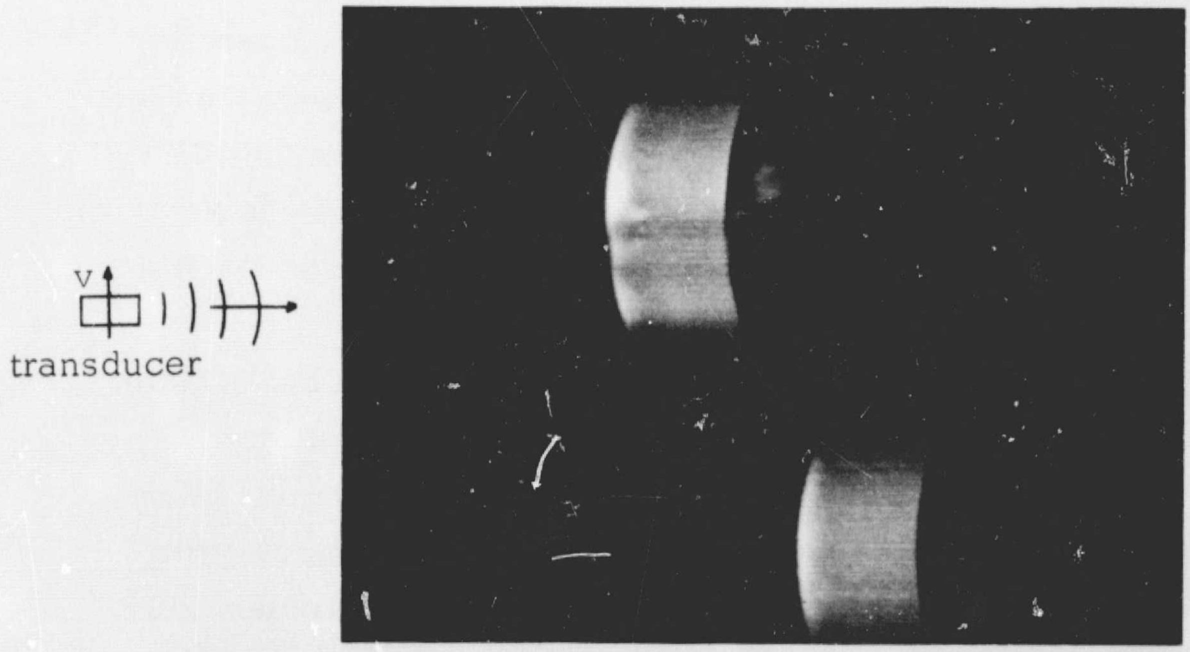

(b) Swept frequency image of two spheres
(f = 1.5 MHz ± 10%)

Figure 2.8 Effect of frequency average on image of sphere targets. (from Rouse, 1968).

like that shown in the comparison of laser and panchromatic illumination in the visible region.

2.2.2 Polypanchromatic Illumination

No one has yet produced polypanchromatic or continuous spectral data in the microwave region. A number of investigators have made polychromatic measurements at a limited number of discrete frequencies. Some measurements of the effect of polarization are available at these limited frequencies, however, most programs have concentrated on the variation of backscatter with incidence angle. The aim of most prior programs incorporating polychromatic measurements has been to produce design data for specific monochromatic systems.

2.2.2.1 Naval Research Laboratory Experiments

NRL has operated for several years a four-frequency radar system mounted in a WV-2 aircraft. This system operates at 428 MHz (P-band), 1225 MHz (L-band), 4455 MHz (C-band), and 8910 MHz (X-band). The antennas look forward along the flight track and the angle of incidence may be varied by antenna movement. Beamwidths of the four antennas are 12° (P-band), 5.5° (L-band), and 5° (C- and X-band). At each frequency the system is capable of transmitting or receiving either a vertical or horizontal polarized signal, thus the full polarization matrix may be recorded (Ament, et al., 1959).

The system described above has been used to record backscatter characteristics from a wide variety of targets, although the primary usage has been the measurement of sea clutter. Due to the narrow beamwidths the variation in angle data must be collected by making multiple passes with different antenna tilts. While this poses little problem over the ocean (which may be considered homogeneous over large stretches) the difficulty in repeating flight lines leads to a rather gross definition of terrain categories. Figure 2.9 is a sample of the NRL aircraft program data for the categories "New Jersey Woods" and "City of Chicago".

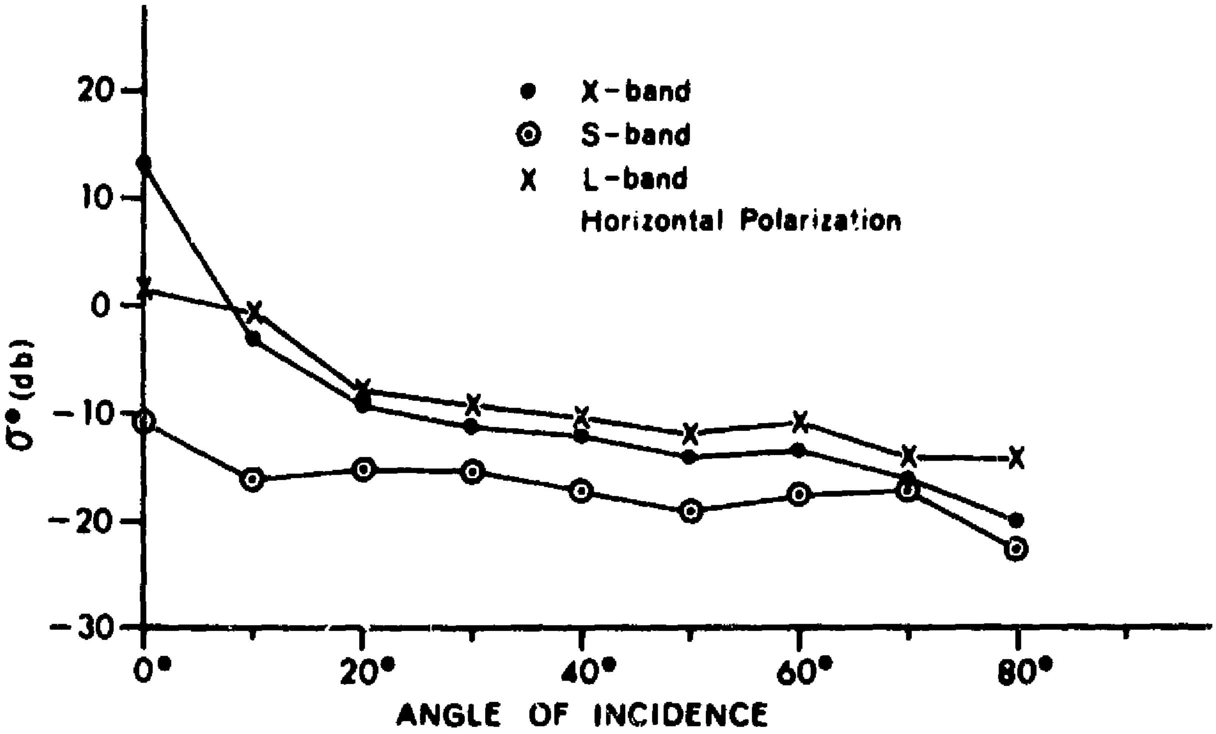

(a) City of Chicago

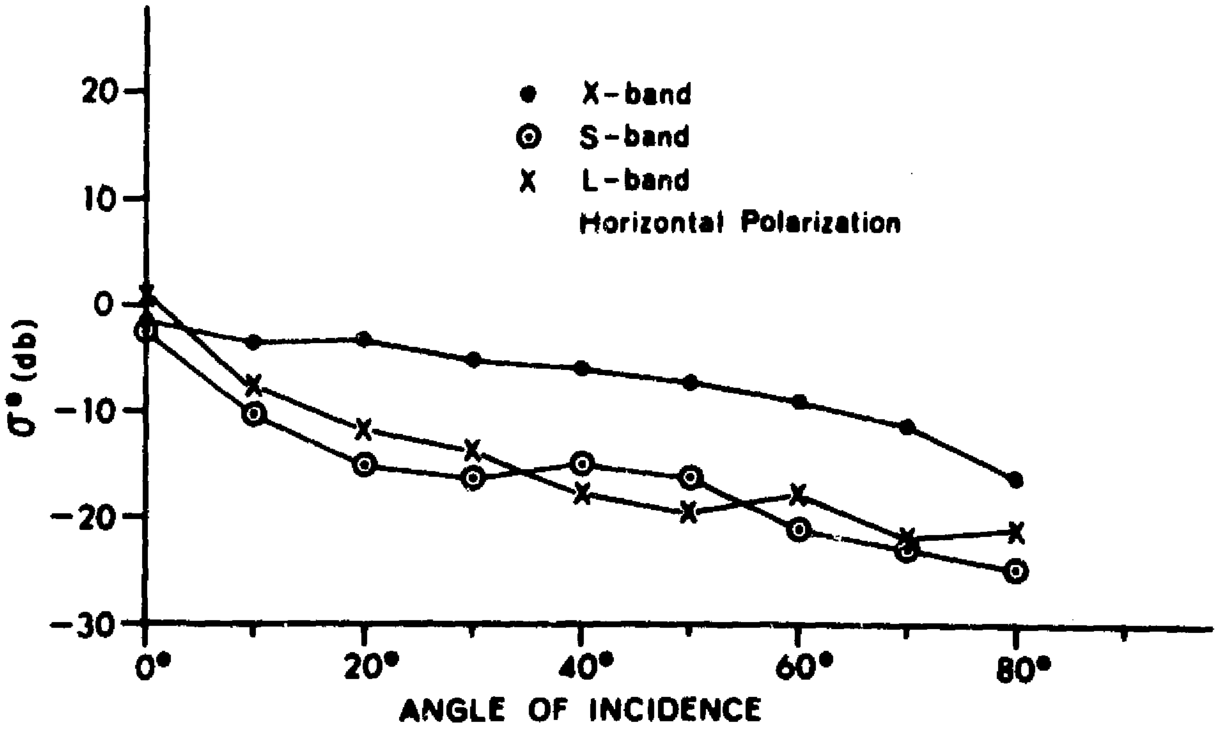

(b) New Jersey woods

Figure 2.9 Naval Research Laboratory airborne backscatter measurements.

NRL also supported a brief three-frequency ground measurement program (Grant and Yaplee, 1957). The operating wavelengths were 3.2 cm, 1.25 cm, and 8.6 mm. Measurements were recorded for a wide variety of terrain types and with reasonable definition. Figure 2.10 shows examples of these measurements.

2.2.2.2 Sandia Corporation Experiments

Sandia Corporation conducted a measurement program using a two-frequency (415 MHz and 3800 MHz) pulsed airborne system (Edison et al., 1960). Angular variations were obtained by tracking the annular illuminated region provided by narrow pulse modulation. Unfortunately, the program objective was to provide altimeter design data; hence, the technique used restricted the angular range to near vertical incidence (less than 30° from the nadir). The targets measured are reasonably well documented and samples of the measurements are shown in Figure 2.11.

2.2.2.3 Ohio State University Experiments

Probably the most carefully controlled and repeatable series measurements of natural surfaces has been conducted by the Ohio State University Antenna Laboratory (Cosgriff et al., 1960). A three-frequency truck-mounted system operating at 10 GHz (X-band), 15.5 GHz (Ku-band), and 35 GHz (Ka-band) was used. The antennas were mounted on an elevated boom and were adjustable over a range of incident angles. The measurements were taken by moving the truck along an assumed homogeneous stretch of terrain while recording.

The principal disadvantage with this system lies in the relatively small illuminated area (approximately 1 meter in diameter) due to the low altitude of the antennas. This restricts measurements to small scale terrain features such as grass, concrete roads, etc. The apparent accuracy and repeatability of these measurements offers a valuable insight into the behavior of radar backscatter from natural terrain. Figure 2.12 shows examples of Ohio State University data.

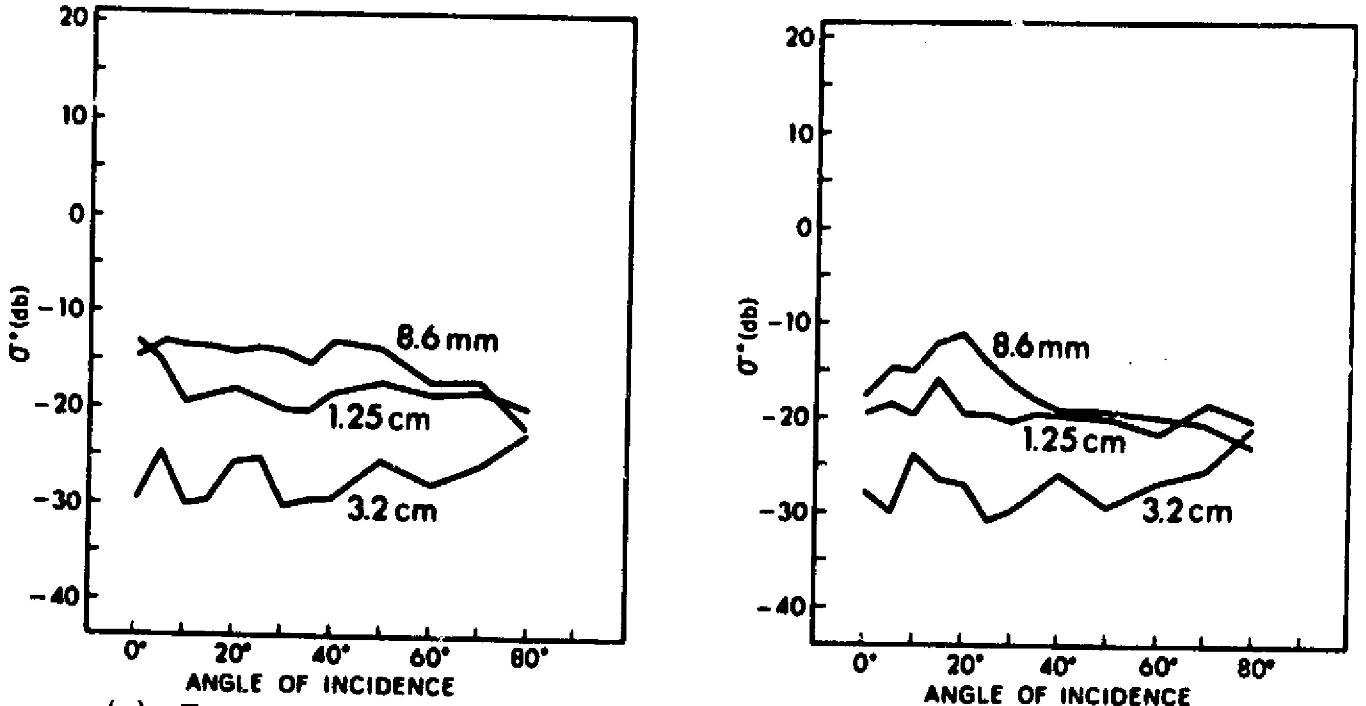

(a) Tree-covered terrain.

(b) Terrain covered with tall dry weeds

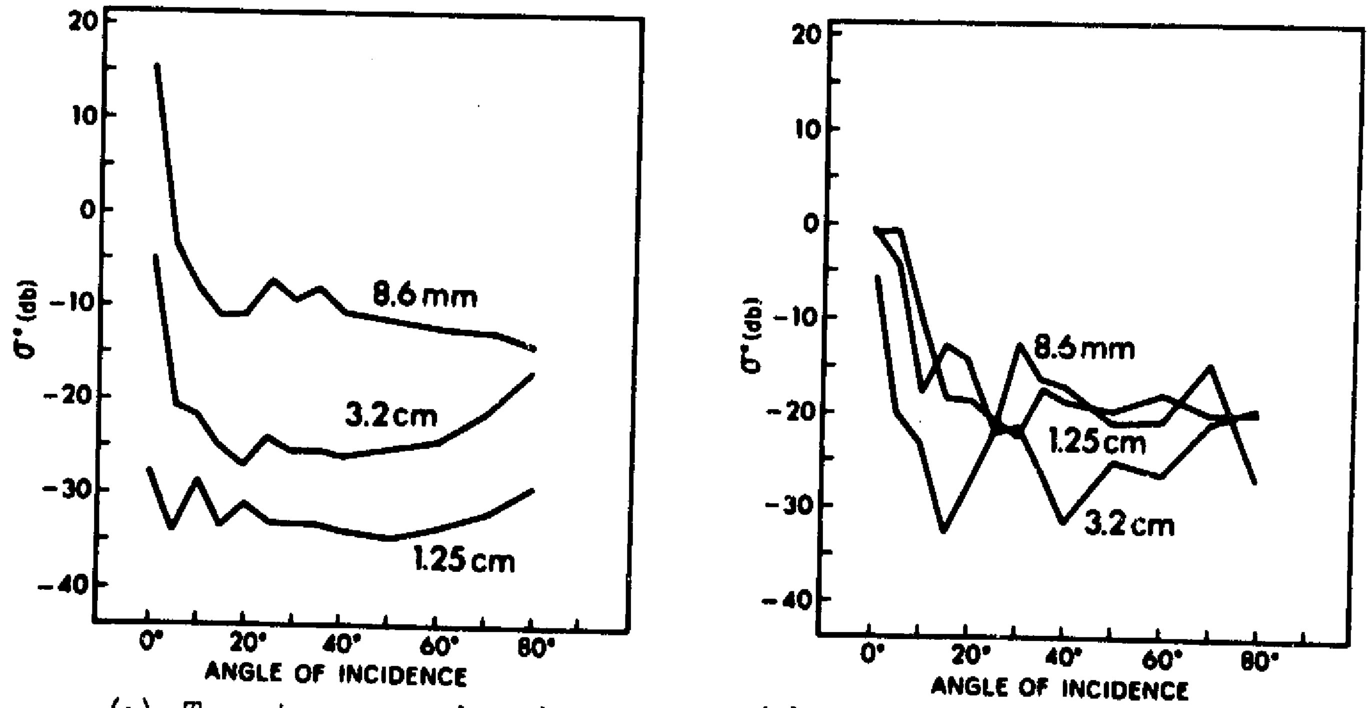

(c) Terrain covered with tall green weeds or flags.

(d) Terrain partially covered with short dry grass.

Figure 2.10 Naval Research Laboratory ground-based backscatter measurements (after Grant and Yaplee, 1957).

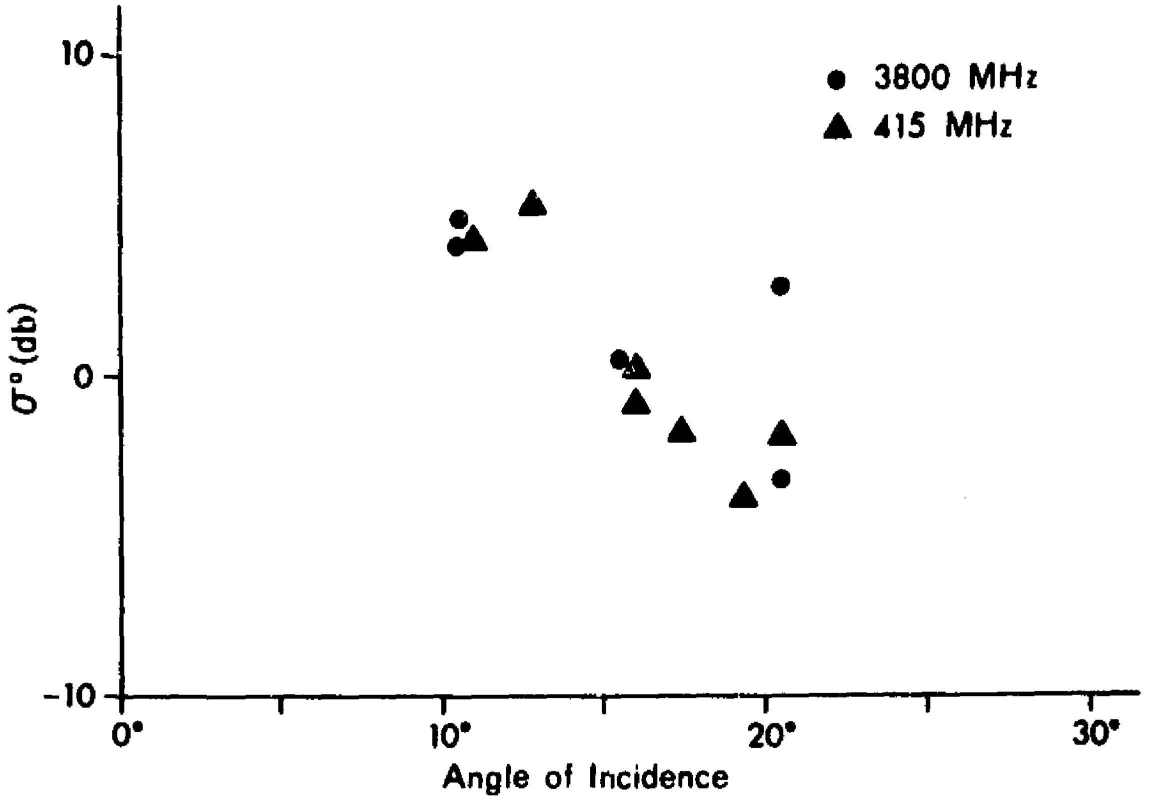

(a) Farmland near Cameron, Missouri.

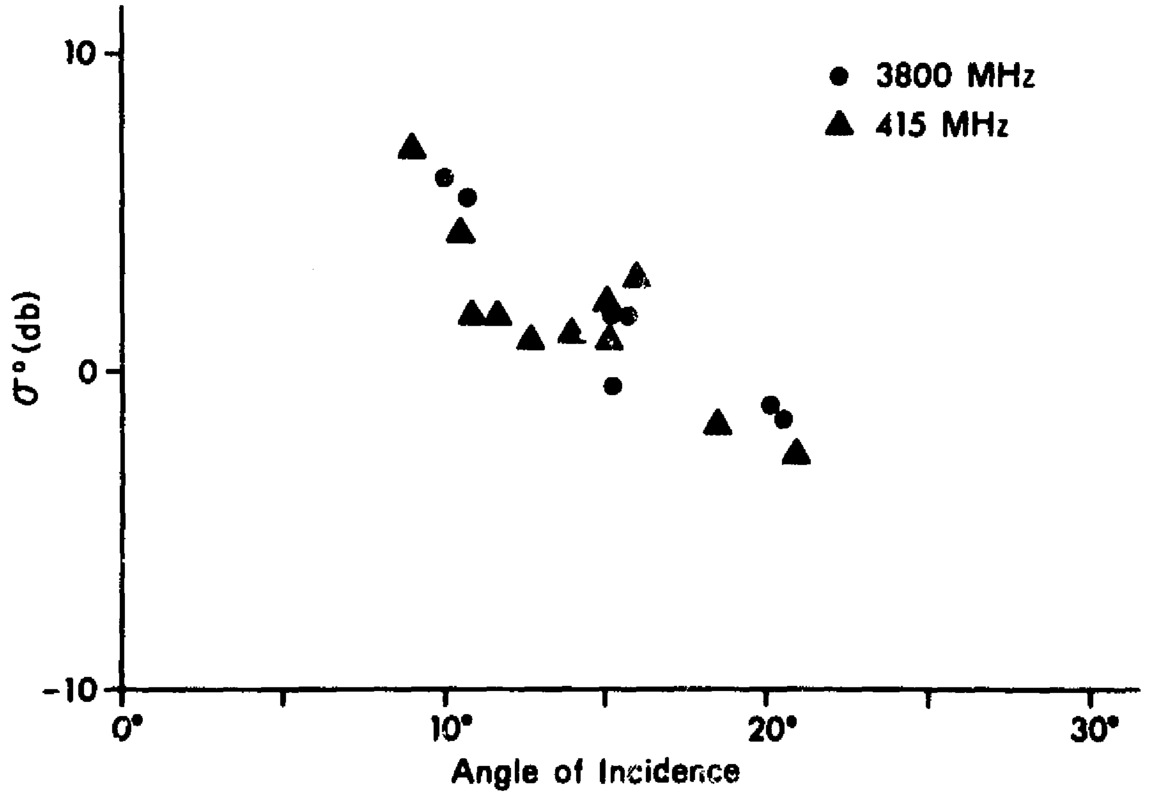

(b) Area of apartment buildings in Kansas City, Missouri.

Figure 2.11 Sandia Corporation airborne backscatter measurements (after Edison et al., 1960).

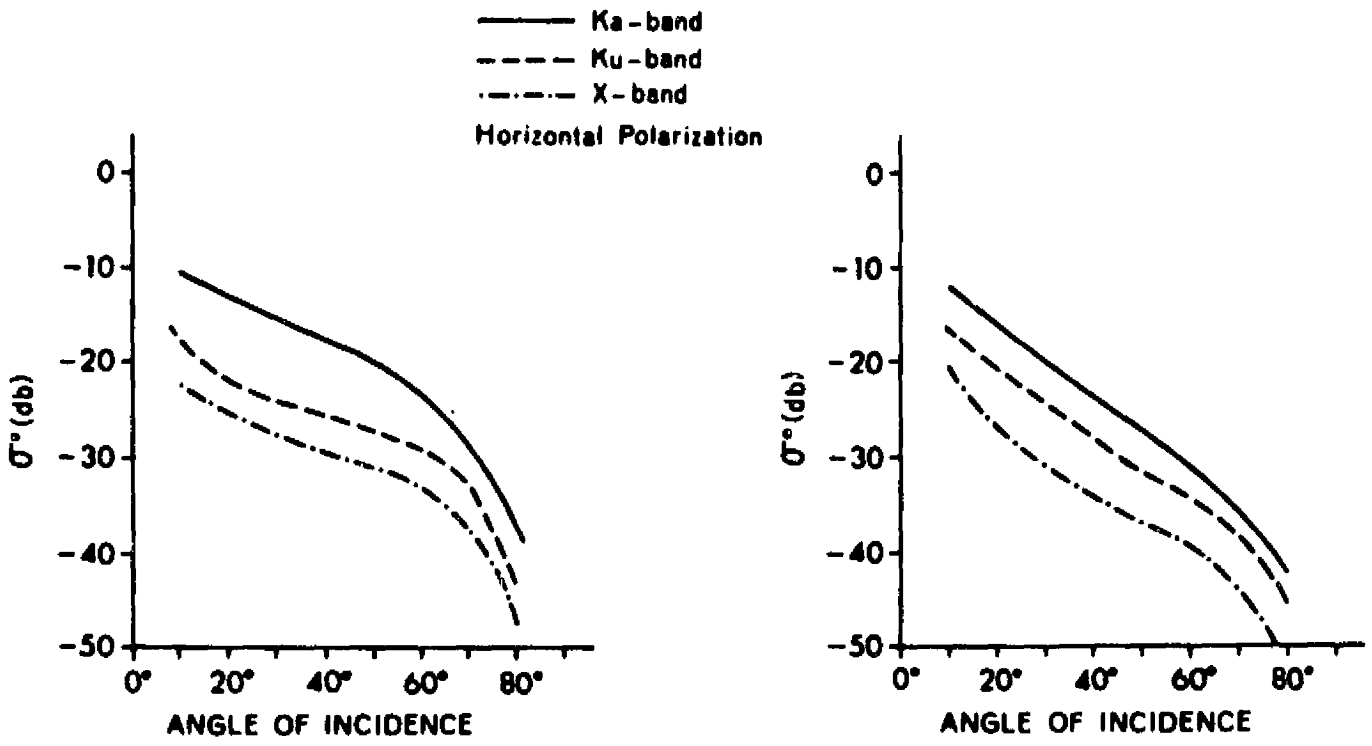

(a) Asphalt road.

(b) Concrete road.

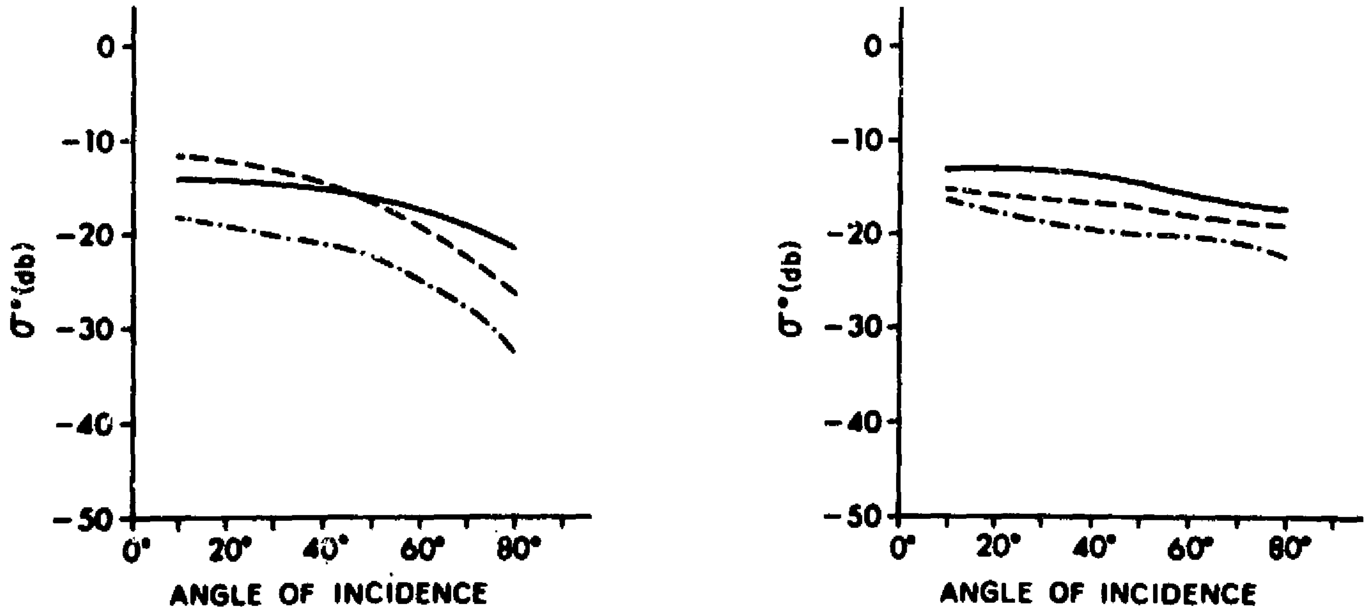

(c) Disked ground.

(d) Three-foot green oats (June).

Figure 2.12 Ohio State University ground-based backscatter measure- (after Cosgriff et al., 1960).

2.2.2.4 Waterways Experiment Station Experiments

The U.S. Army Waterways Experiment Station operates a four-frequency system mounted on a 50-foot radius wooden arch. The antennas travel along tracks mounted inside the arch and may view an approximately 4-foot diameter target sample at the center of the arch over an angular range of 210 degrees. The system frequencies are 297 MHz (P-band), 5879 MHz (C-band), 9375 MHz (X-band), and 35,543 MHz (Ka-band).

Measurements conducted with this system have been principally concerned with determining the amount of penetration into soil and the effect of moisture content upon the backscattered return (Lundien, 1966). These measurements are made on carefully prepared soil samples. A limited amount of data from more natural targets has been taken and a sample of these results is shown in Figure 2.13.

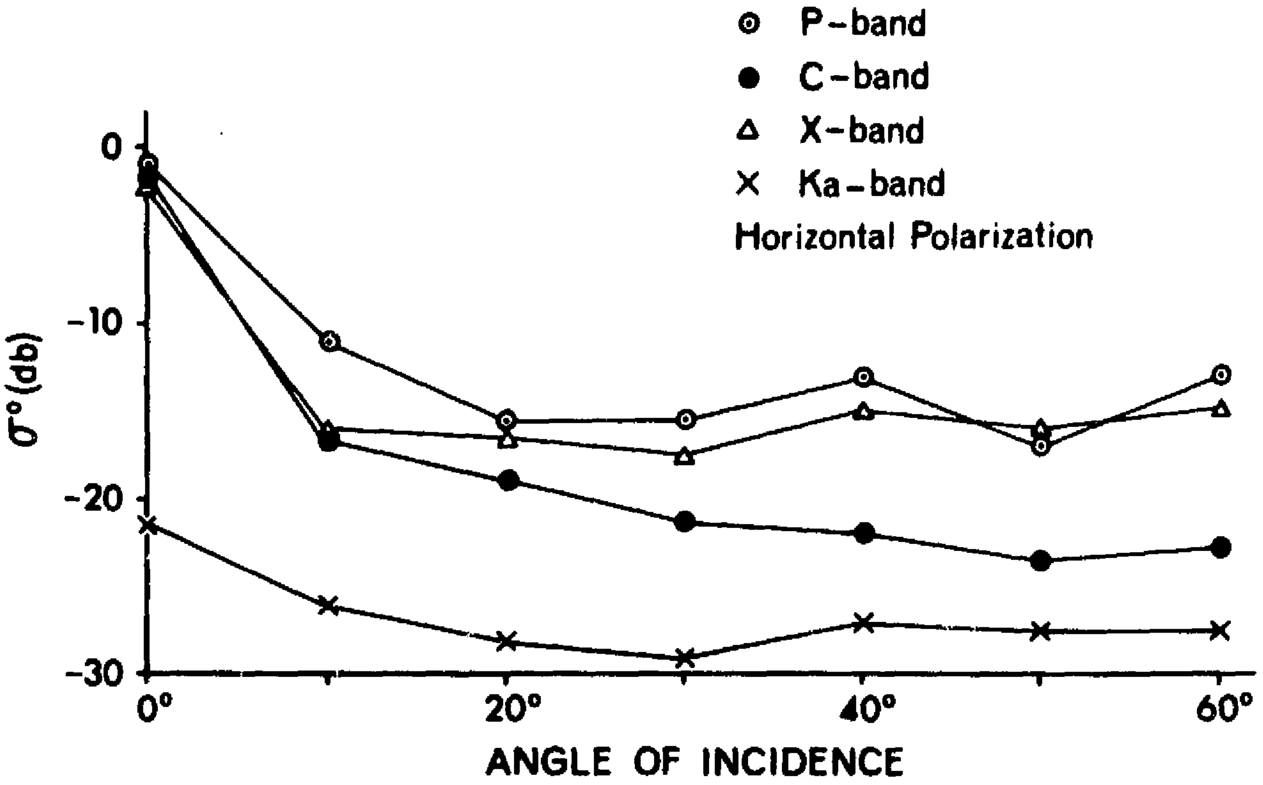

(a) Wheat sample - 3 1/2 inch vegetation height.

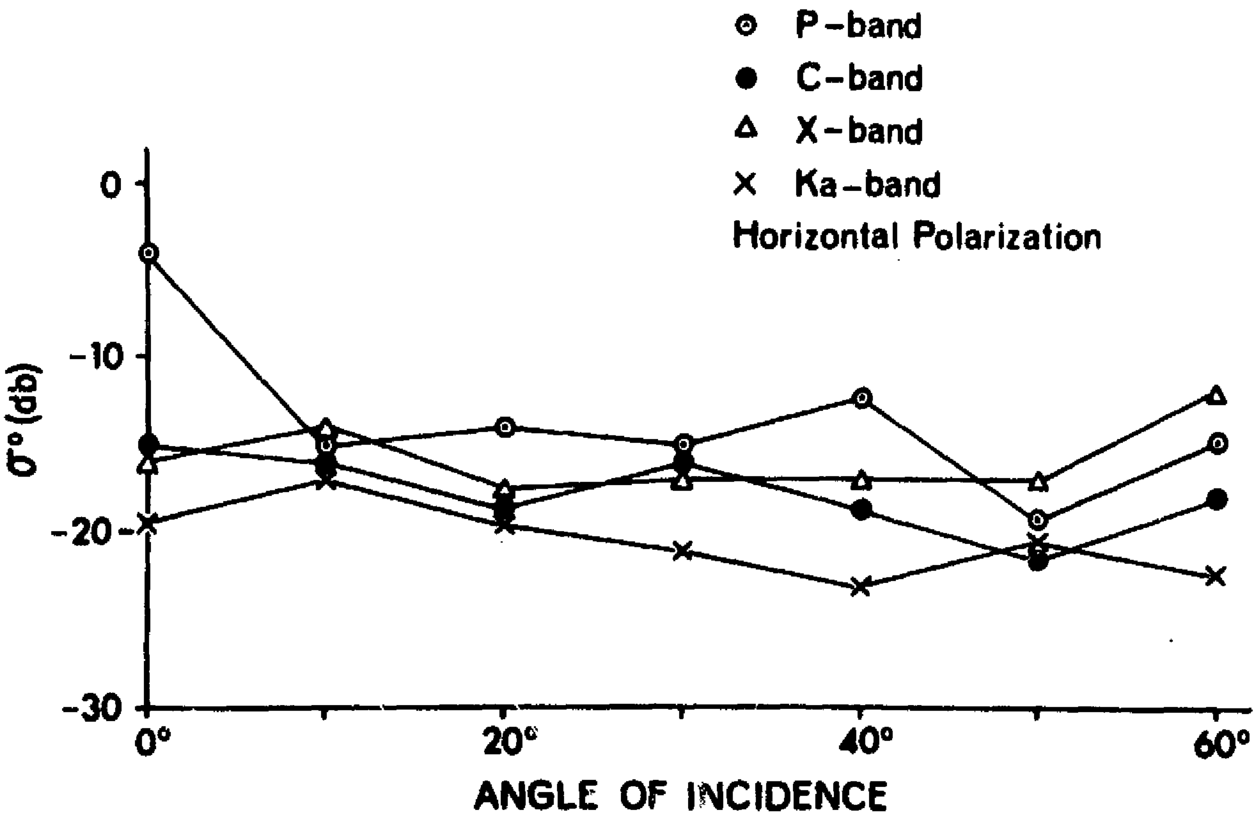

(b) Wheat sample - 29 inch vegetation height.

Figure 2.13 Waterways Experiment Station ground-based backscatter measurements (after Lundien, 1966).

CHAPTER 3

VARIANCE REDUCTION OF RADAR BACKSCATTER WITH BROAD-SPECTRUM ILLUMINATION

In this chapter we shall investigate the effect of broad-spectrum illumination upon the fading statistics of a target model assumed to represent a distributed target. It is assumed that the targets of interest are sufficiently complex that they may be represented by an equivalent set of point scatterers. The behavior and, in particular, the variance of the signal return from the postulated model is then examined for a variety of transmitted signals both monochromatic and broad-spectrum.

3.1 Target Model

We shall assume that the targets of interest are sufficiently complex that they may be represented by a random collection of discrete independent scatterers. Each scatterer reradiates isotropically with an amplitude proportional to its effective radar cross-section. The amplitude distribution is random and is assumed to have a gaussian distribution with zero mean and variance, σ_a^2. For a given target area or class the average density of scatterers per unit area, γ, is constant, i.e scatterers are uniformly distributed within the target.

Figure 3.1 shows the target model illuminated by a radar system. Angular resolution of the target is provided by the antenna beam width, β. The antenna gain is assumed constant over the illuminated area and zero elsewhere. Range resolution is obtained by modulation of the transmitted waveform. The dimensions of the target may be either larger or smaller than the corresponding dimenions of the radar system resolution cell. For instance, the resolution cell of an imaging radar system may occupy only a small portion of a large homogeneous field. At the other extreme, the target for a search radar system is frequently an aircraft with an area or volume much less than that of the system resolution cell.

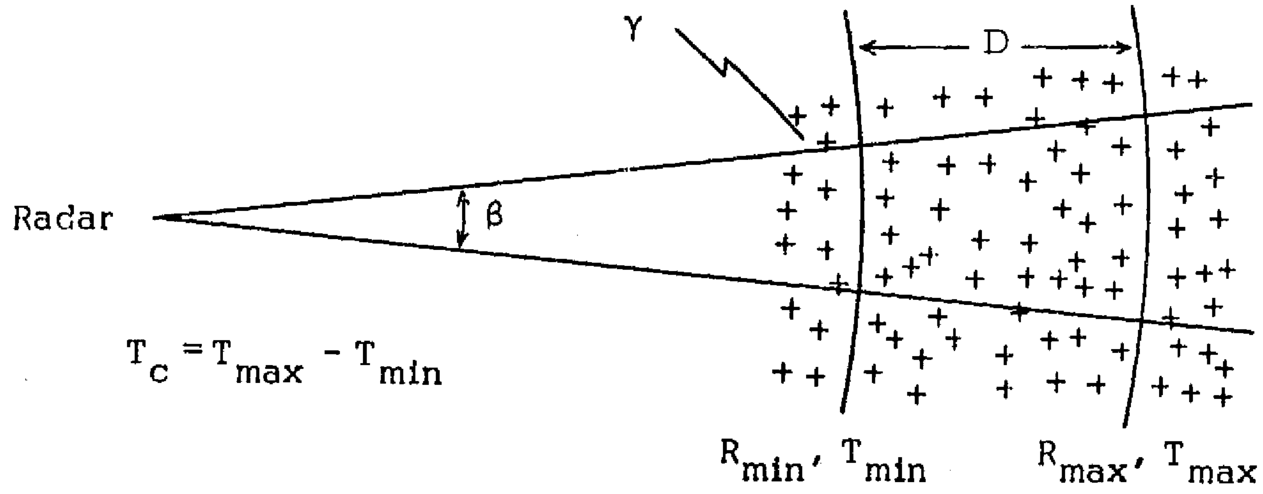

Figure 3.1 Discrete scatterer model of target area.

Within the target complex each scattering element is characterized by its return signal amplitude and its range from the radar. In all instances it is assumed that the target range dimension, D, is much less than the minimum range of the system such that the return signal amplitude of the scattering elements may be considered independent of range.

The signal returned to the radar from a single scattering element is

$$s_r(t) = a_n s(t - t_n) \tag{3.1}$$

where s(t) = transmitted waveform

t_n = round-trip time delay corresponding to the scatterer range

a_n = scattering amplitude adjusted for system parameters.

The local return from the target is the summation of the returns from all scattering elements located within the illuminated area. Thus,

$$S_r(t) = \sum_{n=1}^{N} a_n \, s(t-t_n) \tag{3.2}$$

The delayed transmitter signal may be expressed as the convolution of the transmitted waveform with an impulse function.

$$s(t-t_n) = \int_{-\infty}^{\infty} s(t_n) \, \delta(t-t_n) \, dt_n \tag{3.3}$$

where

$$\delta(t-t_n) = \begin{cases} 0 & \text{if } t \neq t_n \\ 1 & \text{if } t = t_n \end{cases}$$

The total received signal may now be expressed as

$$S_r(t) = \sum_{n=1}^{N} a_n \int_{-\infty}^{\infty} s(t_n) \, \delta(t-t_n) \, dt_n \tag{3.4}$$

Interchanging the order of integration and summation, we have

$$S_r(t) = \int_{-\infty}^{\infty} s(t_n) \sum_{n=1}^{N} a_n \, \delta(t-t_n) \, dt_n \tag{3.5}$$

The return signal is, thus, the convolution of the transmitted signal with what might be considered the impulse response of the target model. We may express equation (3.5) in a simpler fashion by

$$S_r(t) = s(t) \otimes c(t) \tag{3.6}$$

where the symbol, $\otimes$, denotes convolution and c(t) is the pulse response of the target model given by

$$c(t) = \sum_{n=1}^{N} a_n \, \delta(t - t_n) \tag{3.7}$$

The frequency response, C(f), of the target model is given by the Fourier transform of the impulse response. Thus,

$$\begin{aligned} C(f) &= \int_{-\infty}^{\infty} \sum_{n=1}^{N} a_n \, \delta(t - t_n) \, e^{j2\pi f t} \, dt \\ &= \sum_{n=1}^{N} a_n \, e^{-j2\pi f t_n} \end{aligned} \tag{3.8}$$

C(f) may be characterized as a vector sum with random amplitude and phase. For any frequency $f \gg 1/0$, the phase distribution will be effectively uniform over the basic phase interval 0 to 2π. By taking the minimum range to always be significantly greater than zero, it is assumed that the effective scattering amplitudes are not only independent of range, but that they meet the requirements of the Central Limit Theorem, i.e the variance of any one term is negligible compared to the variance of the sum.

With the above conditions the random vector sum is recognizable as a complex gaussian variable with a Rayleigh distributed envelope and a uniformly distributed phase. Thus, if

$$C(f) = z \, e^{j\theta} \qquad z = |C(f)|$$

we have the density functions

$$p(z) = \frac{z}{\alpha^2} \, e^{-z^2/2\alpha^2} \tag{3.9}$$

$$p(\theta) = \begin{cases} \frac{1}{2\pi} & 0 \le \theta \le 2\pi \\ 0 & \text{elsewhere} \end{cases} \tag{3.10}$$

where

$$\alpha^2 = \frac{1}{2}\sum_{n=1}^{N} E\left[a_n^2\right] = \frac{1}{2}\sum_{n=1}^{N} \sigma_{a_n}^2 \tag{3.11}$$

The mean, mean square and variance of the Rayleigh distribution are given by

$$\mu_z = E[z] = \alpha\sqrt{\pi/2} \tag{3.12}$$

$$E\left[z^2\right] = 2\alpha^2 \tag{3.13}$$

$$\sigma_z^2 = E\left[(z-\bar{z})^2\right] = 2\alpha^2\left[1-\pi/4\right] \tag{3.14}$$

Thus, the magnitude of the spectral response of the target model is given by a Rayleigh distribution at any frequency.

The frequency response autocorrelation function of the target model may be obtained from the expression developed for C(f), thus

$$\begin{aligned} R_c(\nu) &= E\left[C(f)\,C^*(f-\nu)\right] \\ &= E\left[\sum_{n=1}^{N} a_n e^{-j2\pi f t_n} \sum_{m=1}^{M} a_m e^{j2\pi(f-\nu)t_m}\right] \\ &= E\left[\sum_{n=1}^{N}\sum_{m=1}^{M} a_n a_m e^{-j2\pi f(t_n-t_m)} e^{-j2\pi\nu t_m}\right] \end{aligned} \tag{3.15}$$

Since the amplitudes of the individual scattering elements are statistically independent, the expected value of the double summation will be zero except when n = m. Therefore,

$$R_c(\nu) = \sum_{n=1}^{N} E\left[a_n^2 \, e^{-j2\pi\nu t_n}\right] \tag{3.16}$$

The strength and position, i.e. amplitude and phase, of the individual scattering elements are statistically independent. So

$$R_c(\nu) = \sum_{n=1}^{N} E\left[a_n^2\right] E\left[e^{-j2\pi\nu t_n}\right] \tag{3.17}$$

We further assume that not only are the scattering elements uniformly distributed, but that the distribution of time delay is likewise uniform.

$$p(t_n) = \frac{1}{T_c} \qquad\qquad \frac{T_c}{2} \leq t_n \leq \frac{T_c}{2}$$

For the case of a homogeneous area target of greater extent than the system resolution, this involves approximating the angular sector of Figure 3.1 by parallel lines over the range interval of interest. Taking the target center as the zero time reference, we have

$$\begin{aligned} E\left[e^{-j2\pi\nu t_n}\right] &= \int_{-\infty}^{\infty} p(t_n)\, e^{-j2\pi\nu t_n} \, dt_n \\ &= \int_{-T_c/2}^{T_c/2} \frac{1}{T_c}\, e^{-j2\pi\nu t_n} \, dt_n \\ &= \frac{\sin \pi\nu T_c}{\pi\nu T_c} \end{aligned} \tag{3.18}$$

Let

$$\sigma_c^2 = \sum_{n=1}^{N} E[a_n^2] \tag{3.19}$$

We now have

$$R_c(\nu) = \sigma_c^2 \frac{\sin \pi \nu T_c}{\pi \nu T_c} \tag{3.20}$$

Recalling that $T_c = 2D/c$, we have in terms of target size

$$R_c(\nu) = \sigma_c^2 \frac{\sin 2\pi \nu D/c}{2\pi \nu D/c} \tag{3.21}$$

The spacing between independent frequency samples of the model may be determined from the autocorrelation function of equation (3.21). If we assume independence to be achieved at the first zero of the autocorrelation function, the required frequency spacing, Δf, is given by

$$\Delta f = \frac{c}{2D} = \frac{150}{D} \text{ MHz} \tag{3.22}$$

The above result agrees with those shown earlier in Chapter 2, which is not surprising as the model is basically the same. We may now examine the effect of this model upon the return signal. If we transmit a signal, s(t), with corresponding spectrum, S(f), the received signal from the target model will be given by

$$s_r(t) = s(t) \otimes c(t) = \int_{-\infty}^{\infty} S(f)\, C(f)\, e^{j2\pi f t}\, df \tag{3.23}$$

where c(t) and C(f) are the impulse response and corresponding spectrum of the target model. The total received energy from the target is given by

$$W_r = \int_{-\infty}^{\infty} |s_r(t)|^2 \, dt = \int_{-\infty}^{\infty} |S(f)|^2 \, |C(f)|^2 \, df \tag{3.24}$$

The received energy, W_r, is itself a random variable that will change as we examine different sample functions of the target process. The expected value of the received energy is

$$\begin{aligned} E[W_r] &= E\Big[\int_{-\infty}^{\infty} |S(f)|^2 \, |C(f)|^2 \, df \\ &= E\Big[|C(f)|^2 \int_{-\infty}^{\infty} |S(f)|^2 \, df \end{aligned} \tag{3.25}$$

The integral portion of equation (3.25) is recognized as the transmitted signal energy, W_s, while the mean square value of C(f) was previously determined to be

$$E\left[|C(f)|^2\right] = 2\alpha^2 = \sum_{n=1}^{N} \sigma_{q_n}^2 = \sigma_c^2$$

The expected value of the total received energy, then, is given by

$$E[W_r] = \sigma_c^2 \, W_s \tag{3.26}$$

Of perhaps even greater interest is the variance of the received energy about its expected value. This is given by

$$\sigma_{W_r}^2 = E[W_r^2] - E^2[W_r] \tag{3.27}$$

We may express W_r^2 as

$$W_r^2 = \int_{-\infty}^{\infty} |S(f)|^2 |C(f)|^2 \, df \int_{-\infty}^{\infty} |S(f')|^2 |C(f')|^2 \, df'$$

$$= \int_{-\infty}^{\infty}\int_{-\infty}^{\infty} |S(f)|^2 |C(f)|^2 |S(f-\nu)|^2 |C(f-\nu)|^2 \, df \, d\nu \qquad (3.28)$$

where $f' = f - \nu$

The expected value of W_r^2 is

$$E[W_r^2] = \int_{-\infty}^{\infty}\int_{-\infty}^{\infty} E[|C(f)|^2 |C(f-\nu)|^2 |S(f)|^2 |S(f-\nu)|^2 \, df \, d\nu$$

$$= \int_{-\infty}^{\infty} E[|C(f)|^2 |C(f-\nu)|^2] \left[\int_{-\infty}^{\infty} |S(f)|^2 |S(f-\nu)|^2 \, df \right] d\nu \qquad (3.29)$$

The second integral is recognized as the autocorrelation function of the transmitted signal energy spectral density, $K_s(\nu)$. Thus,

$$E[W_r^2] = \int_{-\infty}^{\infty} E[|C(f)|^2 |C(f-\nu)|^2 \, K_s(\nu) \, d\nu \qquad (3.30)$$

The target model spectrum, C(f), was shown to be a complex gaussian variable with zero mean and uniformly distributed phase. For this type variable it can be shown in general that (see Appendix A)

$$E[|z_1|^2 |z_2|^2] = E^2[|z|^2] + E^2[z_1 z_2^*] \qquad (3.31)$$

0

Applying the above relationship to the expected value portion of equation (3.31) yields

$$E[|C(f)|^2|C(f-\nu)|^2] = E^2[|C(f)|^2] + E^2[C(f)C^*(f-\nu)]$$

where $E^2[|C(f)|^2] = \sigma_c^4$

and $E^2[C(f)C^*(f-\nu)] = R_c^2(\nu) = \sigma_c^4\left[\frac{\sin 2\pi\nu D/c}{2\pi\nu D/c}\right]^2$

We now have for the mean square

$$E[W_r^2] = \int_{-\infty}^{\infty}[\sigma_c^4 + R_c^2(\nu)]\,K_s(\nu)\,d\nu \tag{3.32}$$

The integral of $K_s(\nu)$ is equal to the square of the transmitted signal energy. Thus,

$$E[W_r^2] = \sigma_c^4 W_s^2 + \int_{-\infty}^{\infty} R_c^2(\nu)\,K_s(\nu)\,d\nu \tag{3.33}$$

The square of the mean is

$$E^2[W_r] = \sigma_c^4\,W_s^2 \tag{3.34}$$

The variance of the return energy is then given by

$$\sigma_{W_r}^2 = \int_{-\infty}^{\infty} R_c^2(\nu)\,K_s(\nu)\,d\nu \tag{3.35}$$

The variance of the total received signal energy is, thus, a function of the autocorrelation functions of the target frequency spectrum and the signal energy spectral density.

3.2 Monochromatic Illumination

True monochromatic illumination implies an infinite duration time signal and cannot, of course, provide range resolution of the target. This condition might be approached in practice by a system sensing a self-bounded target, such as an aircraft, with a single frequency pulse of spatial extent greatly exceeding that of the target. Since the monochromatic signal has infinite energy, it is necessary to use the power spectral density rather than the energy spectral density.

We shall assume a signal of the form

$$s(t) = e^{j2\pi f_0 t} \tag{3.36}$$

The spectrum of this signal is an impulse and is given by

$$S(f) = \delta(f - f_0) \tag{3.37}$$

The power spectral density is likewise an impulse located at the same frequency

$$|S(f)|^2 = \delta(f - f_0) \tag{3.38}$$

The autocorrelation function of the power spectral density, $K_S(\nu)$ is thus,

$$\begin{aligned} K_s(\nu) &= \int_{-\infty}^{\infty} |S(f)|^2 |S(f-\nu)|^2 \, d\nu \\ &= \int_{-\infty}^{\infty} \delta(f-f_0)\, \delta(f-f_0-\nu) \, d\nu \\ &= \delta(0) \end{aligned} \tag{3.39}$$

The variance of the average power returned by the monochromatic signal is given by equation (3.35) as

$$\begin{aligned} \sigma_{W_r}^2 &= \int_{-\infty}^{\infty} R_c^2(\nu)\, K_s(\nu)\, d\nu \\ &= \sigma_c^4 \int_{-\infty}^{\infty} \frac{\sin^2(2\pi\nu D/c)}{(2\pi\nu D/c)^2}\, \delta(0)\, d\nu \\ &= \sigma_c^4 \end{aligned} \tag{3.40}$$

Recall from equation (3.34) that

$$E[W_r] = \sigma_c^2\, W_s$$

where W_s is the transmitted signal energy or, in this case, the average power transmitted

$$\begin{aligned} W_s &= \int_{-\infty}^{\infty} |S(f)|^2\, df = \int_{-\infty}^{\infty} |s(t)|^2\, dt \\ &= 1 \end{aligned} \tag{3.41}$$

Thus, for the monochromatic signal the expected value of the average return power is

$$E[W_r] = \sigma_c^2 \tag{3.42}$$

while

$$\sigma_{W_r}^2 = \sigma_c^4$$

We note that the variance of the return is simply the square of the expected value. This is not surprising since the point scatterer model used is known to give rise to the Rayleigh distribution when monochromatically illuminated. The Rayleigh power or exponential distribution is characterized by equal mean and standard deviation, thus the variance of return power is equal to the square of the mean.

3.3 Broad-Spectrum Illumination

3.3.1 Rectangular Spectrum

For the case of broad-spectrum illumination we shall first consider the case of a broad-band rectangular spectrum of the form shown in Figure 3.2.

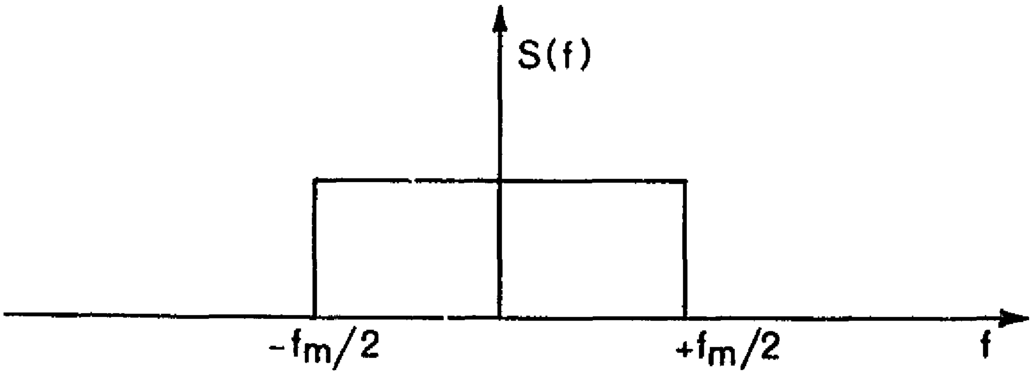

Figure 3.2 Rectangular frequency spectrum.

The total energy transmitted is normalized to the average power value obtained with monochromatic illumination. This will facilitate later comparison with the monochromatic result and that of other types of illumination. The total energy for this signal is given by

$$W_s = \int_{f_m/2}^{f_m/2} |S(f)|^2 \, df = \int_{f_m/2}^{f_m/2} A^2 \, df$$

$$= A^2 f_m \tag{3.43}$$

Normalizing the above result to one requires that

$$A = \frac{1}{\sqrt{f_m}}$$

The signal energy spectral density and its autocorrelation function are shown in Figure 3.3.

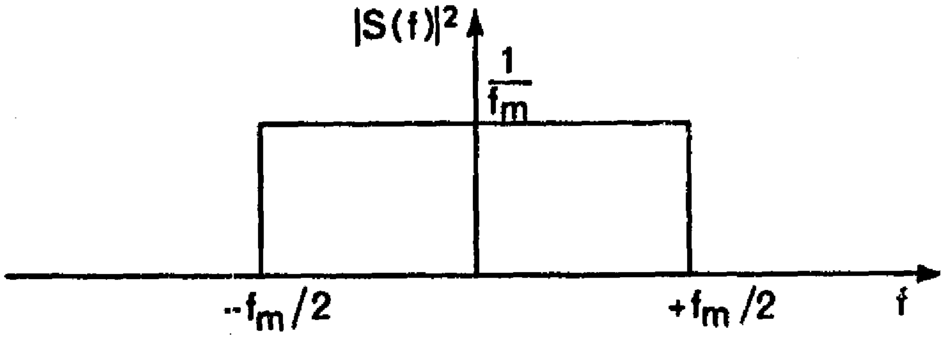

(a) Energy spectral density

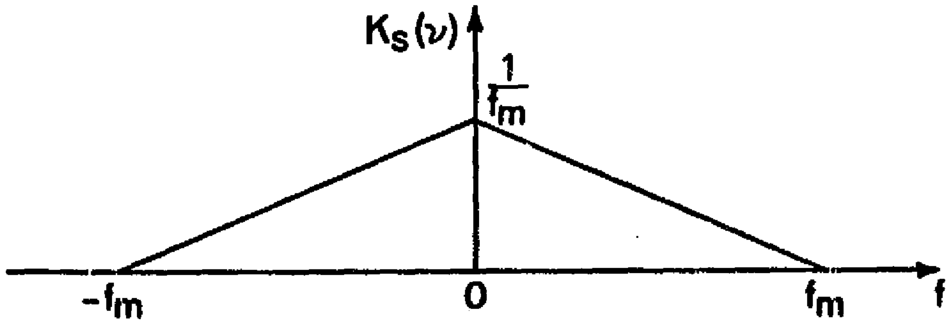

(b) Autocorrelation function of energy spectral density

Figure 3.3 Rectangular spectrum.

We have, then, for $K_s(\nu)$

$$K_s(\nu) = \int_{-\infty}^{\infty} |S(f)|^2 |S(f-\nu)|^2 \, df$$

$$= \frac{1}{f_m} \left[1 - \frac{|\nu|}{f_m} \right] \quad -f_m \leq \nu \leq f_m \tag{3.44}$$

The variance of the return energy is now given by

$$\sigma_{W_r}^2 = \int_{-f_m}^{f_m} R_c^2(\nu) \frac{1}{f_m} \left[1 - \frac{|\nu|}{f_m} \right] d\nu$$

$$= \frac{2\sigma_c^4}{f_m} \int_0^{f_m} \frac{\sin^2(2\pi\nu D/c)}{(2\pi\nu D/c)^2} \left[1 - \frac{|\nu|}{f_m} \right] d\nu \tag{3.45}$$

Making the following change of variables

$$\chi = 2\pi\nu D/c \quad \text{and} \quad R = 2 f_m D/c$$

we have

$$\sigma_{W_r}^2 = \frac{2\sigma_c^4}{\pi R} \int_0^{\pi R} \frac{\sin^2 x}{x^2} \left[1 - \frac{x}{\pi R} \right] dx \tag{3.46}$$

Not too surprisingly, the result turns out to be dependent only upon the signal bandwidth-target size product. Since the time extent of the target, 2D/c, is inversely related to the resolution bandwidth of the system we might also consider R to represent the ratio of transmitted signal bandwidth to system resolution bandwidth. This ratio will, of course, depend upon precisely how the system resolution is defined.

While the integration indicated by equation (3.46) cannot be performed directly, it is relatively simple to evaluate by means of rational approximation (see Appendix B). The results of the approximate integration are shown in Figure 3.4.

The variance of the return energy as shown in Figure 3.4 is normalized with respect to σ_c^4. This may be interpretted as a normalization with respect to the variance of the monochromatic result, or the quantity ${}_{W_r}{}^2/\sigma_c^4$ may be considered the square of the ratio of the standard deviation and mean of the return energy distribution.

$$\frac{\sigma_{W_r}^2}{\sigma_c^4} = \frac{\sigma_{W_r}^2}{E^2[W_r]} = \frac{\sigma_{W_r}^2}{\mu_{W_r}^2} = \left(\frac{\sigma_{W_r}}{\mu_{W_r}}\right)^2 \qquad (3.47)$$

It is interesting to note that the addition of signal bandwidth causes an appreciable reduction in return variance even for R equal to or less than one. For any practical system this means one should expect a return distribution with slightly less variance than the Rayleigh distribution which corresponds to the monochromatic example. For instance, the rectangular spectrum considered here will, with linear phase variation, give a $\frac{\sin x}{x}$ type time waveform. If we consider the system resolution to be defined by the separation between the first zeros of the $\frac{\sin x}{x}$ function the resolution bandwidth will correspond to $R = 1$ and the variance of the return energy will be 0.656 that of the Rayleigh distribution.

3.3 2 $\frac{\sin x}{x}$ Spectrum

The $\frac{\sin x}{x}$ spectrum is particularly interesting as its transform in the time domain is a perfectly rectangular pulse. With this pulse adjacent range resolution cells are completely independent as there is no overlapping illumination on the leading and trailing edges. We shall assume a spectrum of the form shown in Figure 3.5.

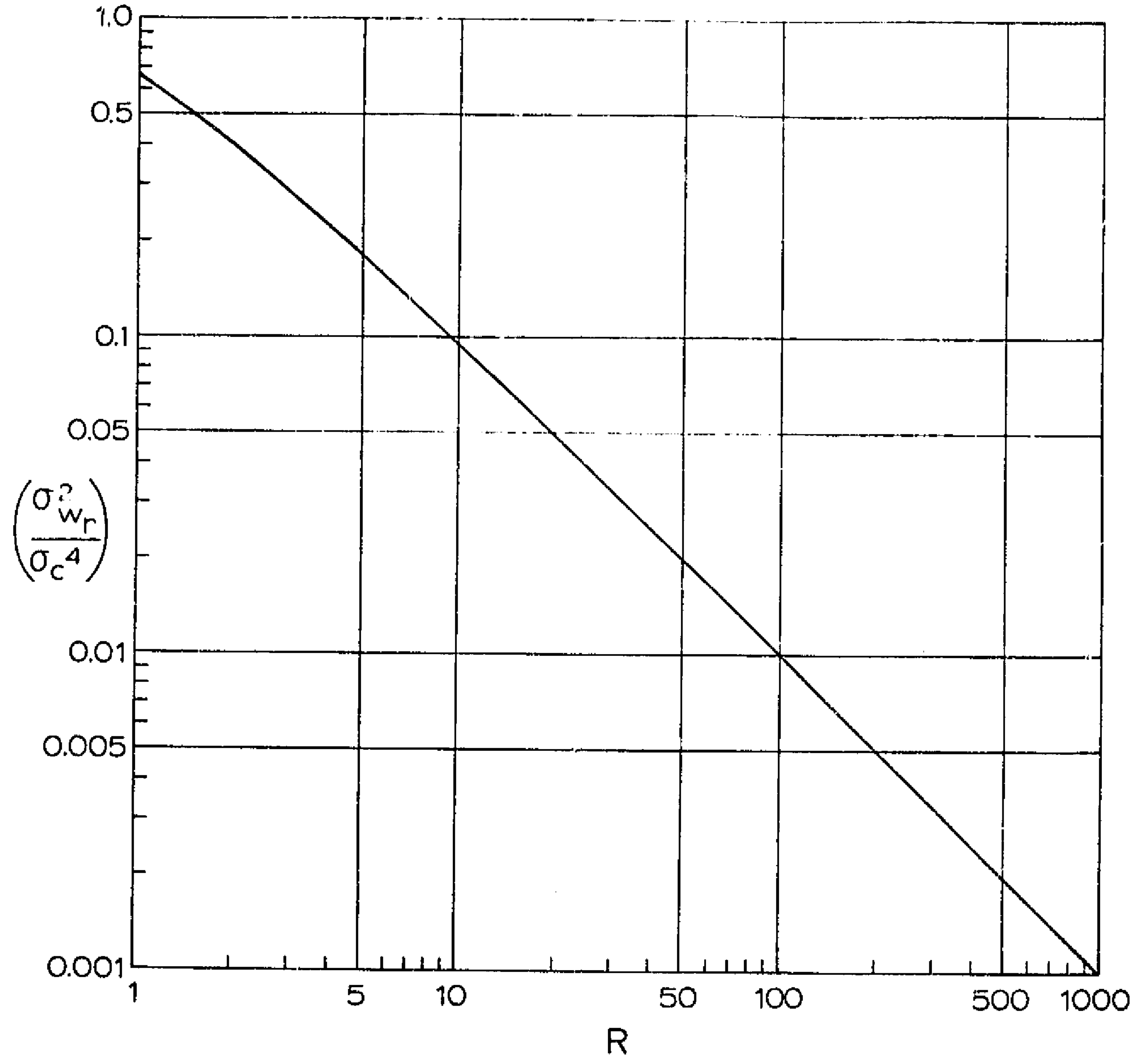

Figure 3.4 Variance reduction with rectangular spectrum panchromatic illumination.

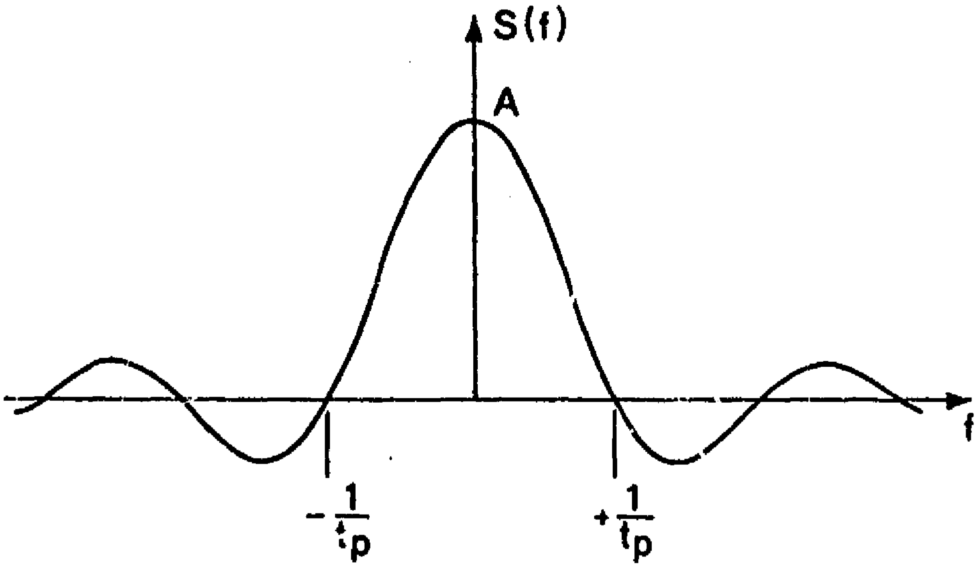

Figure 3.5 $\frac{\sin x}{x}$ frequency spectrum.

Again, the total energy transmitted is normalized to facilitate comparison with other types of illumination.

$$W_s = \int_{-\infty}^{\infty} |S(f)|^2 \, df = \int_{-\infty}^{\infty} A^2 \frac{\sin^2 \pi f t_p}{(\pi f t_p)^2} \, df$$

$$= \frac{A^2}{t_p} \tag{3.48}$$

Normalization yields a spectral amplitude of

$$A = \sqrt{t_p}$$

The autocorrelation function of the signal energy spectral density is given by

$$K_s(\nu) = \int_{-\infty}^{\infty} |S(f)|^2 |S(f-\nu)|^2 \, d\nu$$

$$= \int_{-\infty}^{\infty} |R_s(\tau)|^2 e^{-j2\pi\nu\tau} \, d\tau \tag{3.49}$$

The time domain representation is somewhat easier to work with for this type signal, thus, the second integral is used. The time domain function, its autocorrelation function, and the square of the autocorrelation function are shown in Figure 3.6.

$$K_s(\nu) = \frac{2}{t_p^2} \int_0^{t_p} [t_p^2 - 2t_p\tau + \tau^2] \cos 2\pi\nu\tau \, d\tau$$

$$= \frac{4}{t_p^2} \left[\frac{t_p}{(2\pi\nu)^2} - \frac{\sin 2\pi\nu t_p}{(2\pi\nu)^3} \right] \quad -t_p \le \nu \le t_p \tag{3.50}$$

The variance of the return energy is now given by

$$\sigma_{W_r}^2 = \frac{4}{t_p^2} \int_{-\infty}^{\infty} R_c^2(\nu) \left[\frac{t_p}{(2\pi\nu)^2} - \frac{\sin 2\pi\nu t_p}{(2\pi\nu)^3} \right] d\nu$$

$$= \frac{8\sigma_c^4}{t_p^2} \int_0^{\infty} \frac{\sin^2(2\pi\nu D/c)}{(2\pi\nu D/c)^2} \left[\frac{t_p}{(2\pi\nu)^2} - \frac{\sin 2\pi\nu t_p}{(2\pi\nu)^3} \right] d\nu \tag{3.51}$$

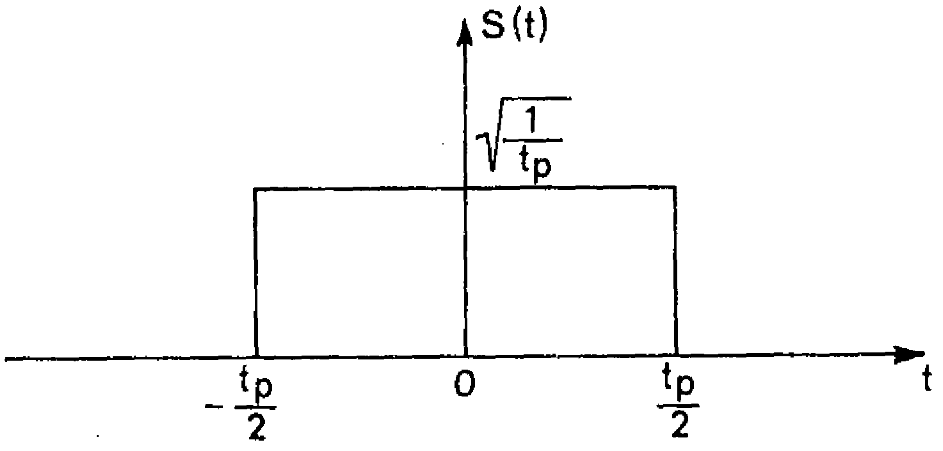

(a) Time domain function

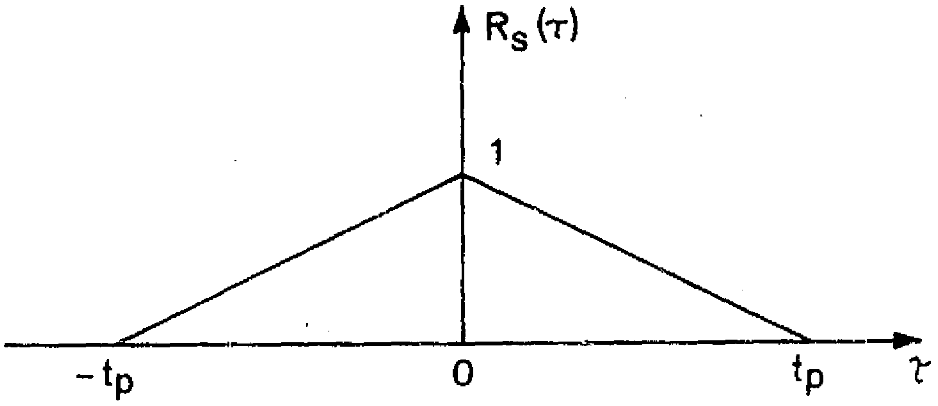

(b) Time domain autocorrelation function

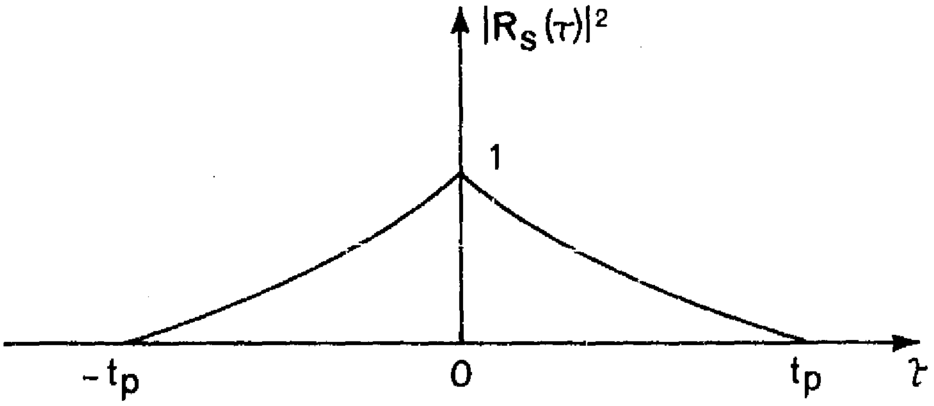

(c) Square of autocorrelation function

Figure 3.6 $\frac{\sin \chi}{\chi}$ spectrum.

Making the following change of variables

$$T_c = \frac{2D}{c} \quad \text{and} \quad x = \pi \nu T_c$$

we have

$$\sigma_{w_r}^2 = \frac{8\sigma_c^4}{\pi} \frac{t_p}{T_c} \int_0^\infty \frac{\sin^2 x}{x^2} \left[\frac{\left(2x \frac{t_p}{T_c}\right) - \sin\left(2x \frac{t_p}{T_c}\right)}{\left(2x \frac{t_p}{T_c}\right)^3} \right] dx \qquad (3.52)$$

Let $K = \frac{t_c}{t_p}$, then

$$\sigma_{w_r}^2 = \frac{8\sigma_c^4}{\pi K} \int_0^\infty \frac{\sin^2 x}{x^2} \left[\frac{\left(\frac{2x}{K}\right) - \sin\left(\frac{2x}{K}\right)}{\left(\frac{2x}{K}\right)^3} \right] dx \qquad (3.53)$$

The similarity between the above result and that obtained previously for the rectangular spectrum is obvious. Again the parameter, K, is subject to various interpretations. It may as before be considered a signal bandwidth-target size product, a ratio of signal bandwidth and resolution bandwidth or a ratio of target time extent and system time resolution. The precise nature of the parameter, K, will again depend upon how the resolution bandwidth is defined.

The integral in equation (3.53) is likewise intractable, however, a series expansion of the $\sin(\frac{2x}{K})$ term results in a form easily integrated by computer. The results of the approximate integration are shown in Figure 3.7.

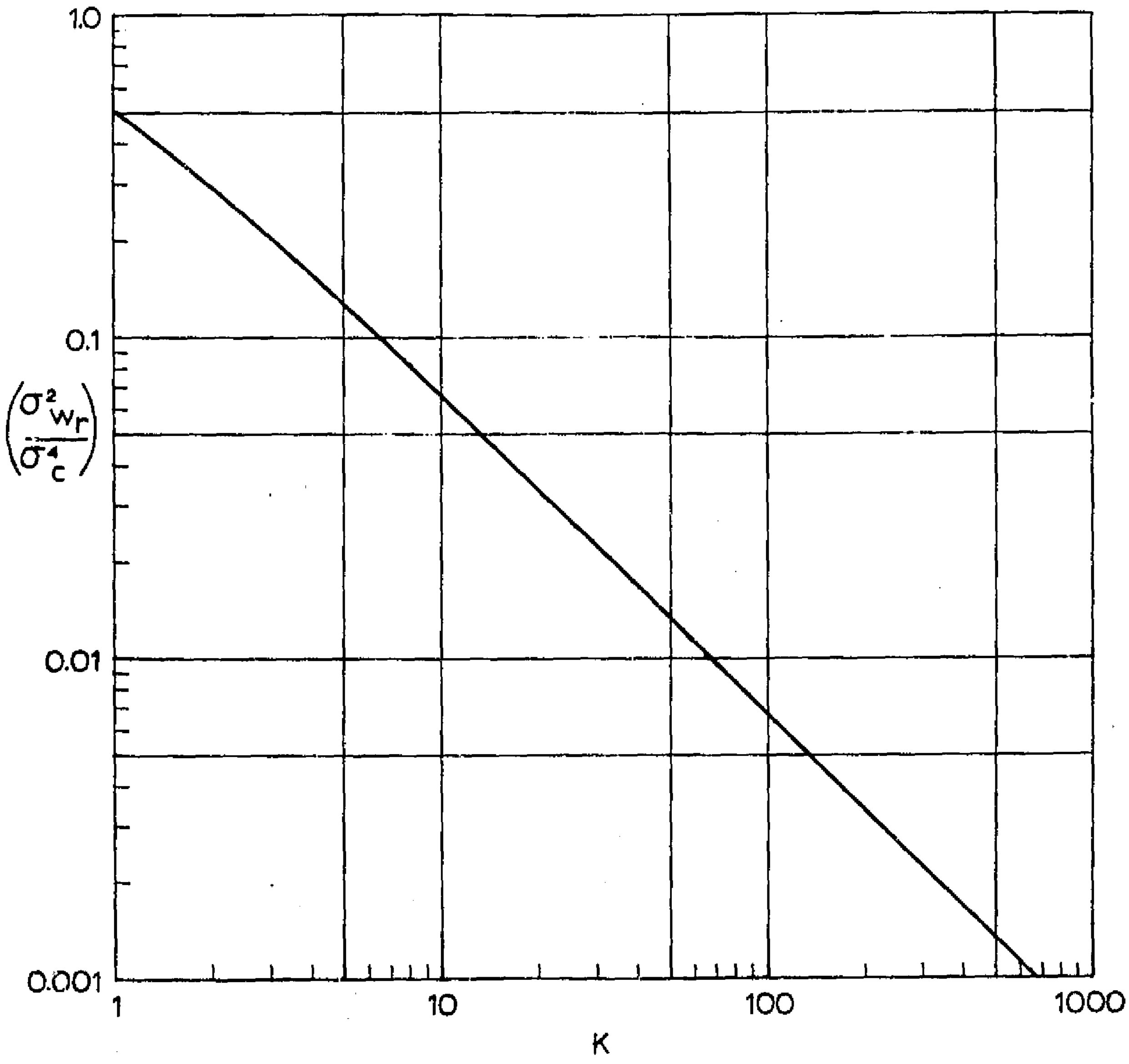

Figure 3.7 Variance reduction with $\frac{\sin x}{x}$ spectrum panchromatic illumination.

3.4 Postdetection Averaging of Independent Resolution Cells

Figures 3.4 and 3.7 illustrate the decrease in variance of the energy distribution obtainable with panchromatic illumination (excess range bandwidth). Let us compare this with the improvement that may be obtained with a system that processes bandwidth for maximum resolution and then subsequently averages the return from different resolution cells.

We shall assume that the return distribution for a maximum resolution system is the same as that obtained with monochromatic illumination (Rayleigh distributed). As shown previously, the return energy distribution with monochromatic is given by

$$p(w) = \frac{1}{2\sigma_c^2} e^{-w/2\sigma_c^2} \tag{3.54}$$

The above distribution is recognized as the Rayleigh power or exponential distribution and also as a Chi-square distribution with two degrees of freedom, for

$$p(\chi^2) = \frac{1}{(2\sigma_c^2)^{n/2}(n/2-1)!} (\chi^2)^{(n/2-1)} e^{-\chi^2/2\sigma_c^2} \tag{3.55}$$

where n is the number of degrees of freedom. The mean value and variance of the Chi-square distribution are given by

$$\text{mean} = n\sigma_c^2 \qquad \text{variance} = 2n\sigma_c^4$$

The return from each resolution cell of an assumed homogeneous target will be characterized by the above distribution. Averaging of these returns involves the addition of random variables each distributed with a Chi-square distribution with two degrees of freedom. If we assume each distribution to come from a totally disjoint segment of the target area the distributions will be statistically independent. The additive property of the Chi-square distribution says that the sum of independent Chi-square distributions will yield a Chi-square distribution with the number of degrees of freedom equal to the sum of the degrees of freedom of the individual distributions.

From the above we may calculate the reduction in normalized variance as more resolution cells are averaged, by

$$\left(\frac{\sigma}{\mu}\right)^2 = \frac{2n\,\sigma_c^4}{n^2\,\sigma_c^4} = \frac{2}{n} \qquad (3.56)$$

Since each independent sample of the return distribution has two degrees of freedom, the number of independent samples averaged is one-half the number of degrees of freedom. Figure 3.8 shows the linear curve of normalized variance as a function of degrees of freedom and independent samples.

3.5 Comparison of Averaging Methods

Figure 3.9 shows the variance reduction obtainable with the methods investigated. Again, note that each result is normalized to that obtained with monochromatic illumination and that the total energies transmitted are equal.

At first sight it appears that the panchromatic illumination methods actually produce a slightly better result than that produced by postdetection averaging of independent resolution cells. However, this appearance is due to a number of simplifying assumptions made during the course of the development.

First, consider the difference between the rectangular spectrum and postdetection averaging curves. As pointed out earlier with regard

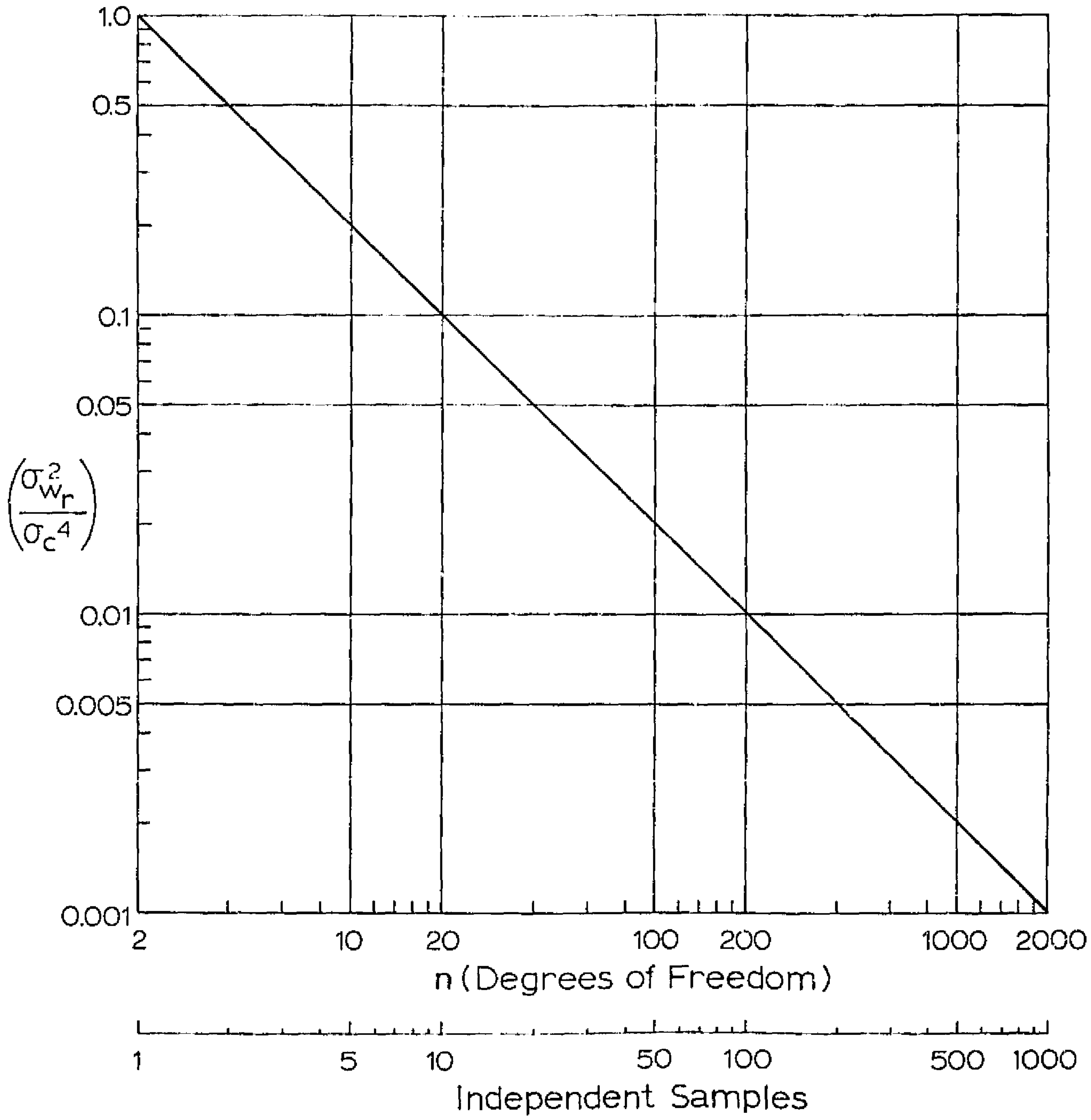

Figure 3.8 Variance reduction through postdetection averaging of independent resolution cells.

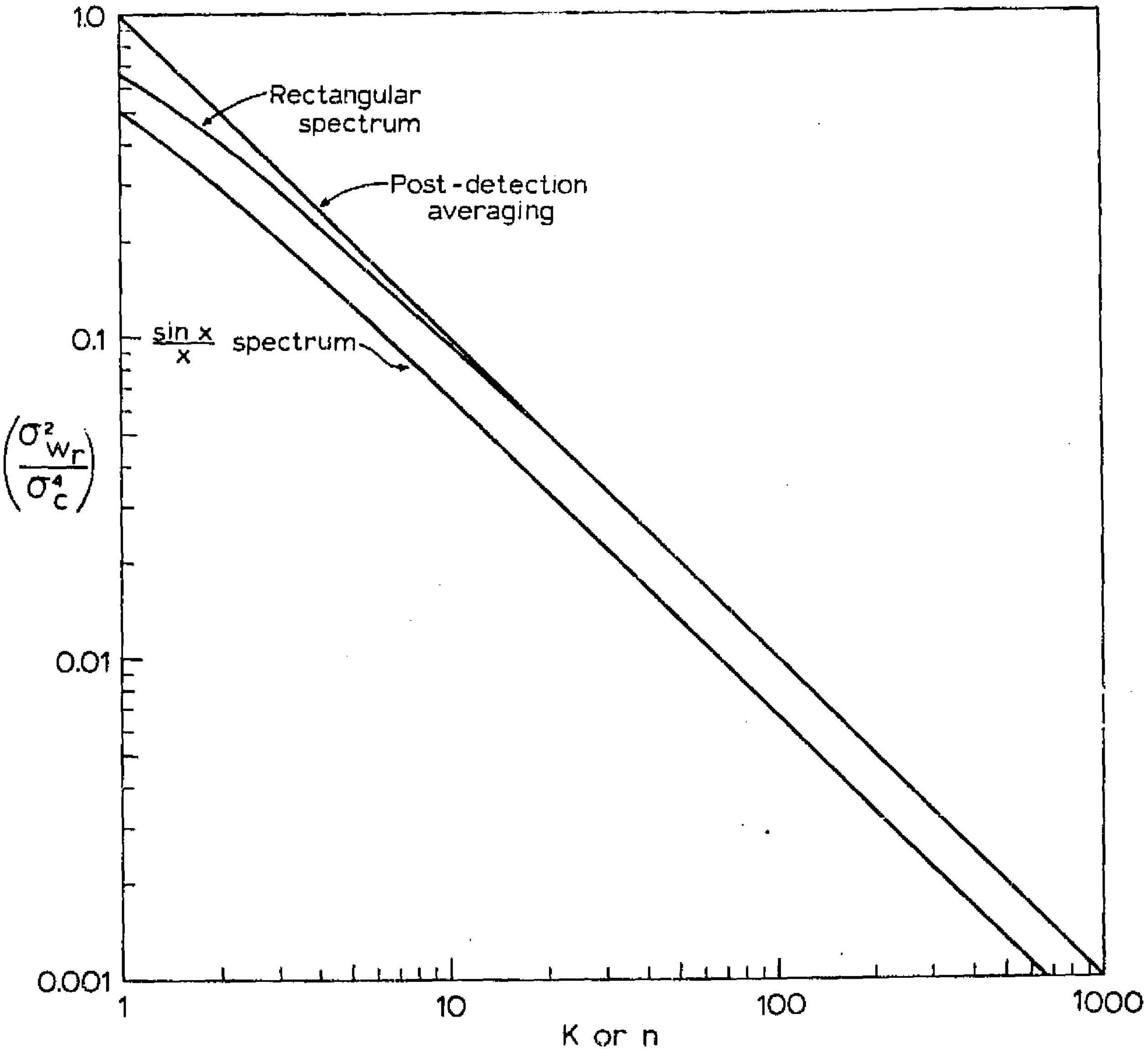

Figure 3.9 Comparison of averaging methods.

to the rectangular spectrum, the addition of sufficient bandwidth to merely resolve a resolution cell significantly reduces the normalized variance and causes a departure from the Rayleigh result obtained with monochromatic illumination. For instance, assuming the resolution bandwidth to be given by the reciprocal of the target time extent, $2D/c$, the bandwidth-target size parameter, R, must equal one in order to resolve the target. This, in turn, says that the return from each resolution cell is characterized by a distribution with less variance than that of the Rayleigh distribution. Thus, the postdetection averaging estimate is actually somewhat higher than the result one would expect from an actual system.

On the other hand, the rectangular spectrum is known to yield a $\frac{\sin x}{x}$ time signal of infinite duration. Thus, consideration of statistically independent resolution cells actually involves an approximation as to how much overlapping illumination may be permitted while still assuming essentially zero correlation between cells.

While these points are minor, they do account for the discrepancies between the two curves. In addition, one is led to the conclusion that the curve for the rectangular spectrum is probably the better approximation to a physically realizable system. If this is the case, we may expect the result of averaging over a relatively narrow panchromatic band or averaging a small number of resolution cells to produce slightly less variance than that normally predicted by consideration of independent sample averages.

Let us now consider the differences noted in the curve for the $\frac{\sin x}{x}$ spectrum. This spectrum yields a perfectly rectangular time signal and, thus there is no problem in considering disjoint independent resolution cells. However, this spectrum has the rather undesirable characteristic of requiring an infinite system bandwidth.

In comparing the rectangular and $\frac{\sin x}{x}$ results we are again faced with the problem of defining resolution. If we define resolution in the time domain, this presents no problem for the $\frac{\sin x}{x}$ spectrum gives a rectangular pulse. The rectangular spectrum, however, produces a $\frac{\sin t}{t}$ pulse in the time domain and some approximation must be made regarding what constitutes resolution. If we consider the resolution to be defined by the region between the first zeros of the $\frac{\sin t}{t}$ function, the resolution bandwidth is given by $1/2\ t_r$. For the same time domain resolution, however, the central lobe of the $\frac{\sin x}{x}$ spectrum will have twice this width or $1/t_r$. Conversely, if we match central lobe and rectangle in the frequency domain we obtain a two-to-one difference in the time domain.

Applying this two-to-one difference to the result for the $\frac{\sin x}{x}$ spectrum we have the result shown in Figure 3.10. Of course, defining resolution or bandwidth as extending to the first zeros of the $\frac{\sin x}{x}$ function is arbitrary and the difference will be correspondingly less if the 3 db points are selected for this definition.

For a practical system confined to finite time and bandwidth, the actual results will lie somewhere between the curves shown in Figure 3.10. We note that each of the curves of Figure 3.10 approach a straight line with the same slope. Considering the resolution bandwidth to be

$$f_r = \frac{c}{2D}$$

and, likewise to be the bandwidth necessary to achieve independent samples, we may calculate the frequency separation between independent samples as

$$\Delta f = f_r = \frac{150}{D}\ \mathrm{MHz} \tag{3.57}$$

This is a familiar result and merely states again the equivalence between what is considered an independent sample and the bandwidth required to resolve the sample. Again, this result is dependent upon the definition used for resolution.

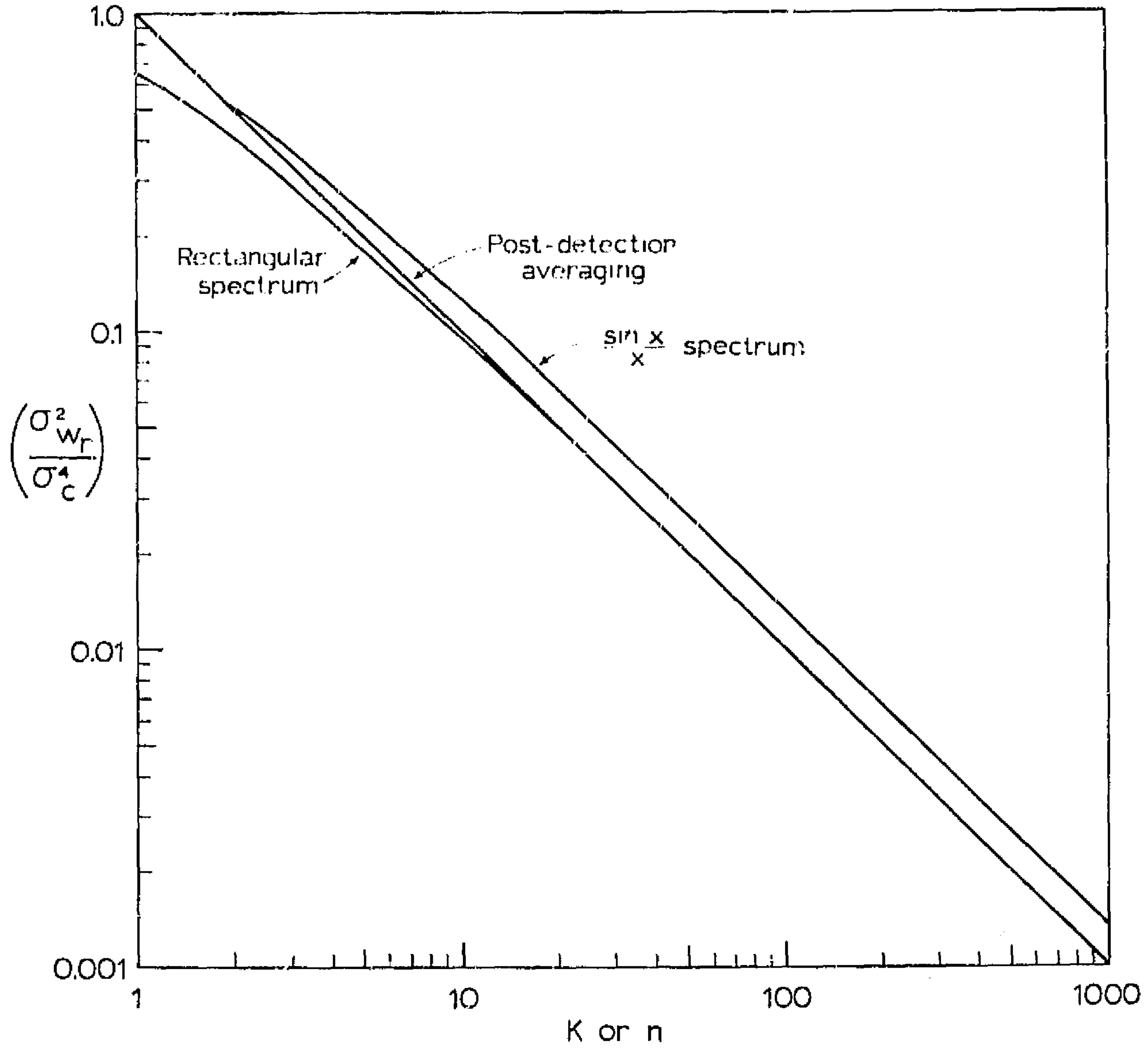

Figure 3.10 Comparison of averaging methods.

From the preceding development we may conclude that the means of frequency averaging is immaterial so long as energy is conserved. With this conclusion the question arises as to what advantage is gained by using panchromatic illumination. The answer to this lies in the actual means of system implementation. While the result is essentially the same for a maximum resolution system with post-detection averaging and a panchromatic system, the point at which the averaging is performed may be significantly different.

To realize any advantage from the panchromatic technique the averaging operation must be performed prior to the final video output or recording. This may yield a substantial savings in the bandwidth necessary in the main receiver amplification stage and for imaging systems in the bandwidth of the recording system. Since the recording bandwidth of high resolution systems is one of the prime constraints this offers the possibilities of a significant savings.

CHAPTER 4

EXPERIMENTAL INSTRUMENTATION

The system used to produce the measurement data for this study was designed and built as a portion of the research program. The design of the measurement system was considerably influenced by the desire to produce a flexible instrument capable of a wide variety of broad-spectrum measurements rather than one restricted to the limited goals of this specific program. The choice of subassemblies for the system was determined as much by this desire for flexibility as by the normal constraint of cost.

To fully investigate the capabilities of broad-spectrum illumination or "polypanchromatic" radar requires an illuminating source capable of extreme broad-bandwidth transmission. This is not in principle a difficult task since sub-nanosecond pulse-width radars have been built and operated by numerous investigators (Micronotes, 1967). Techniques for pulse compression to increase bandwidth are likewise common in today's operational systems. If the spectrum of the scattered broad-bandwidth return is to be processed for spectral information content it is also necessary that the system have multiple receiving channels, each responsive to a different bandwidth of the illuminating spectrum.

The above requirements for broad-bandwidth and multiple receiving channels, while within the state-of-the-art, were well outside the budget for this program. It was possible, however, through the use of a so-called "slow-sweep" mode of operation to build a flexible system for investigation of a wide range of illuminating conditions.

In line with the desire for maximum flexibility the entire system is mobile including its own source of power furnished by a diesel motor-generator set. The antenna is mounted on a 40-foot hydraulically operated boom and may be positioned for any incidence angle or azimuth setting by a remote controlled antenna positioner. The complete system is shown in Illustration 4.1.

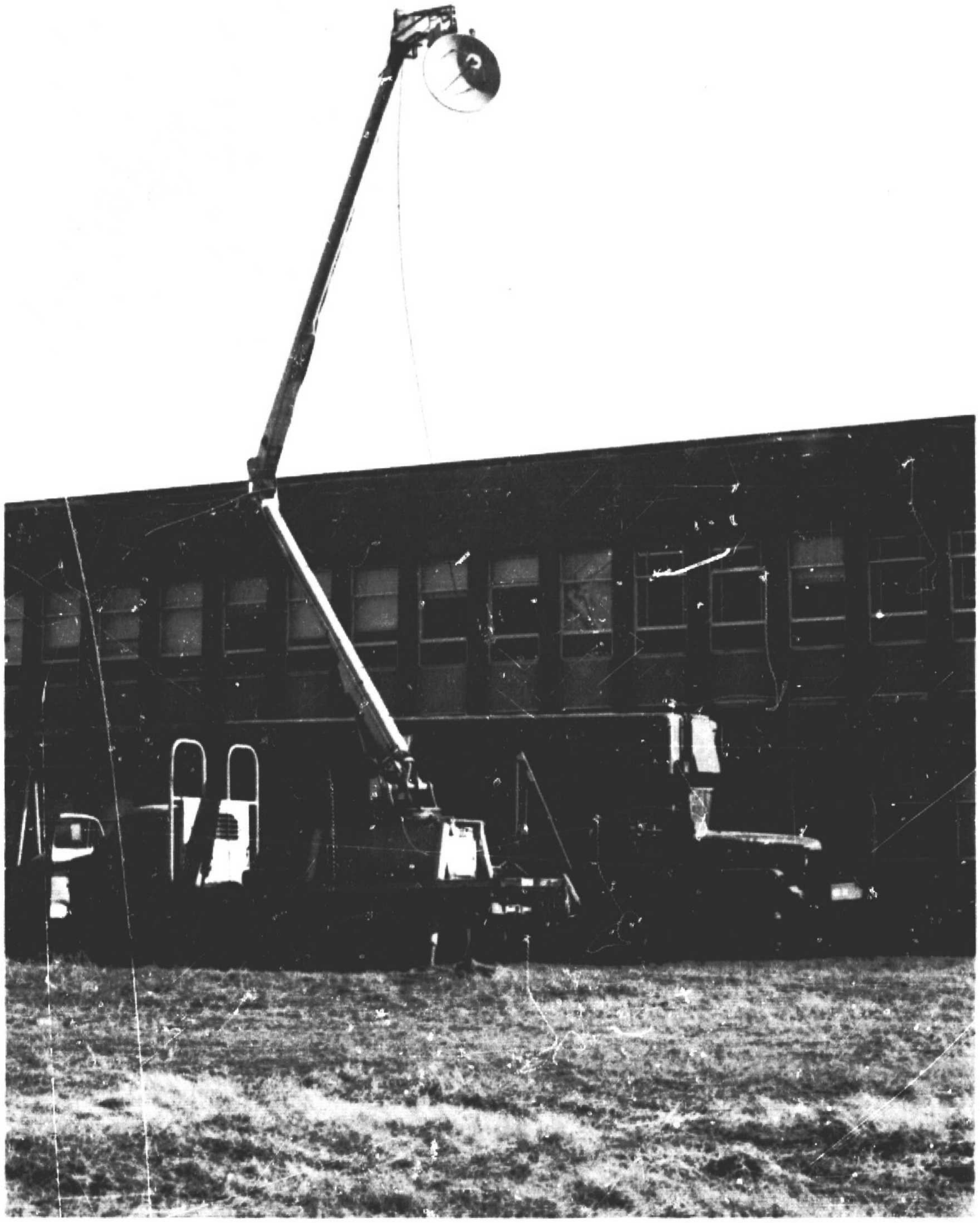

Illustration 4.1 Broad-bandwidth radar measurement system.

4.1 System Function

In the "slow-sweep" mode of operation the transmitter frequency is continuously swept across the full operational bandwidth at a relatively slow rate. This continuously swept signal is pulse modulated at a pulse repetition rate much faster than the sweep rate, thus the transmitter output is a succession of pulses each at a slightly different carrier frequency. By suitable choice of the relative repetition rates and the pulse width, the spectra of the pulses are overlapped giving an almost uniform output spectrum over the sweep range. This technique is illustrated in Figure 4.1.

The average amplitude of the return pulses is, in essence, a sampled data record of the target spectral response across the swept band. The sampling window spectral width is that of the individual amplitude modulated pulse. Postdetection averaging of successive pulses enables one to increase the effective bandwidth by small increments up to the full sweep width. The fine control of effective bandwidth permitted by such averaging in frequency permits investigation of the effect of bandwidth or panchromatic illumination upon the fading return of complex targets.

The need for multiple receiving channels to investigate possible spectral signature identification is met by recording B-scan images of area extensive targets for several panchromatic bands. The resultant images are then optically or electronically combined to produce false color "polypanchromatic" images (Dalke, 1969).

4.2 System Description

The block diagram of the measurement system is shown in Figure 4.2. The system is composed of six main sections: 1) transmitter, 2) receiver, 3) local oscillator, 4) digital controller, 5) scattering coefficient data processor, and 6) imaging data processor.

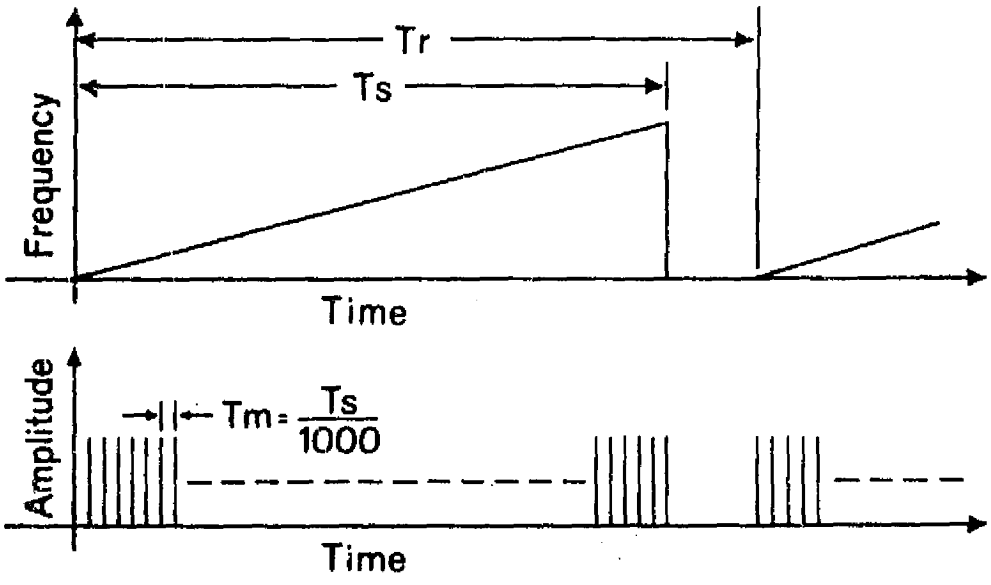

(a) Sweep modulation.

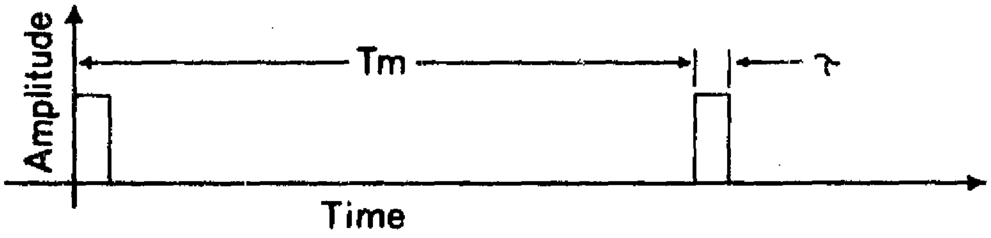

(b) Pulse modulation.

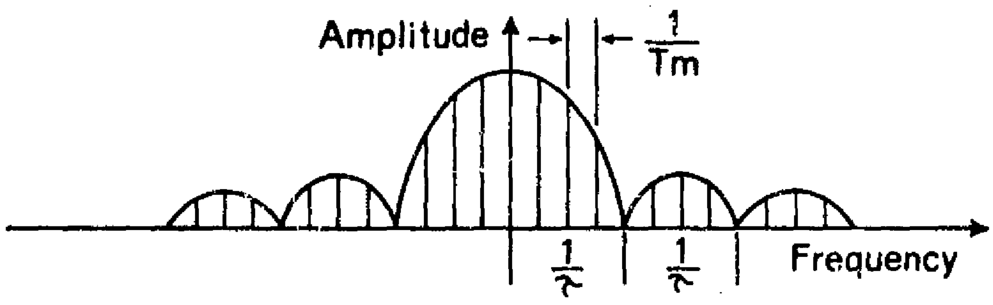

(c) Spectrum of single pulse.

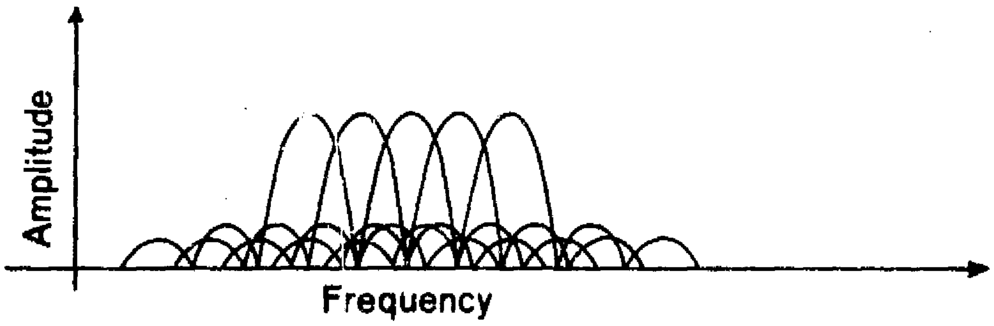

(d) Overlapping spectra due to slow change of carrier frequency.

Figure 4.1 Slow-sweep method of obtaining broad-bandwidth.

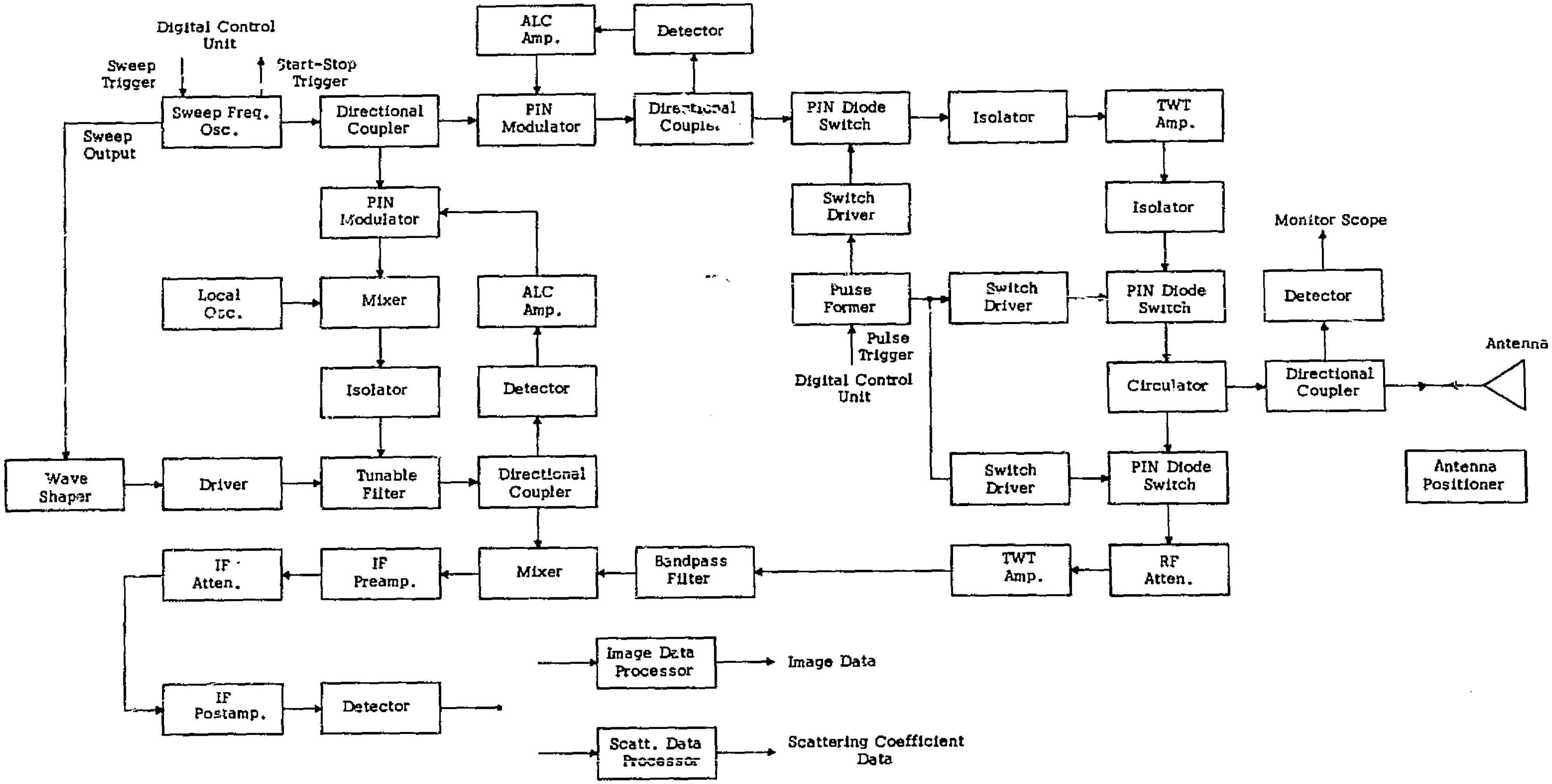

Figure 4.2 System block diagram.

4.2.1 Transmitter Section

The transmitter section consists of a general-purpose sweep frequency oscillator, signal splitter, PIN diode leveling loop, microwave modulation switch, power amplifier, microwave noise blocking switch, duplexer, and antenna.

4.2.1.1 Sweep Frequency Oscillator

This oscillator is a commercial Hewlett-Packard Model 8690A sweep oscillator with a Model 8693B plug-in module that covers the range of 4-8 GHz. The sweep output may be externally triggered to sweep between two variable frequency settings within the 4-8 GHz range. External trigger outputs are available synchronous with the start and stop of the linear frequency sweep as well as a blanking pulse coincident with the generator retrace and stabilization interval. Sweep time is continuously variable between 0.01 and 100 seconds, and the minimum power output across the full range is 15 milliwatts when leveled. The PIN diode leveling components originally mounted in this unit were removed for external use after division of the output signal. A sweep reference ramp voltage is available from the unit and is used to drive a swept frequency filter in the local oscillator section.

In normal operation the sweep is externally triggered by the digital control unit to sweep from 4-8 GHz with a sweep time of 0.01 seconds. The blanking pulse output is used in the digital control unit to suppress spurious trigger signals during the retrace and stabilization interval.

4.2.1.2 Signal Splitter

The output from the sweep oscillator is divided to both drive the transmitter power amplifier and to provide a local oscillator reference signal. This division is accomplished with a -10 db parallel line directional coupler, Narda Model 3004-10. The -10 db output is used for the transmitter drive while the straight through output is used for the local oscillator reference signal.

4.2.1.3 PIN Diode Leveling Loop

The transmitter line power is leveled using the PIN modulator and automatic level control amplifier originally used to internally level the sweep oscillator. The leveling signal is obtained by sampling the transmitter line with a Narda maximally-flat -20 db coupler, Model 3044B-20, and a Hewlett-Packard Model 423A detector. This arrangement reduces the transmitter line power variation at the sampling point to within ± 0.4 db across the full 4-8 GHz band.

4.2.1.4 Microwave Modulation Switch

The swept frequency transmitter signal is pulse modulated by means of a Hewlett-Packard Model 3570 microwave switch. This unit uses two PIN diodes in a grounded cathode configuration and provides a 1.5 db maximum insertion loss and a 38 db minimum isolation across the 4-8 GHz band. In the actual system two of these units are used in series with parallel switching to give sufficient isolation in the off condition. The switching speed of the series combination is approximately 12 nanoseconds off-to-on and 8 nanoseconds on-to-off. With these speeds it is possible to operate the system with a pulse width of as low as 20 nanoseconds with no appreciable loss of peak power output.

The relatively fast switching speeds used in the system make adjustment of relative switching time rather critical since the variation in propagation time and switch delay is significant in comparison to rise time and pulse width. In order to precisely adjust switching times a switch drive circuit was designed to permit independent delay of the leading and trailing edges of the driving pulse. The circuit diagram of the switch driver is shown in Figure 4.3.

4.2.1.5

While the peak power required to meet the system design goal of 20 watts is quite modest, the need for 4-8 GHz operation virtually dictates the use of a travelling wave tube (TWT) power amplifier. A grid-modulated TWT would seem to be called for, howevever, the need for

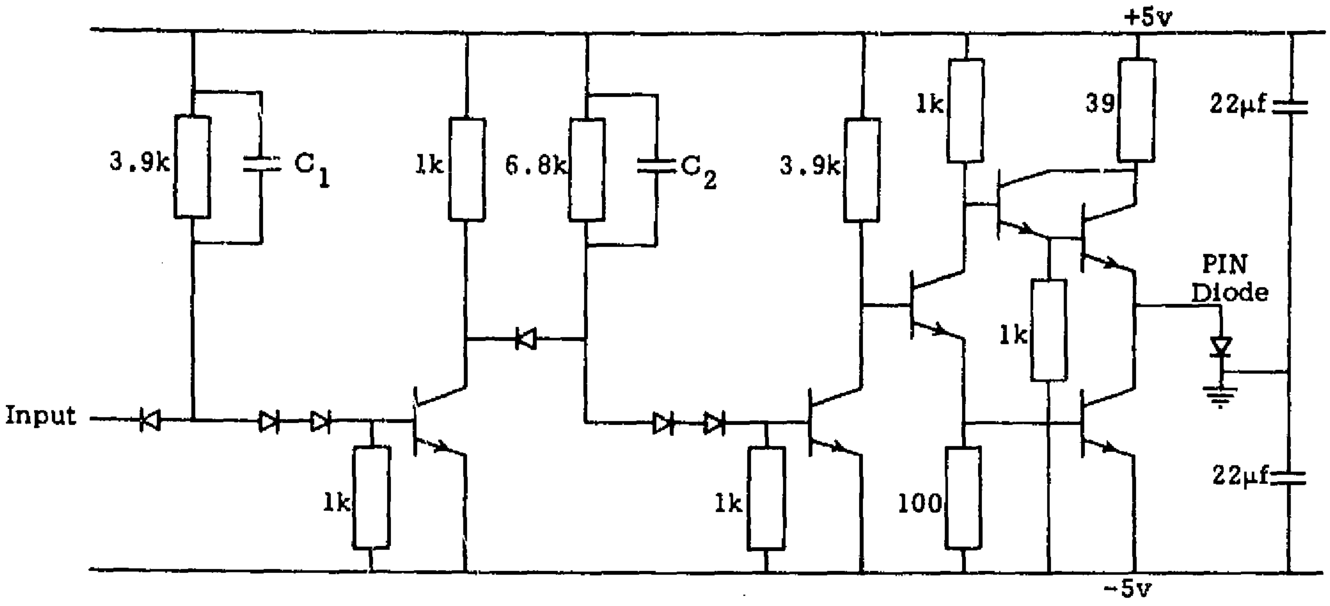

All resistances in ohms
Diodes: 1N4009 Transistors: NPN 2N4420
C_1 and C_2 selected for required delay
Input: -5 volts: switch OFF to RF
0 volts: switch ON to RF

Figure 4.3 Driver circuit for grounded cathode microwave PIN diode switch.

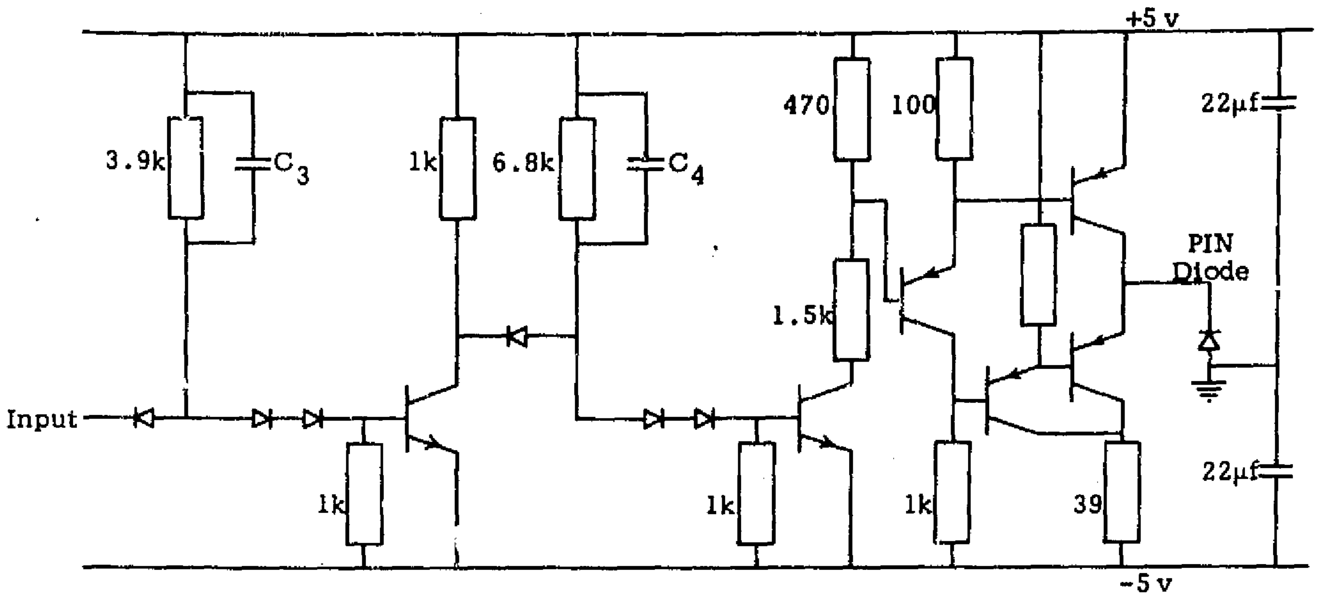

All resistances in ohms
Diodes: 1N4009 Transistors: NPN 2N4420; PNP 2N4423
C_3 and C_4 selected for required delay
Input: -5 volts: switch ON to RF
0 volts: switch OFF to RF

Figure 4.4 Driver circuit for grounded anode microwave PIN diode switch.

extremely fast rise time and relatively low cost led to specification of a standard commercial unit with 20 watt CW capability. The CW operation required that external modulation be provided and further necessitated an extremely high duplexer isolation to keep the TWT amplifier noise from the receiver input during reception. The amplifier used is an Alto Scientific Company Model 20C 4.0-8.0 Q60. This unit has a 20 watt CW rating with a 60 db small signal gain and a maximum noise figure of 35 db.

The TWT amplifier is operated with PIN diode switches at both the input and output. In order to reduce the VSWR and prevent possible damage to the amplifier, load isolators are used at both the input and output of the TWT. These units are Melabs Model H-317-264-T internally terminated ferrite circulators with a maximum insertion loss of 0.4 db and a minimum isolation of 18 db across the 4-8 GHz band.

4.2.1.6 Microwave Noise Blocking Switch

The CW operation of the relatively noisy TWT power amplifier makes it necessary to provide an exceptionally high transmitter-to-receiver isolation. This problem is further complicated by the wide bandwidth operation which prohibits the use of sharply tuned passive devices. In this system the required isolation is obtained with a Hewlett-Packard Model C0043 3603A microwave switch following the TWT power amplifier. This unit uses two PIN diodes in a common anode configuration and provides a 1.5 db maximum insertion loss and a 60 db minimum isolation across the 4-8 GHz band.

The switch drive circuit used with the noise blocking switch is shown in Figure 4.4. Note that the circuit is basically the same as that of Figure 4.3, however the common anode configuration of this switch requires the use of PNP transistors in the output stage.

4.2.1.7 Duplexer

The duplexing or coupling of both transmitter and receiver to a common antenna is accomplished with a 3-part ferrite circulator. The circulator used is a Melabs Model H-317-264 which has a maximum insertion loss of 0.4 db and a minimum isolation of 18 db across the 4-8 GHz band.

The relatively short minimum range (40 feet) of the system requires that the IF amplifier in the receiver not saturate during transmission since the recovery time is well beyond the minimum range. This obviously requires a much higher isolation during transmission than that provided by the ferrite circulator. As described previously, the high noise output of the CW TWT requires a high isolation during reception. The requirements for greater isolation than can be obtained with broad-band passive devices are met by switching both the transmitter and receiver lines.

The complete modulation and duplexing arrangement including isolation switches are shown in Figure 4.5. The timing sequence is likewise shown in Figure 4.5. During transmission the combined isolation of the ferrite circulator and the receiver blanking switch is 94 db minimum. During reception the combined isolation of the ferrite circulator and the noise blocking switch is 78 db minimum. The need for relatively fast rise and fall times of the microwave switches and precise adjustment of the driving waveforms can be seen from the timing sequence.

4.2.1.8 Antenna

The antennas used are relatively standard 3-foot or 6-foot parabolic reflectors with broad-band (3.95 - 8.2 GHz), dual polarization ridged waveguide feeds. The units are Scientific Atlanta Models 22-6/A and 22-3/A reflectors with Model 28-3.9/6 and 28-3.9/3 feeds. E-plane patterns at the band extremes are shown for both antennas in Figures 4.6 and 4.7.

The antenna is positioned for scattering measurements and scanned for imaging by means of a standard antenna positioner, Scientific-Atlanta Model 5403-1. The positioner control, Scientific-Atlanta Model 4112, and indicator assembly, Scientific-Atlanta Model 4422-(3)(3), permit a readout precision of ±0.03° in both azimuth and elevation.

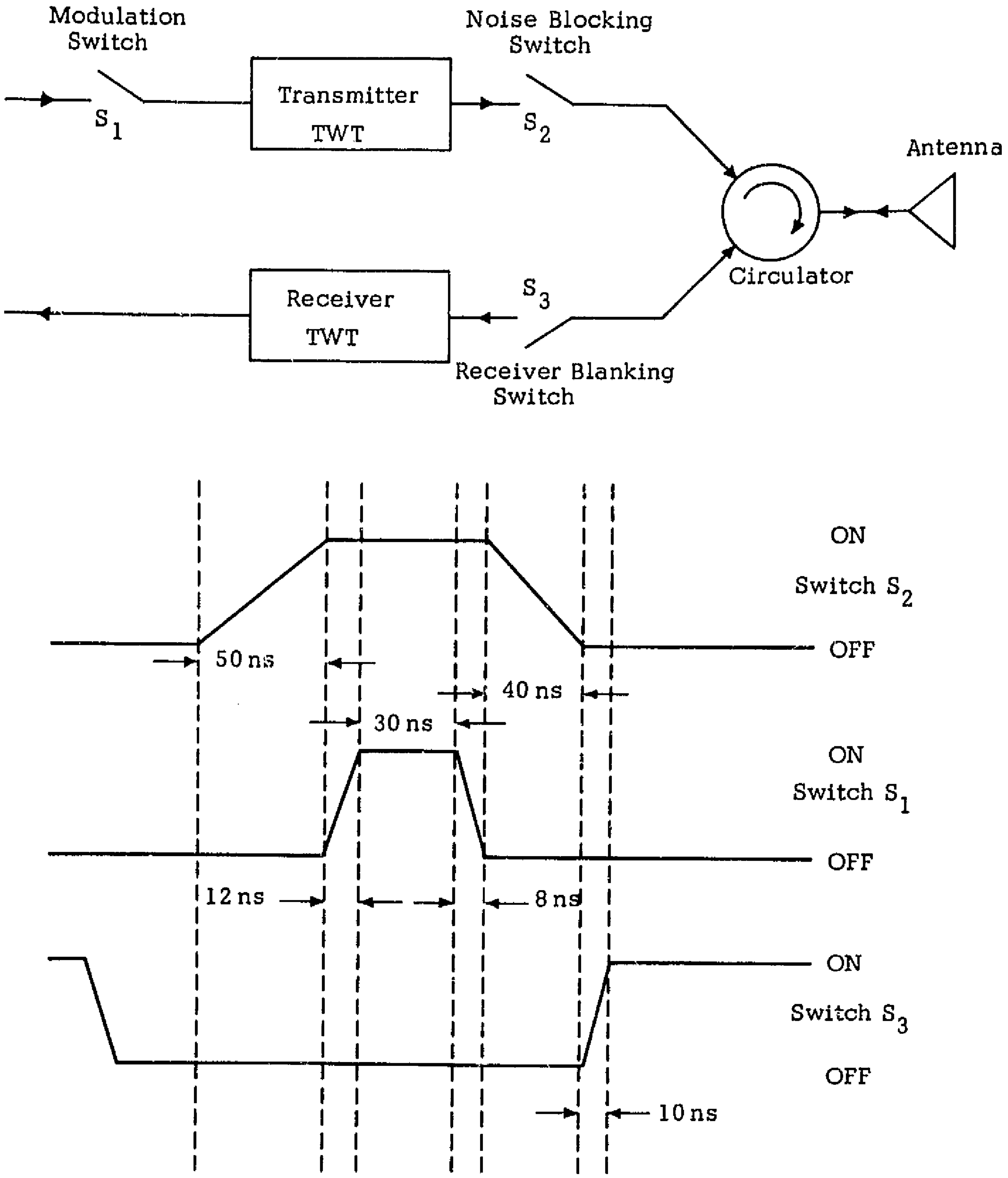

Figure 4.5. Duplexing arrangement and timing sequence.

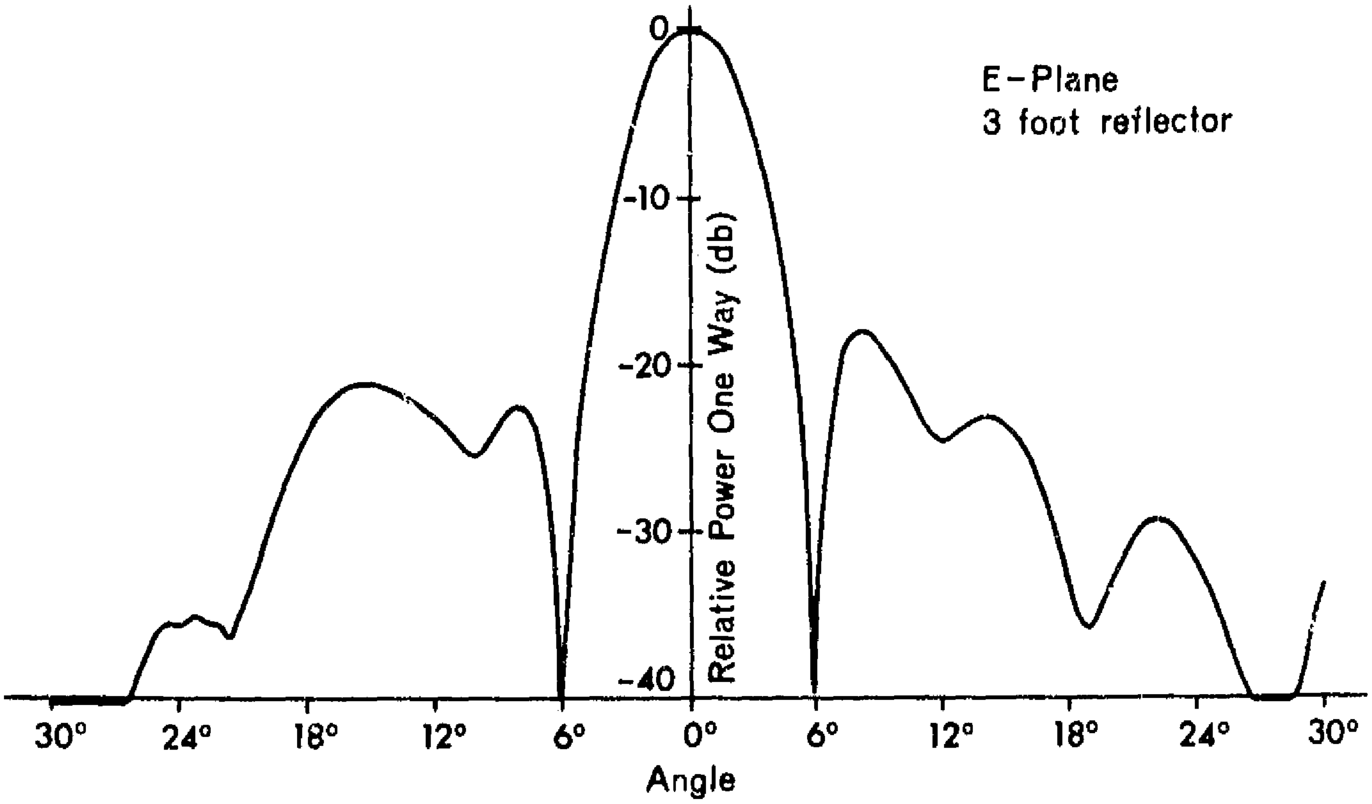

(a) Frequency 4 GHz.

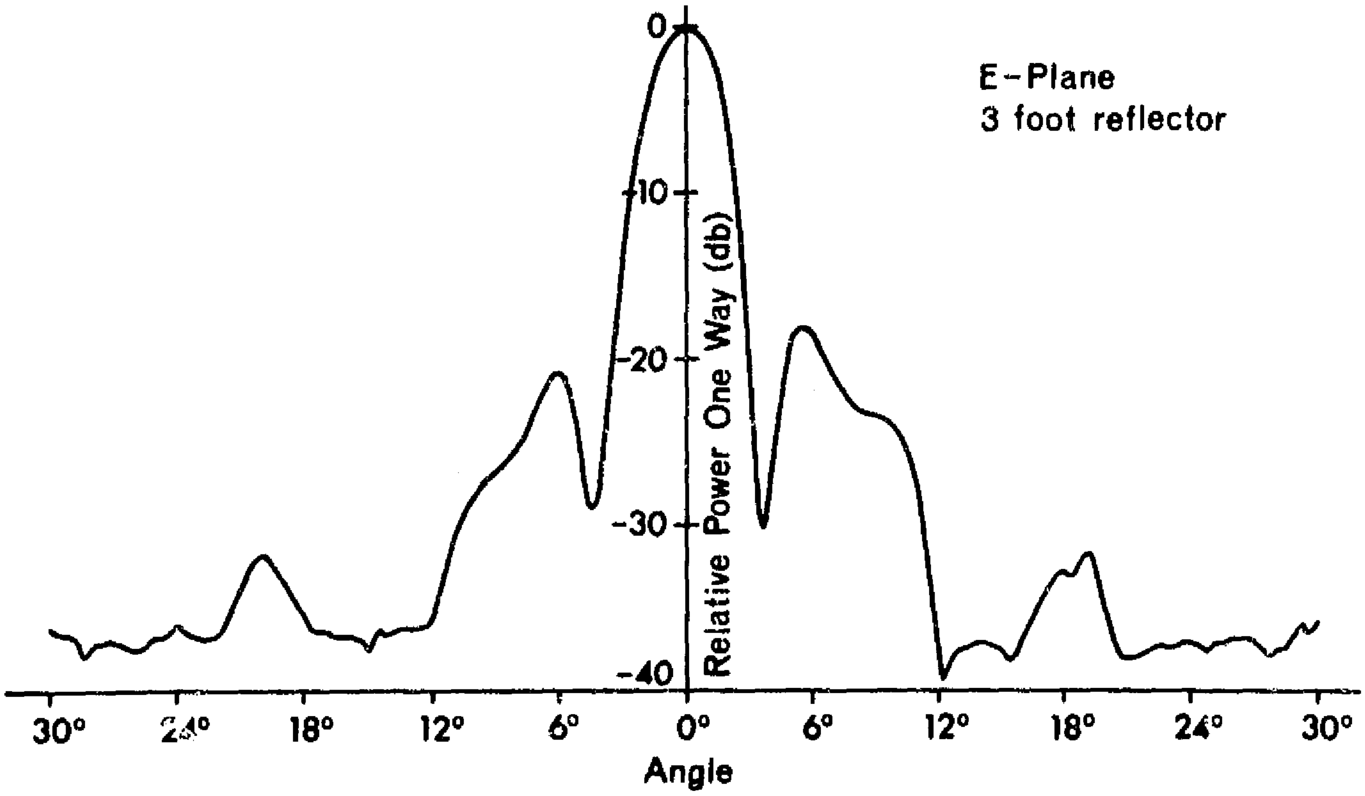

(b) Frequency 8 GHz

Figure 4.6. E-plane patterns for 3-foot reflector.

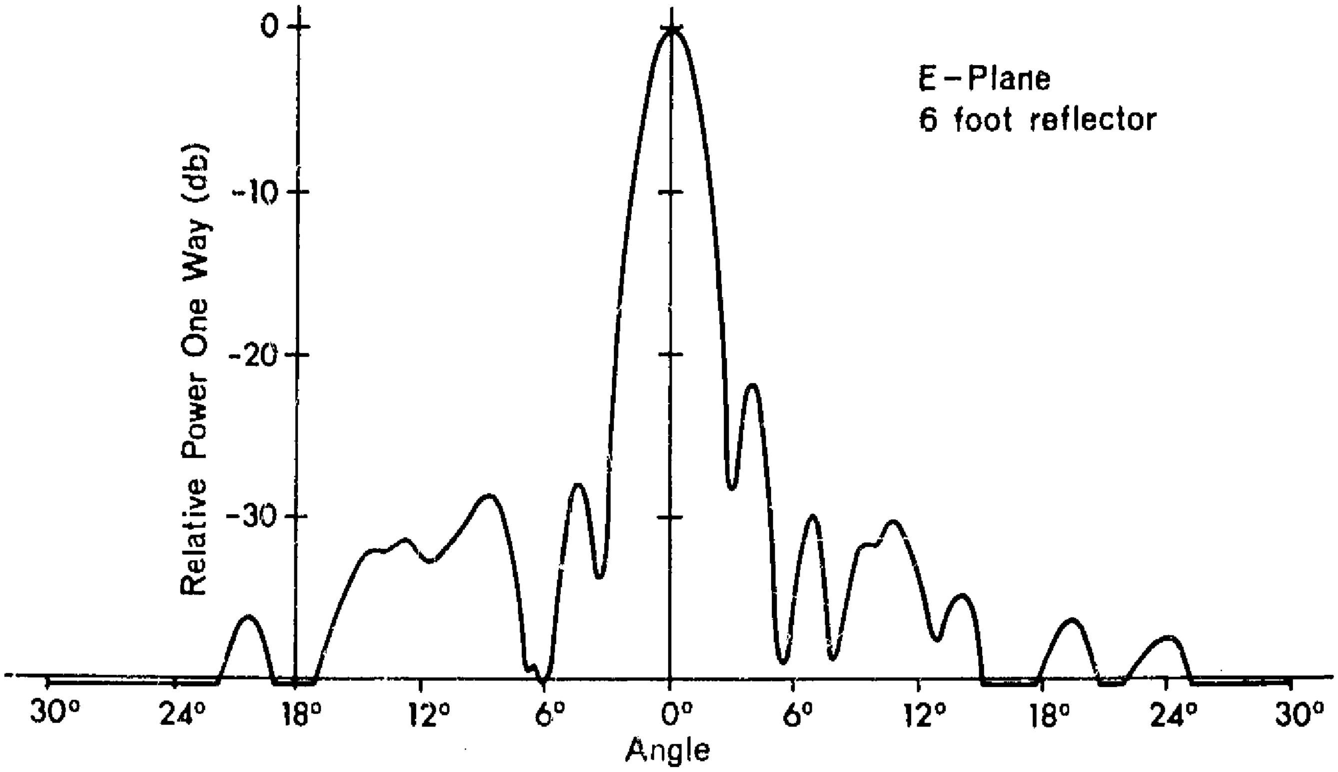

(a) Frequency 4 GHz.

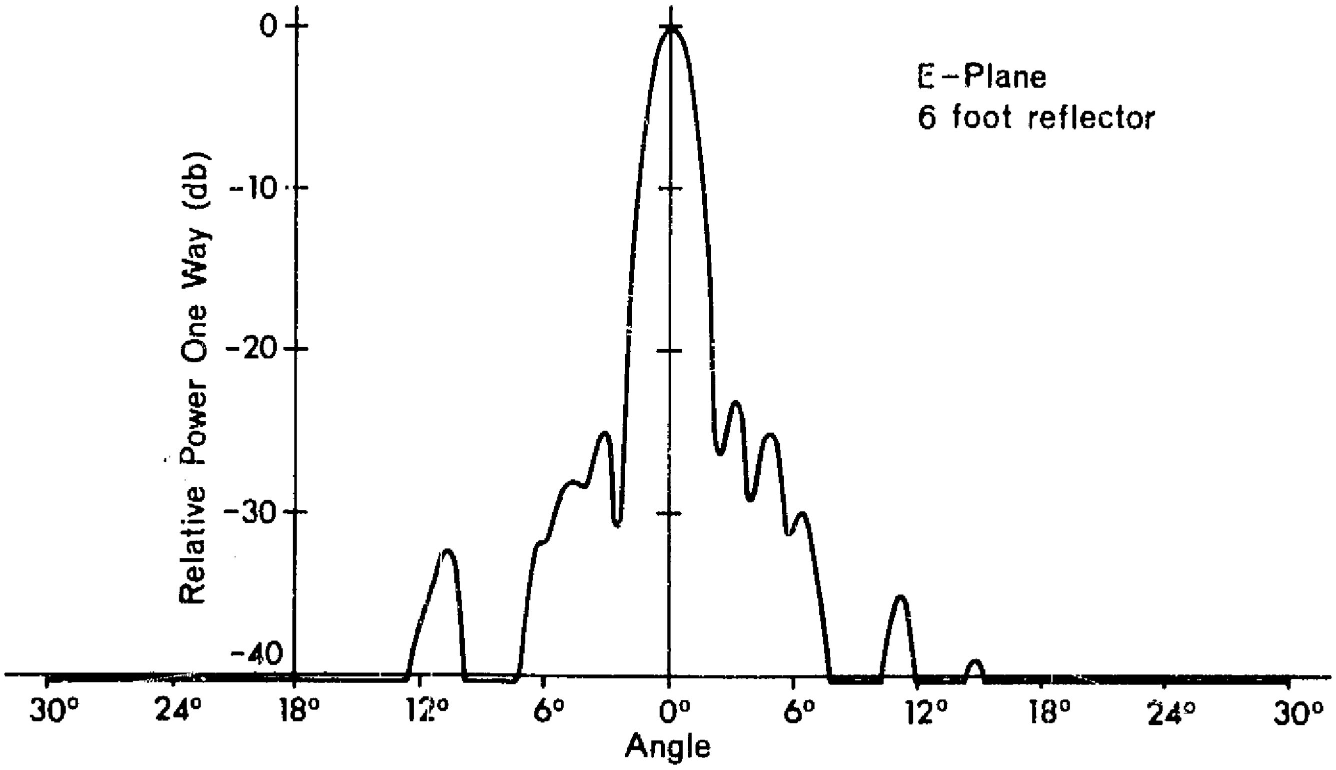

(b) Frequency 8 GHz.

Figure 4.7. E-plane patterns for 6-foot reflector.

The positioner was modified for inverted mounting to conform to the geometry of the measurements performed. In this configuration the elevation axis permits viewing the ground from the nadir to grazing. The azimuth axis permits positioning and is also the scan axis for production of B-scan images.

4.2.2 Receiver Section

The receiver section consists of a low noise figure TWT preamplifier, microwave receiver blanking switch, bandpass filter, mixer-preamplifier, IF postamplifier-detector, and signal attenuators.

4.2.2.1 Low-Noise Preamplifier

The received signal is preamplified with a Watkins-Johnson low-noise travelling wave tube amplifier, Model WJ-423. This unit has a maximum noise figure of 7.3 db across the 4-8 GHz operating range. The minimum small signal gain is 31.8 db and the saturation power output is +13 dbm.

4.2.2.2 Microwave Receiver Blanking Switch

The minimum range capability of the system requires that the receiver be prevented from saturating during transmission. This requires a transmitter-to-receiver isolation considerably in excess of that provided by the duplexing circulator. Additional isolation is provided by a microwave PIN diode switch in the receiver line. The switch used is a series arrangement of two Hewlett-Packard Model 3570 microwave switches and drivers identical to those used for the modulation switch.

4.2.2.3 Bandpass Filter

A bandpass filter is used prior to the mixer-preamplifier to eliminate video transients introduced onto the RF line by the microwave switching circuits. The filter is a Hewlett-Packard Model 8435A 4-8 GHz bandpass filter. This unit has a maximum passband insertion loss of 2 db and a rejection of over 45 db ten percent away from the band edges.

4.2.2.4 Mixer-Preamplifier

The bandwidth of the IF amplifier must be great enough to accommodate the maximum bandwidth of the individual pulses. The minimum pulse length, τ, of 20 nanoseconds requires approximately $1.2/\tau$ or a 60 MHz bandwidth. In order to allow for possible future reduction of the pulse width an IF bandwidth of 100 MHz was used for the system.

The incoming signal is translated to a center frequency of 250 MHz. This mixing operation is accomplished in a coaxial integrated mixer-IF amplifier, RHG Electronics Laboratory Model MP 4-8/437. This unit has a signal bandwidth of 4-8 GHz, an IF bandwidth of 100 MHz, an IF noise figure of 4 db and a combined mixer-preamplifier power gain (RF to IF) of 23 db.

4.2.2.5 IF Postamplifier-Detector

The final stage of amplification is obtained with either a linear or logarithmic IF postamplifier. For most scattering coefficient measurements the greater precision linear amplifier is used. The mean of the fading return is positioned near the middle of the usable dynamic range by means of signal attenuators in both RF and IF lines. For most imaging applications the wide variety of returns as well as the range variation necessitates a much wider dynamic range. For this reason, a logarithmic final IF amplifier is provided for this application.

The linear section is an RHG Electronics Laboratory Model EBT 106 MGC IF postamplifier. This unit has a 250 MHz center frequency and a 100 MHz bandwidth . The amplifier gain is 55 db with a noise figure of 5 db. Both IF and video outputs are available with output capabilities of 1 milliwatt into 50 ohms and 2 volts into 90 ohms, respectively.

The logarithmic section is an RHG Electronics Laboratory Model LT16040RFI IF postamplifier. This unit has a center frequency of 160 MHz and a bandwidth of 40 MHz. Amplifier linear gain is 62 db with a noise figure of 8 db. Video output is 2 volts into a 90 ohm load. When using the logarithmic amplifier, the 160 MHz IF frequency is obtained with a Sage

Laboratories Model 2543ND mixer. This unit has a maximum noise figure of 8.5 db and a maximum conversion loss of 8.5 db.

4.2.2.6 Signal Attenuators

The dynamic range required in making backscatter measurements over a range of incidence angles is far outside the capability of a linear system. Reference to the measured results presented in Chapter 2 shows that the scattering coefficient may easily vary from near +20 db at vertical incidence to less than -30 db at 60° incidence angle. Range variations in the measurements will add at least 10 db to this figure requiring a total dynamic range of approximately 60 db to measure differences in the mean value of the return. The dynamic range must accommodate not only the variation in σ^{o} but also the fading of the individual returns about this value. The 5% to 90% range assuming a Rayleigh distribution for the return is 18 db (+8 db to -10 db). The total dynamic range required is in the order of 68 db.

The system cannot handle this range even if the less accurate logarithmic IF postamplifier is used. In order to accommodate this range it is necessary to effectively step the receiver gain for different measurements. This is accomplished by placing variable attenuators in the system prior to each amplification stage. Sufficient attenuation is placed in the system to prevent saturation of any amplifier and to place the mean signal level in the center of the available dynamic range.

4.2.3 Local Oscillator Section

In a swept frequency system such as this the local oscillator frequency must accurately track that of the transmitter to keep the heterodyned return signal within the IF passband. This is accomplished by developing the local oscillator signal from the same sources as the transmitter. A sample of the transmitted signal, f_c, is mixed with a 250 MHz reference signal to produce sidebands at $f_c \pm 250$ MHz. This mixer output is passed through a narrow band tunable filter which tracts the upper sideband, $f_c + 250$ MHz. This offset sample of the transmitter signal is then mixed with the return to produce the 250 MHz IF frequency used for subsequent amplification.

The local oscillator section consists of a PIN diode leveling loop, first mixer, reference signal source, and tunable filter-driver.

4.2.3.1 PIN Diode Leveling Loop

The sample of the transmitter signal is leveled using an independent PIN diode leveling loop identical to that in the transmitter. The reference signal used for leveling is taken off with a -10 db directional coupler after the signal has passed through the tunable filter.

4.2.3.2 First Mixer

The sample of the transmitted signal is mixed with a 250 MHz reference signal using an Aertech Model 8000 mixer/modulator. This unit uses doubly balanced Schottky diodes and produces approximately 1 milliwatt of power in the upper sideband across a signal input range of 4-8 GHz.

4.2.3.3 Reference Signal Source

The 250 MHz reference signal is obtained from a Frequency Sources Inc. Model FS-7R cavity controlled mechanically tunable oscillator. Power output is approximately 200 milliwatts at 250 MHz with a 5% tuning range and a ± 5% frequency stability over the operating temperature range of -30° to $+70^{\circ}$C.

4.2.3.4 Tunable Filter-Driver

The upper sideband output of the first mixer is isolated by means of a four-stage YIG tuned filter, Watkins-Johnson Model WJ-617-8. This unit has an integrated voltage-to-current driver, WJ-922-4, and tunes the frequency range of 4.25-8.25 GHz. The 3 db bandwidth is approximately 50 MHz with a maximum passband insertion loss of 5 db, an off-resonance isolation of 70 db, and a selectivity of 24 db per octave. The tuning voltage is 0-10 volts with a maximum deviation from linear of ± 8 MHz.

4.2.4 Digital Control Section

The frequency of the transmitted signal and the signal process sequencing are controlled digitally. A block diagram of the digital control system is shown in Figure 4.8.

A pulse generator, Hewlett-Packard Model 220A, serves as the master clock for the entire system. The generator is synchronized with the sweep frequency oscillator at a period of 1/1000 of the sweep period; thus, 1000 pulses are available for modulation of the transmitted signal. If the sweep is over the full 4-8 GHz range, the pulses are spaced 4 MHz apart. The frequency, f, of the transmitted signal may be selected by triggering the modulating PIN diode switch only after n pulses have been counted from the start of the sweep frequency period, Thus,

$$f = 4 + \frac{4n}{1000} \text{ GHz} \tag{4.1}$$

The effective bandwidth of the signal may likewise be determined by counting the number, b, of consecutive pulses transmitted during a single sweep.

$$BW_{eff} = BW + 4b \text{ MHz} \tag{4.2}$$

where BW = bandwidth of the individual pulse

BW_{eff} = effective bandwidth obtained by averaging of pulse sequence.

Additional counters are **used** to automate data gathering by scanning a set effective bandwidth across the entire range of 4-8 GHz.

The digital control modulation signal is fed to a pulse forming network that generates the driving pulses for all microwave switching. As considerable cable length may be present between the digital control unit and the microwave switch drivers, it is necessary to compensate for

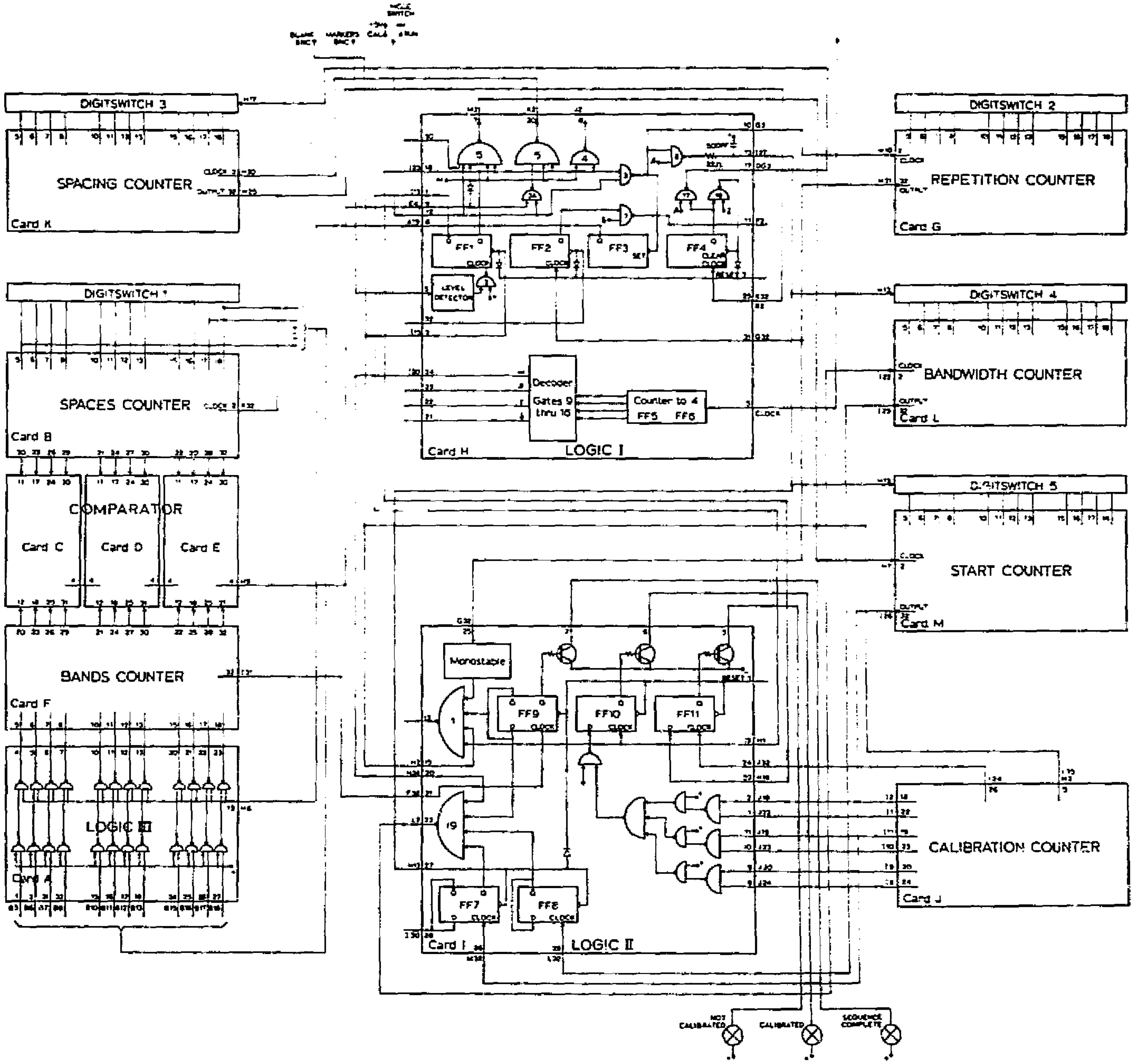

Figure 4.8 Block diagram of digital control system.

pulse distortion effects which may occur. This is done by regenerating a fast-rise and fall time variable width pulse from the sharpened negative-going edge of the input signal. The circuit of this pulse forming network is shown in Figure 4.9.

In addition, the digital control unit provides the sequencing signals for sampling of the return signal, the reading of the integrated average by a digital voltmeter and the drive signals and conversion circuitry required to record the digital voltmeter output on punched paper tape.

4.2.5 Scattering Coefficient Data Processor

In order to determine the differential backscattering coefficient, σ^o, it is necessary to measure the average backscattered power from the target area of interest. This is done by sampling the return signal at a time delay corresponding to the range of the target element. Signal averaging must be performed both to obtain the desired effective bandwidth and to eliminate effects of fading due to spatial variability of the individual scatterers within a resolution cell such as might be caused by wind motion. The averaging for increased effective bandwidth is performed on successive pulses within a single sweep while averaging of spatial fading effects is performed on a sweep-to-sweep basis.

The functional block diagram of the scattering coefficient signal processor is shown in Figure 4.10. This unit is composed of a sampling oscilloscope, integrator, digital voltmeter, paper tape punch, and interface equipment. The signal process timing sequence is shown in Figure 4.11.

4.2.5.1 Sampling Oscilloscope

A Tektronix Type 3S76 plug-in is used as the sample-hold circuit for the system. This unit has a sample gate width of approximately 0.6 nanoseconds and can operate at a repetition rate near 10^5 samples per second. The extremely short gate width insures that the measured amplitude is representative of a single independent sample of the return

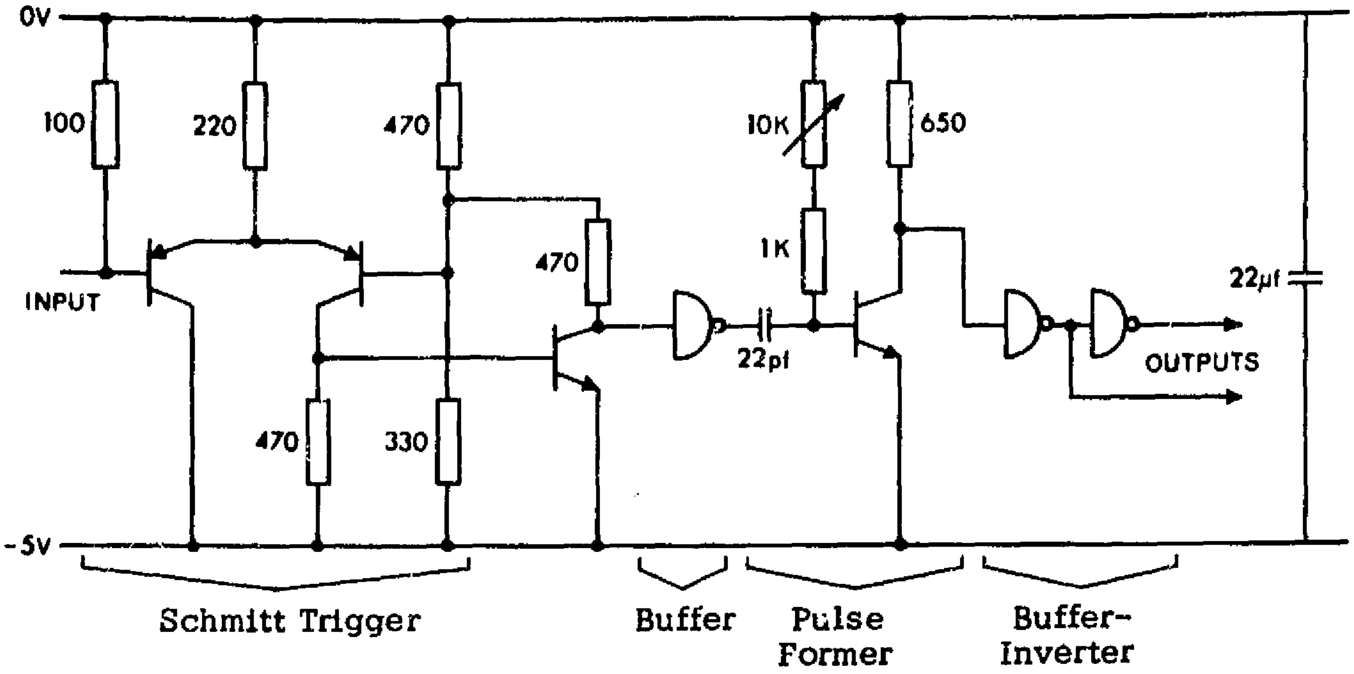

V_{on} = -3 volts

V_{off} = -2 volts

All resistances in ohms
Transistors: NPN 2N4420, PNP 2N4423
Gates: Texas Instruments SN7410N

Figure 4.9. Circuit diagram of pulse forming network.

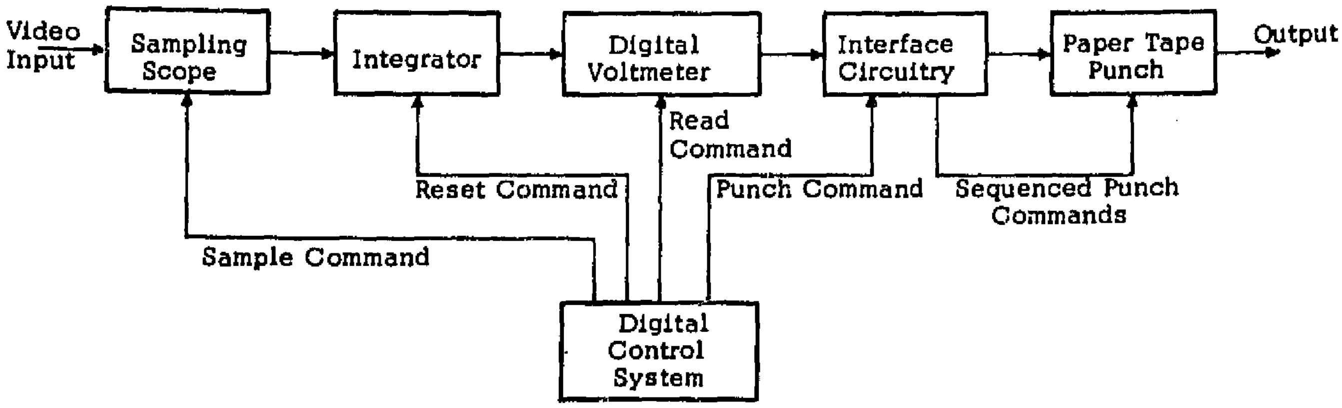

Figure 4.10. Block diagram of scattering coefficient signal processor.

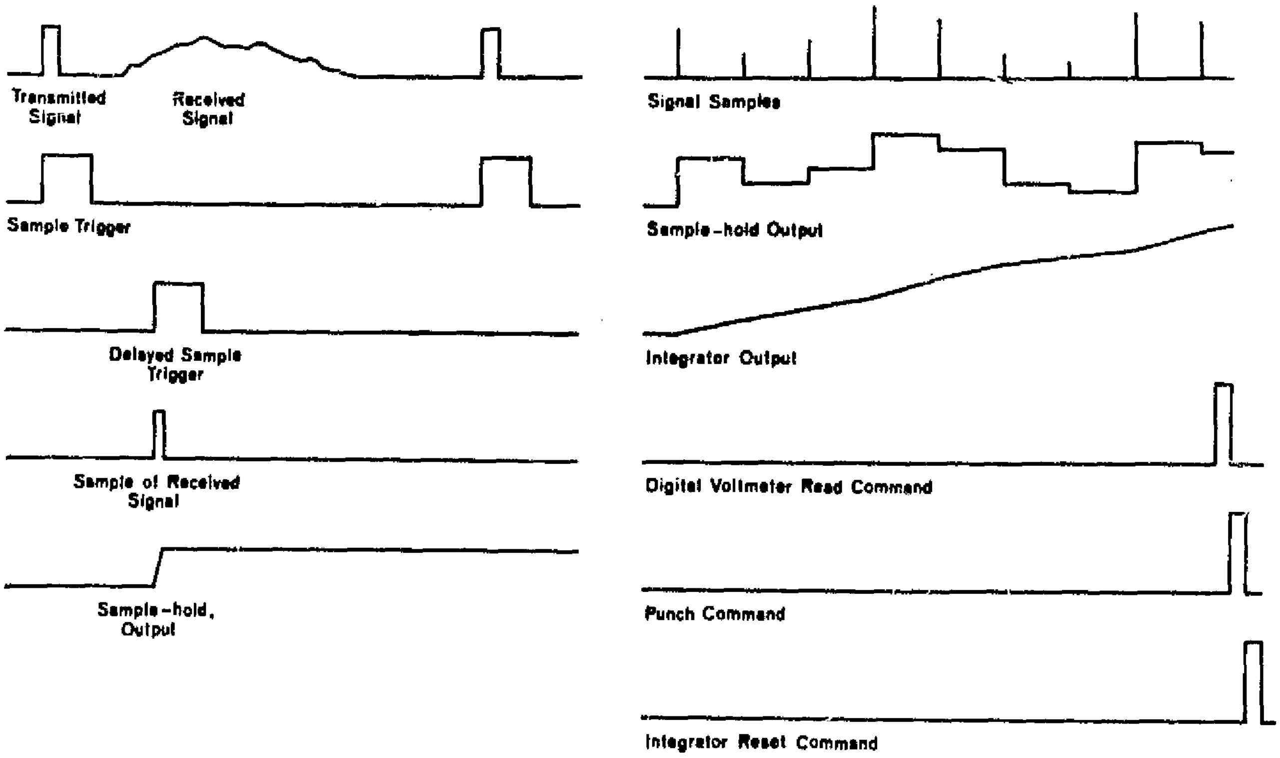

(a) Sampling sequence. (b) Integration and read sequence.

Figure 4.11. Signal process timing sequence.

distribution even when the individual pulse bandwidth is increased to occupy the full IF bandwidth of 100 MHz. The memory circuit of the plug-in retains the sample amplitude until the next sample period, a duration of approximately 10 microseconds at the maximum sample rate. This vertical signal sampled output is available at the front panel of the plug-in.

The sampling plug-in is operated in conjunction with a Type 3577 sampling sweep plug-in with the two units mounted in a standard main frame Type RM561. Operated with an external trigger and in the manual sweep mode it is possible to manually adjust the time delay between the trigger and delayed sample trigger. This variable delay permits positioning of the sample gate at any desired position on the return signal.

4.2.5.2 Integrator

Averaging of the return signal is accomplished by linear integration. With a fixed repetition rate the sample width is constant, hence the mean value of the return may be determined by knowledge of the number of samples integrated.

This application calls for an extremely stable integrator with provision for zeroing out any input offset voltage. Reset is accomplished by a relay closure. The circuit diagram of the integrator is shown in Figure 4.12.

4.2.5.3 Digital Voltmeter

A Hewlett-Packard Model 3440A digital voltmeter with plug-in Model 3443A is used to read the integrator output. This unit has a BCD recorder output that is used to convert the data to a paper tape output.

4.2.5.4 Digital Voltmeter-Tape Punch Interface

The interface between the digital voltmeter and the tape punch provides code translation, level shifting and timing. The BCD output of the digital voltmeter is in a 1-2-2-4 code format. In order to have the

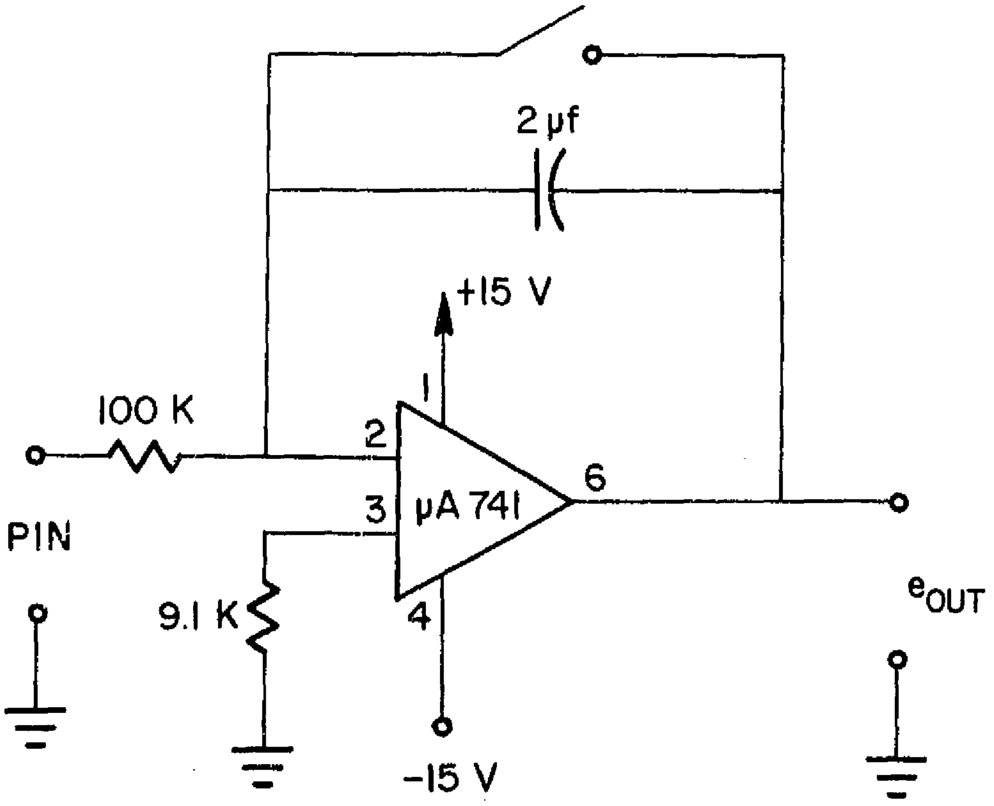

Operational amplifier is Fairchild Linear Integrated Circuit µA741.

Figure 4.12 Circuit diagram of integrator.

paper tape output compatible with existing computer input devices, it is desirable that this code be translated into a standard ASC II code.

The BCD output of the digital voltmeter has logic voltage levels of -1 volt and -24 volts. The Texas Instruments TTL integrated circuits used for all system logic functions operate with levels of 0 volts and -5 volts, while the tape punch requires input levels of 0 volts and -10 volts. Obviously, level shifting is necessary if these units are to be operated in conjunction.

The maximum rate of the tape punch is 12 characters per second and the system sample and read rates must not exceed this limit. The output readings are punched as 4 characters and a multivibrator clock is used to sequence the 4 characters to the appropriate punch driver at the maximum rate.

All interface circuitry is included in the digital control unit shown previously in Figure 4.8. The circuitry described above is part of the logic I and logic II blocks shown in this figure.

4.2.5.3 Paper Tape Punch

The punch used is a Commercial Control Corp Model N255 with a University of Kansas Model TPD/100 tape punch driver. The maximum rate of the punch-driver combination is 12 characters per second.

It should be pointed out that paper tape is used as an output medium because of funding limitations which necessitated use of existing equipment.

4.2.6 Image Data Processor

The basic design of the system concentrated on obtaining backscatter power spectra as a function of transmitted bandwidth and incidence angle. However, the applications of these data are principally to imaging radar systems. For this reason, an imaging capability was incorporated into the system design to facilitate demonstration of the techniques proposed. The images produced are uncalibrated and thus must be judged on strictly a qualitative basis; however, the results shown in Chapter 6 are at least as striking as the earlier comparison of illumination by monochromatic and panchromatic light.

The system records a B-scan presentation of the return signal as a Tektronix 585 oscilloscope. The cathode ray tube of this oscilloscope has a special P-16 phosphor with rapid decay time and broad dynamic range. The image is recorded photographically directly from the cathode ray tube using a sheet film and developing process selected for maximum gray scale rendition.

In normal imaging operation the logarithmic IF postamplifier is used to increase the usable dynamic range of the return signal. The detected video output is fed to a Tektronix 545B oscilloscope operating in the delayed sweep mode. The vertical signal output of the Tektronix 545B is applied to the cathode of the Tektronix 585 cathode ray tube to intensity modulate the beam. The delayed sweep of the Tektronix 545B permits positioning of the return signal so that the intensity modulated raster shows only the desired target return interval. The component arrangement and timing sequence for imaging operation are shown in Figure 4.13.

4.3. System Calibration

4.3.1 Calibration Technique

The system is calibrated by referring all measurements to those made on a target of accurately known radar cross-section. The calibration target used for this system is a 12-inch diameter polished aluminum sphere. A spherical target has the distinct advantage that its cross-section is not aspect-senstive since it remains a sphere no matter from what aspect it is viewed. The normalized radar cross-section of a sphere with infinite conductivity is shown as a function of relative size and wavelength in Figure 4.14 (Rheinstein, 1968).

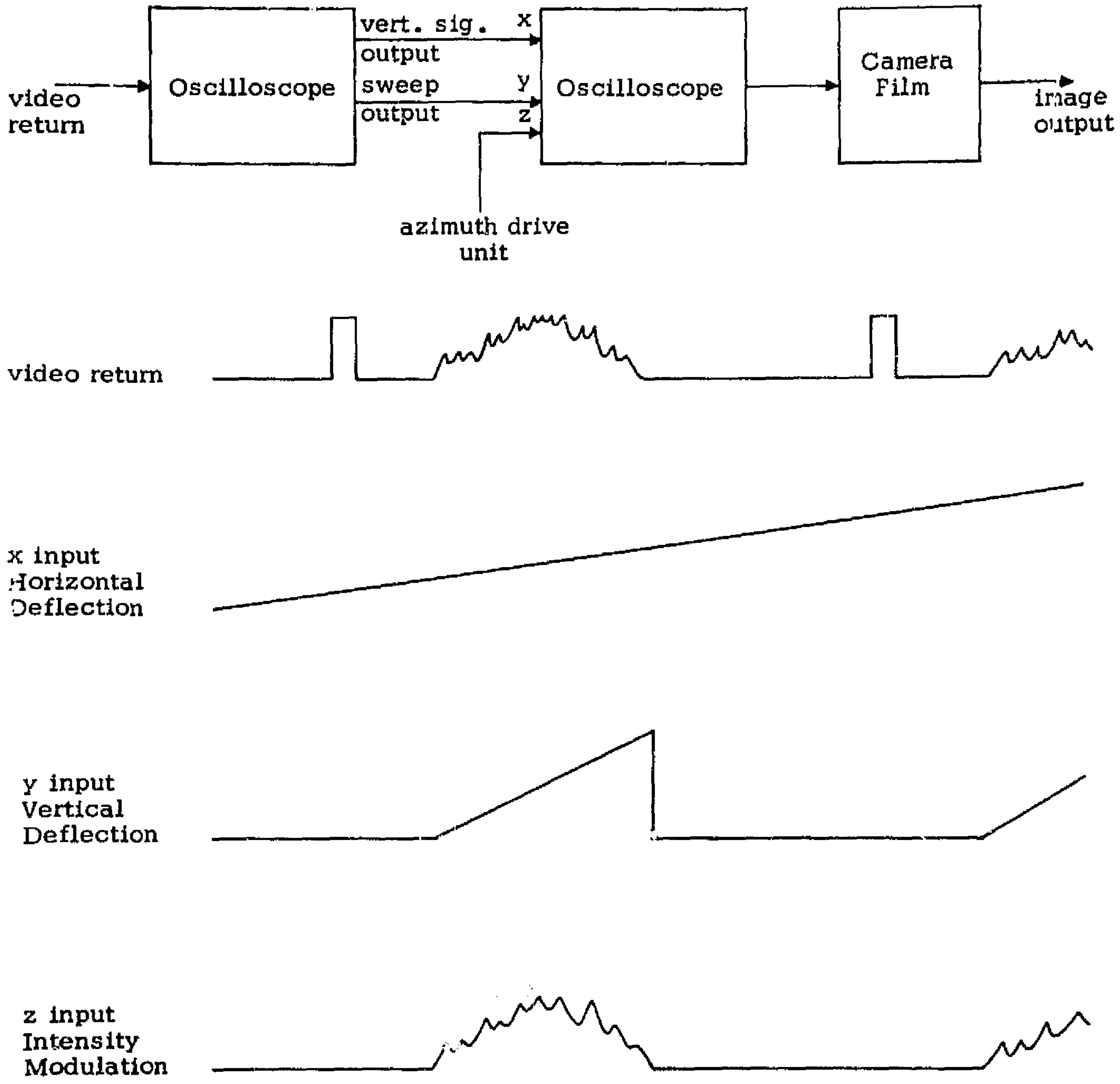

Figure 4.13 Component arrangement and timing sequence for imaging operation.

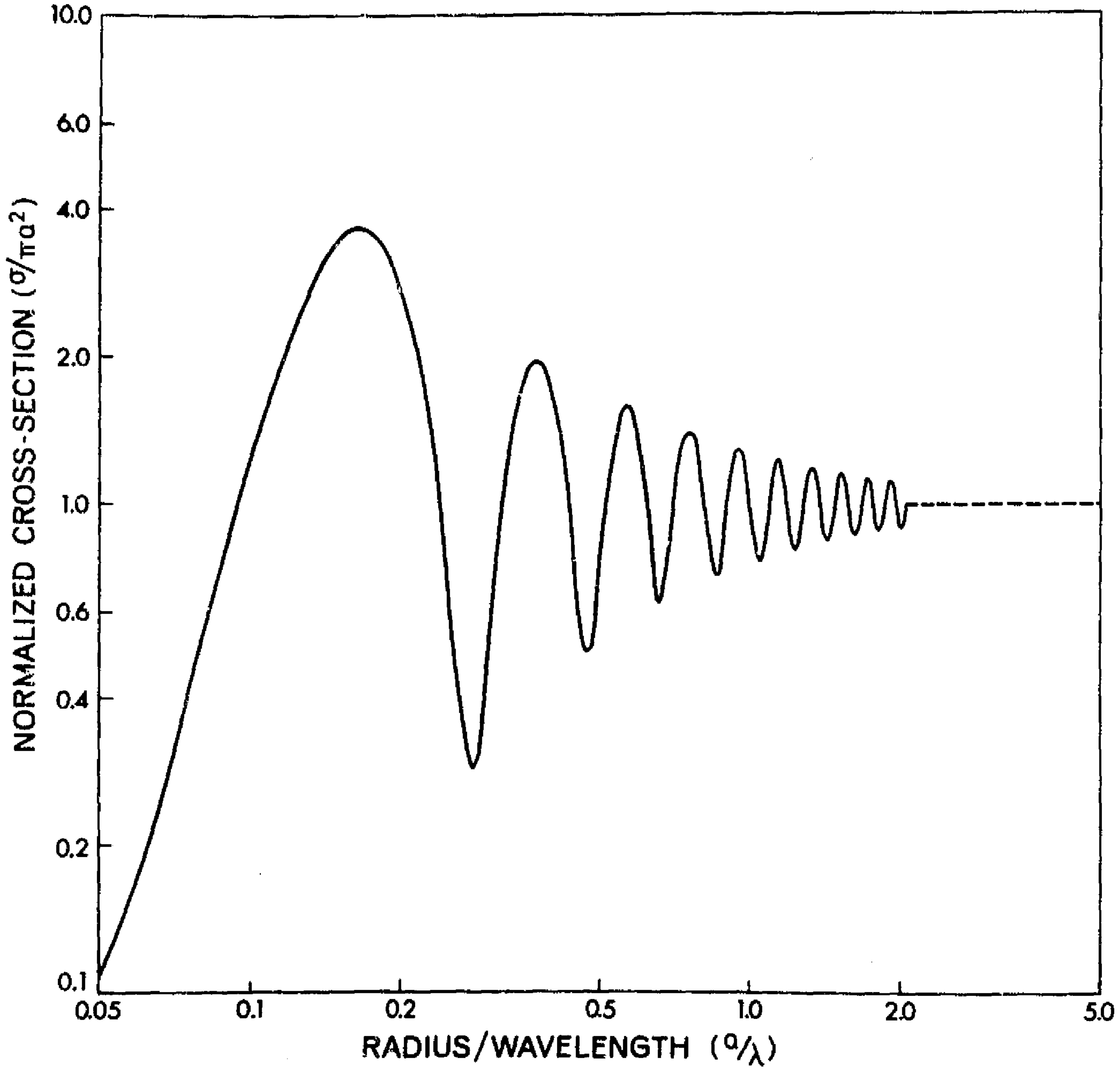

Figure 4.14 Backscatter cross-section of an infinitely conducting sphere (after Rheinstein, 1968).

The ultimate measurement desired is the backscattering cross-section, σ, for discrete targets or the differential backscattering cross-section, σ^{o}, for area extensive targets (Moore, 1969). The actual measurement performed by the system is of the average returned power, which is related to either σ or σ^{o} by the radar equation.

When measuring most discrete targets it may be assumed that the antenna gain is uniform over the target area and equal to the maximum gain; thus the familiar form of the radar equation may be used to give

$$\sigma_t(\lambda) = \frac{(4\pi)^3 \left[P_{rt}(\lambda) / P_T(\lambda) \right] R_t^4}{\lambda^2 \, G^2(\lambda, 0)} \qquad (4.3)$$

where $\sigma_t(\lambda)$ = backscattering cross-section of the target
$P_{rt}(\lambda)$ = return power
$P_T(\lambda)$ = transmitted power
R_2 = range from antenna to target
λ = wavelength
$G(\lambda, 0)$ = antenna gain

A similar measurement made on the calibration sphere yields

$$\sigma_s(\lambda) = \frac{(4\pi)^3 \left[P_{rs}(\lambda) / P_T(\lambda) \right] R_s^4}{\lambda^2 \, G^2(\lambda, 0)} \qquad (4.4)$$

If we assume that during the course of the two measurements the transmitted power, receiver gain and antenna remain the same, equations 4.3 and 4.4 may be combined to give

$$\sigma_t(\lambda) = \sigma_s(\lambda) \, \frac{P_{rt}(\lambda)}{P_{rs}(\lambda)} \left(\frac{R_t}{R_s} \right)^4 \qquad (4.5)$$

The radar backscattering cross-section of a discrete target may thus be referenced to the known backscattering cross-section of the calibration sphere without depending upon determination of the absolute value of each parameter in the radar equation.

The measurement of the differential backscattering cross-section, σ^{o}, of an area extensive target is slightly more complex as the antenna gain may no longer be considered a function of wavelength alone. Use of the differential backscattering cross-section implies that the return from the area extensive target is contributed by a large number of scattering elements where phases are independent. If this condition is met the average return power may be computed by superposition of the power from the individual elements. If we assume that the scattering centers are sufficiently dense within the illuminated area we may pass from the summation to an integral over the illuminated area, thus

$$P_r(\lambda,\theta) = \iint_A \frac{P_T(\lambda)\, G^2(\lambda,\psi)\, \lambda^2\, \sigma^{o}(\lambda,\theta)}{(4\pi)^3 R^4}\, dA \tag{4.6}$$

where $P_r(\lambda,\Theta)$ = average returned power over an ensemble of surfaces

$P_T(\lambda)$ = transmitted power

$G(\lambda,\psi)$ = gain function of the antenna (assumed circularly symmetric with ψ the angle from bore slight)

λ = wavelength

$\sigma^{o}(\lambda,\theta)$ = differential backscattering cross-section

R = range from antenna to target element

A = area illuminated

Technically P_r would be noted as an average since this is a requirement for the superposition of power to be applicable, however, this designation is dropped in line with normal convention and the average is merely implied.

Assuming that targets are selected such that σ^{o} may be considered constant over the illuminated area, we have

$$P_r(\lambda,\theta) = \sigma^{\circ}(\lambda,\theta) \iint_A \frac{P_T(\lambda)\, G^2(\lambda,\psi)\, \lambda^2}{(4\pi)^3 R^4}\, dA \tag{4.7}$$

The return from the calibration sphere may be rewritten as

$$P_{rs}(\lambda) = \frac{P_T(\lambda)\, G^2(\lambda,0)\, \lambda^2\, \sigma_s(\lambda)}{(4\pi)^3 R_s^4} \tag{4.8}$$

Combining equations 4.7 and 4.8 we have

$$\sigma^{\circ}(\lambda,\theta) = \frac{\sigma_s(\lambda)\left[P_r(\lambda,\theta)/P_{rs}(\lambda)\right]}{R_s^4 \iint_A \frac{g^2(\psi)}{R^4}\, dA} \tag{4.9}$$

where $g(\psi)$ is the normalized antenna gain function having a maximum of unity. The integral accounts for the "aperture effect" which is the weighting of the signals from the individual elements by the antenna gain function. This effect has been treated in detail by Parkins (1966). The "aperture effect" integral is calculated separately and is a constant for each λ and Θ combination.

Thus, the differential backscattering cross-section may likewise be referenced to the calibration sphere without depending upon an absolute measure of the radar equation parameters.

4.3.2 Accuracy of Measurements

The fact that the backscattering coefficient or cross-section is determined by a ratio of the average target return and the calibration return rather than an absolute measure of the return power considerably simplifies the calibration procedure. For a single frequency measurement with both target return and calibration return near the same amplitude and measured near the same time, the accuracy is estimated to be within ± 1 db. For swept frequency measurements where the return amplitude must also be adjusted by attenuator insertion the accuracy decreases to approximately ± 2 db.

The principal cause of error is due to the method of frequency determination and the variation of system gain with frequency. Frequency is determined by subdividing the total sweep range (4 GHz) into 1000 pulse intervals and then counting the number of pulses from the start of the sweep. The pulse period may drift between 999 and 1001 counts giving a frequency accuracy of approximately ± 4 MHz near the end of the sweep. The setting of the start and stop points for the sweep introduces an additional error giving an overall accuracy for frequency determination of near ± 10 MHz. The gain variations of the system with frequency are most easily seen in the swept frequency calibration return shown in Figure 4.15.

Another cause of error is the limited dynamic range of the receiving section. With the linear postamplifier the usable dynamic range is approximately 20 db which is barely adequate for the expected fading range from complex targets. For targets of substantially larger radar cross-section than the calibration sphere or targets at a significantly greater range than the calibration measurement the average signal return is adjusted to fall near the center of the dynamic range by insertion or removal of signal attenuators in either RF or IF lines. The tolerance upon the attenuator values gives a corresponding uncertainty in the stability of the system gain which is assumed constant.

To minimize the effect of the error sources, the data runs for each target were repeated a number of times.

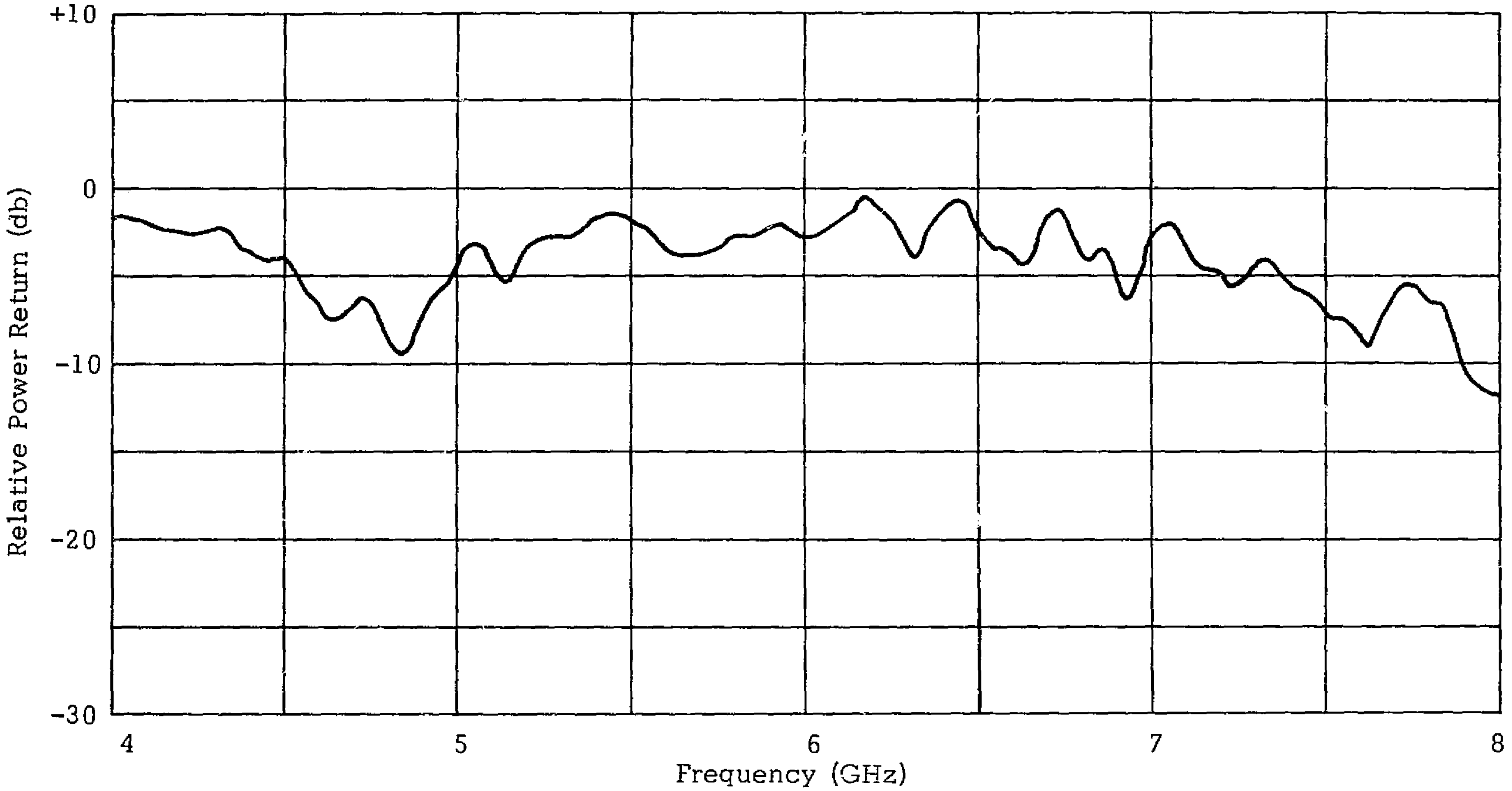

Figure 4.15 Sweep frequency return from 12-inch diameter calibration sphere

CHAPTER 5

SCATTERING EXPERIMENT

The experiment described in this chapter was conducted with two purposes in mind: the first, to verify the reduction of return variance obtained by frequency averaging, and the second, to investigate the spectral response of a variety of targets after averaging out the effects of fading.

The results presented here were obtained with the experimental system described in Chapter 4 with two notable exceptions. During the period of data gathering the sampling oscilloscope and the boom truck were inoperative and undergoing extensive repairs. The loss of the sampling scope necessitated manual recording of the data with the aid of a storage scope. The results were then punched on computer cards for subsequent normalization and averaging. While this procedure did not hamper the reliability of the measurements, it did seriously slow the data gathering and limit the number of measurements that could be made.

The loss of the boom truck destroyed the system mobility and severely limited the choice of targets. The measurements shown here were obtained by mounting the entire system atop a ten-story dormitory and measuring suitable targets within the range of the system. This fixed mode of operation eliminated any investigation of the effects of incidence angle. Illustration 5.1 shows the system located on the dormitory roof.

5.1 Description of Targets

The field of view from the dormitory roof is shown in Illustration 5.2. The following targets were measured and the location of each is shown by corresponding number in Illustration 5.2.

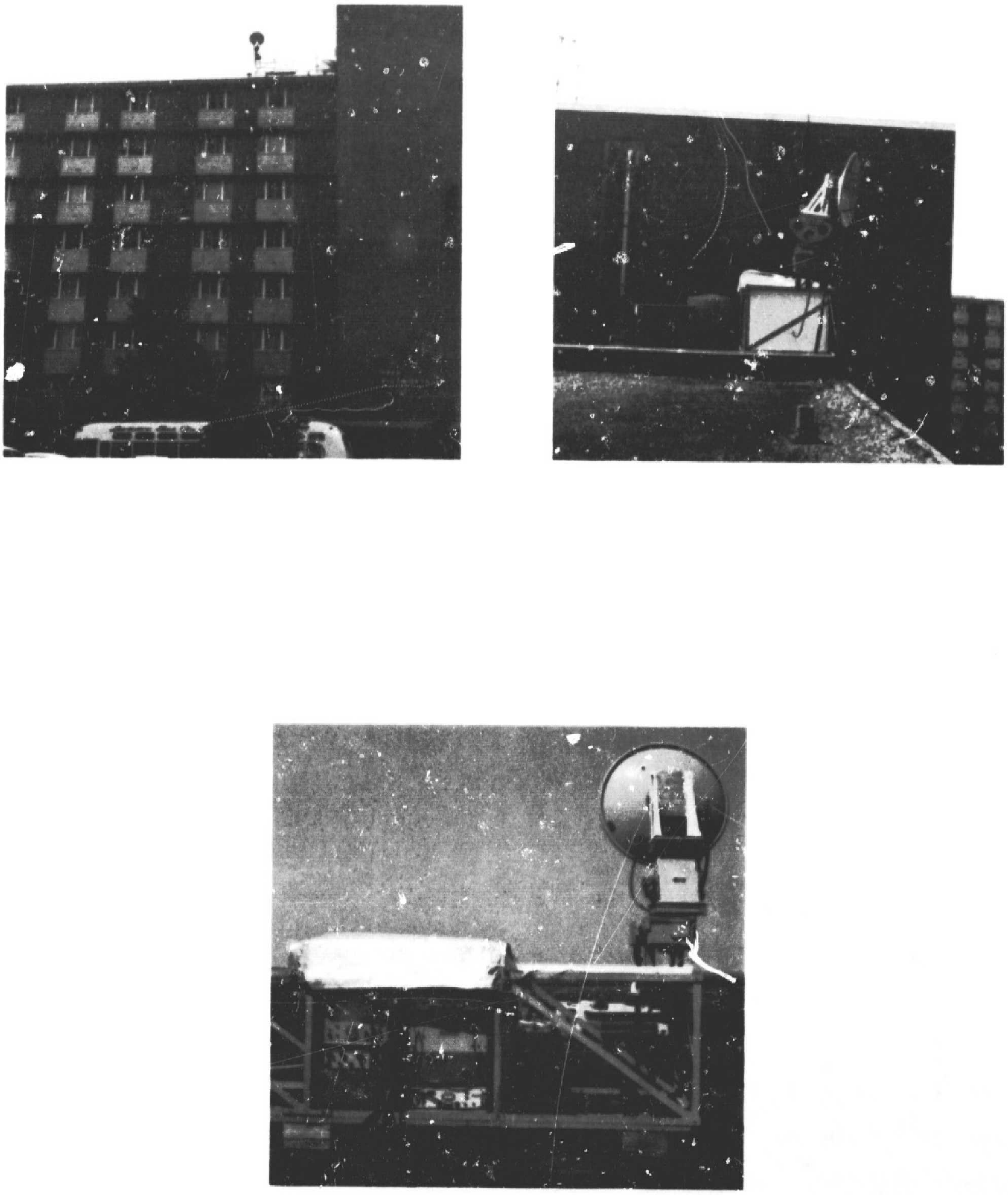

Illustration 5.1 Roof-top installation of measurement system.

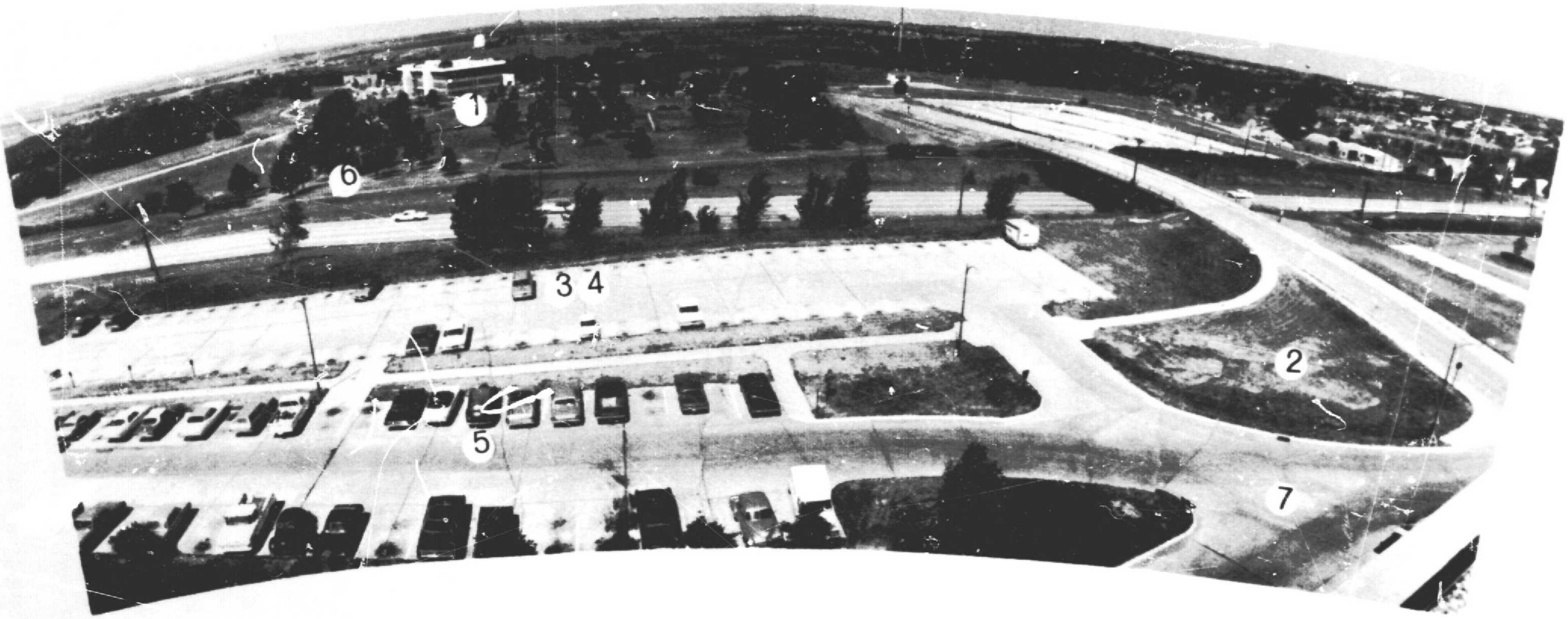

Illustration 5.2 Field of view from dormitory showing target locations.

1. Space Sciences Building -- This target was selected as representative of a large complex cultural target of size comparable to or exceeding that of the system resolution cell. The range to the near wall of the building is 385 meters and the angle of incidence to ground level is 85 degrees. At this range the azimuth resolution is approximately 20 meters, while the range resolution is adjustable with a minimum of 3 meters.

2. Grass -- The grass in this area is regularly mowed and has a uniform height of about 2-1/2 inches. This target is representative of a uniform area extensive target with a low height vegetation cover and is, fortunately, located at a range of 78 meters. The angle of incidence is 63 degrees and the system azimuth resolution is approximately 4 meters.

3. Car -- This target is representative of a small cultural target of a size less than the system resolution cell. For this measurement the car was located approximately in the center of the far parking lot and headed directly at the system as shown in Illustration 5.2. At this angle of incidence (65 degrees) the parking lot surface provides an essentially zero return background. The range is 80 meters and the azimuth resolution approximately 4 meters.

4. Car -- The target and location are identical to that of target 3 with the exception that the car orientation is at right angles to the system line-of-sight.

5. Area of Parked Cars -- This target consists of a sufficient number of cars to totally fill the resolution cell. All cars are oriented to point approximately at the system. The angle of incidence, range and azimuth resolution are respectively 69 degrees, 97 meters and 5 meters.

6. Trees -- This area is representative of a natural vegetation target with a considerable vegetation cover. Unfortunately, the angle of incidence is 79 degrees which is slightly larger than the maximum incidence angle of most imaging systems. The range to the area is 180 meters and the system azimuth resolution is approximately 9 meters.

7. Cement -- This area represents a smooth, near-specular reflective surface over the wavelength range of this system. The angle of incidence to the area measured is 48 degrees and the system sensitivity is barely adequate to obtain the measurement at this angle. The cement parking lot surfaces located at a greater range and higher incidence angle are totally submerged in the system noise. The range to the area measured is 53 meters and the azimuth resolution is approximately 3 meters.

5.2 Measurement Results

The data recording was the same for each target with the only difference that of pulse length or actual resolution bandwidth. Voltage return measurements were recorded at 1000 points across the 4-8 GHz frequency range. The data were then normalized to the return from the calibration sphere and averaged for the desired effective bandwidth.

The degree of averaging and the presentation of results depends upon whether one is interested in the reduction of fading or in the spectral response characteristic that remains after fading effects are averaged out. These data are analyzed separately for investigation of both phenomena.

5.2.1 Measurements of Return Distribution

In an earlier acoustic modeling experiement, Rouse (1968) attempted to measure the probability density function of the scattered return with frequency fading. The results of his experiment were inconclusive as the

9

frequency range of the acoustic system was inadequate to obtain sufficient independent samples of the frequency fading record to adequately define the distribution. With the limited range of his system the best that Rouse could do was to show that the addition of frequency diversity did not disturb the Rayleigh character of the positional fading distribution.

With the increased frequency range of the radar system used for this experiment it was possible to obtain sufficient independent samples to reasonably define the frequency fading distribution through frequency-of-occurrence histograms. The probability density functions of the return distributions from each of the targets are shown in Figures 5.1 and 5.2. No averaging was performed on these data, thus the system resolution and effective bandwidth are equal. It may be seen from Figures 5.1 and 5.2 that despite the dissimilarity of the targets, the behavior of the return distribution is much the same with each curve a reasonable approximation to the Rayleigh power or exponential density function.

Of more significance to our investigations of variance reduction by frequency averaging is the behavior of the mean and standard deviation of the distributions. Table 5.1 shows calculated values of the mean, standard deviation and their ratio for each of the targets measured. These figures were calculated from the data prior to averaging, thus the resolution and effective bandwidth are the same. The theory of Chapter 3 predicts that for a system with equal illumination and effective bandwidths, the ratio, $(\frac{\sigma}{\mu})^2$, should be slightly less than one if the targets are truly representable by the model of Chapter 3. It may be seen from the figures of Table 5.1 that this is not the case for these data.

The explanation for this discrepancy must lie in either the system or the model. One might first suspect variations of the system sensitivity with frequency as the factor contributing to this increased variance; however, repeated measurements of the calibration sphere indicate the system response remains essentially constant with time. A more reasonable explanation is that the model makes no allowance for variations of scattering cross-section with large changes in frequency. Multiband

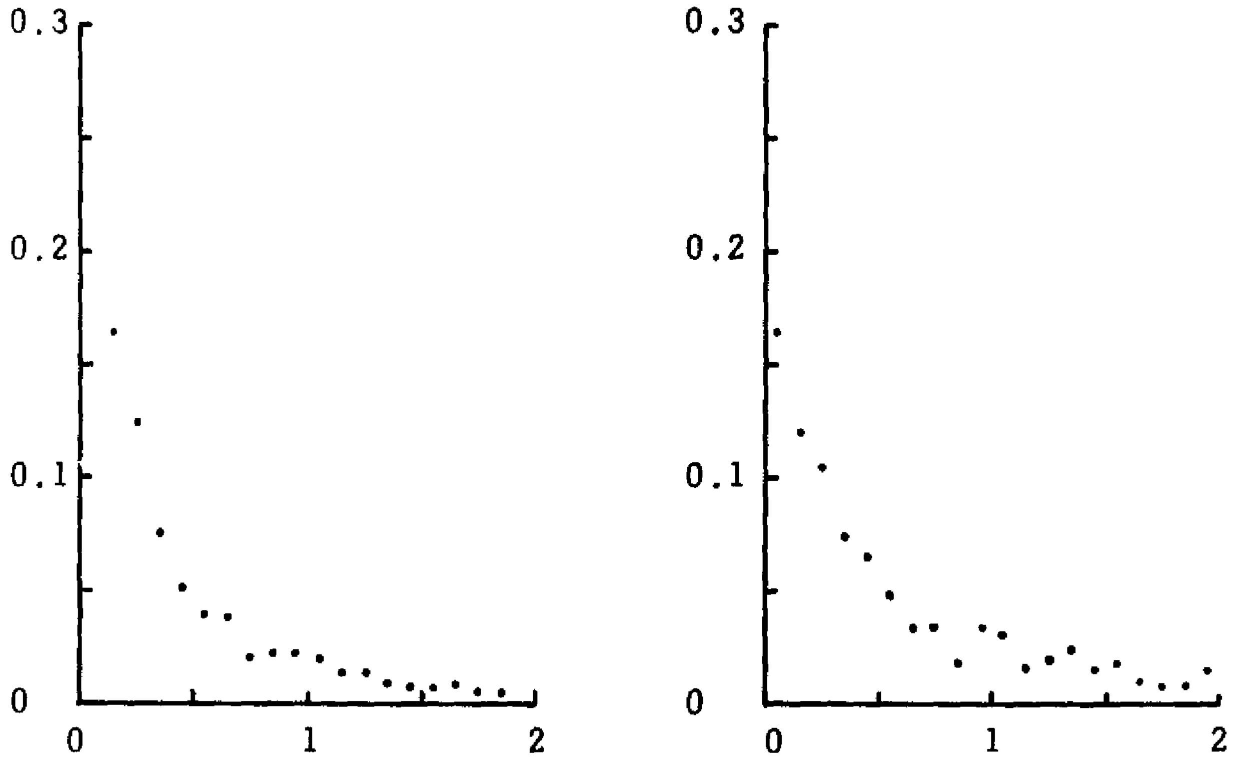

(a) Target 1 - Space Sciences Building

(b) Target 2 - Grass

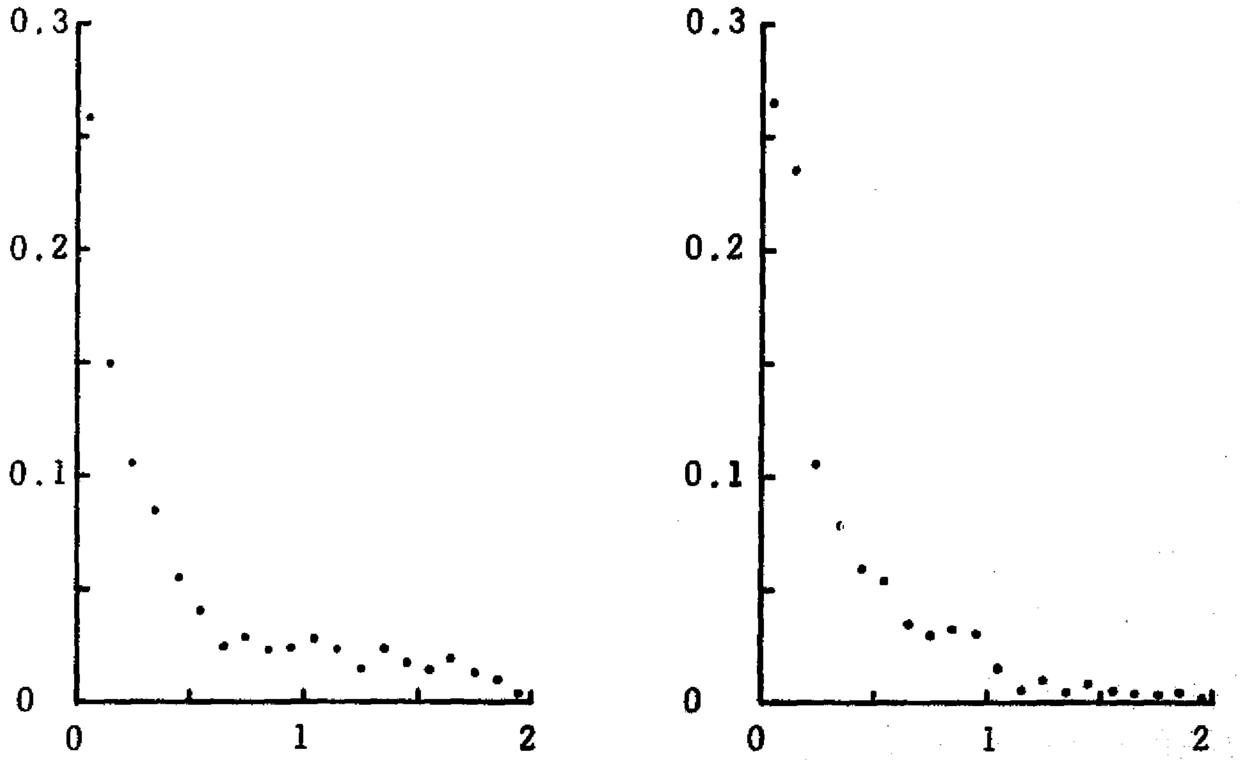

(c) Target 3 - Car

(d) Target 4 - Car (Broadside)

Figure 5.1 Probability density functions of frequency fading distributions for targets 1-4.

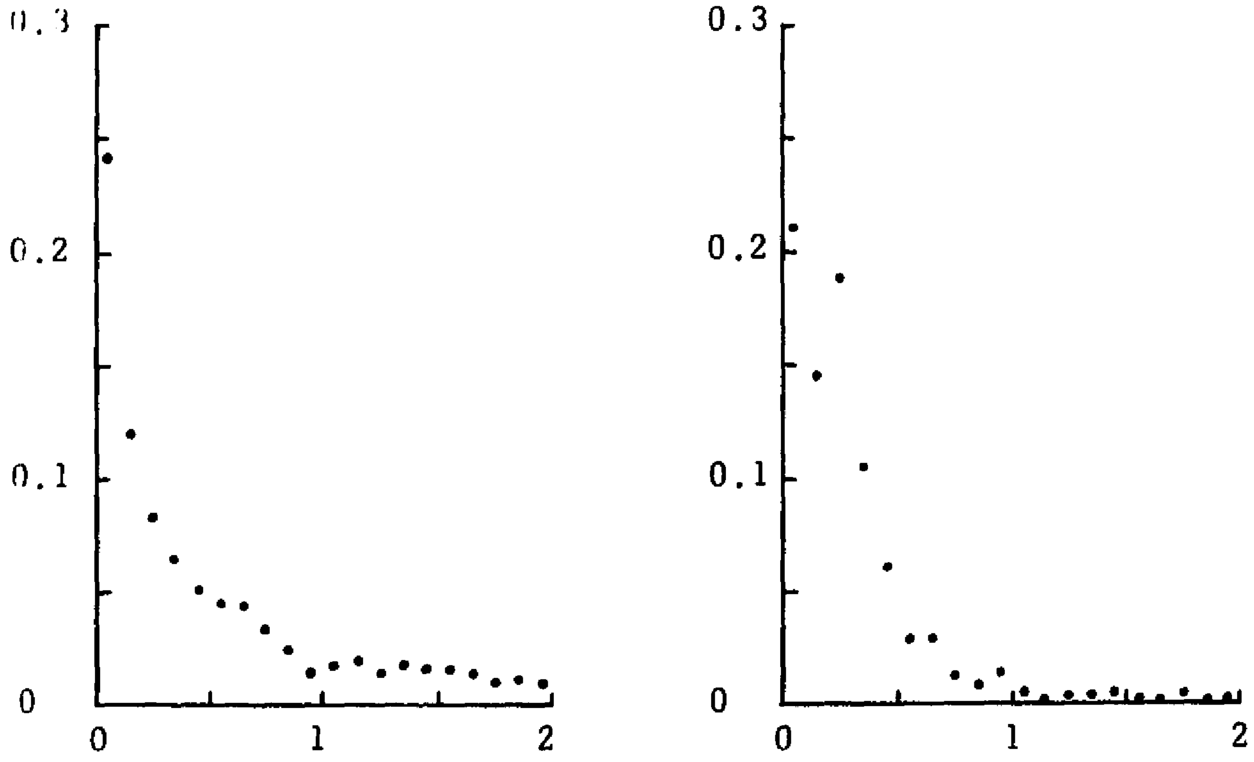

(a) Target 5 - Area of cars

(b) Target 6 - Trees

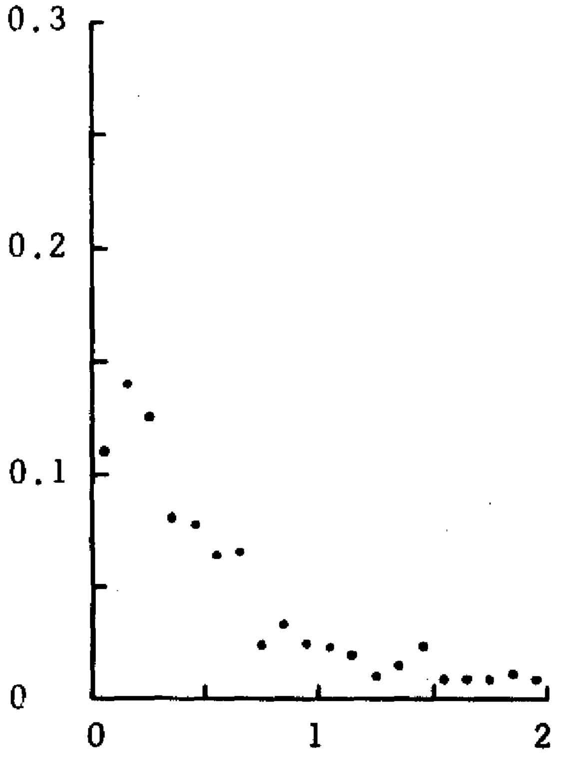

(c) Target 7 - Cement

Figure 5.2 Probability density functions of frequency fading distributions for targets 5-7.

TABLE 5.1

EXPERIMENTAL VALUES OF RETURN MEAN AND VARIANCE

Target	μ	σ	$\left(\frac{\sigma}{\mu}\right)^2$
1	2.166	3.206	2.19
2	1.082	2.104	3.78
3	0.537	0.630	1.37
4	3.944	5.314	1.82
5	2.471	6.290	6.48
6	3.536	5.062	2.06
7	0.953	1.624	2.91

data by previous experimenters show, however, that such variations do exist, and the measurement range of this system approaches that of the discrete frequency measurements made in separate bands (Cosgriff et al., 1960; Lundien, 1966). This argument is treated in greater detail in Section 5.3.

The most graphic illustration of the effects of frequency averaging is examination of the full spectral response curve plotted for differing effective bandwidths. Figures 5.3 and 5.4 show the spectral response curves of targets 2 (grass) and 3 (car) plotted for effective bandwidths of 100 MHz and 500 MHz. It may be seen from these plots that the slightly greater range extent of target 2 gives a higher fading rate and more rapid decorrelation with frequency shift.

5.2.2 Measurements of Spectral Response

Any measurement of scattering coefficient must include sufficient averaging to eliminate fading effects. In most single frequency systems,

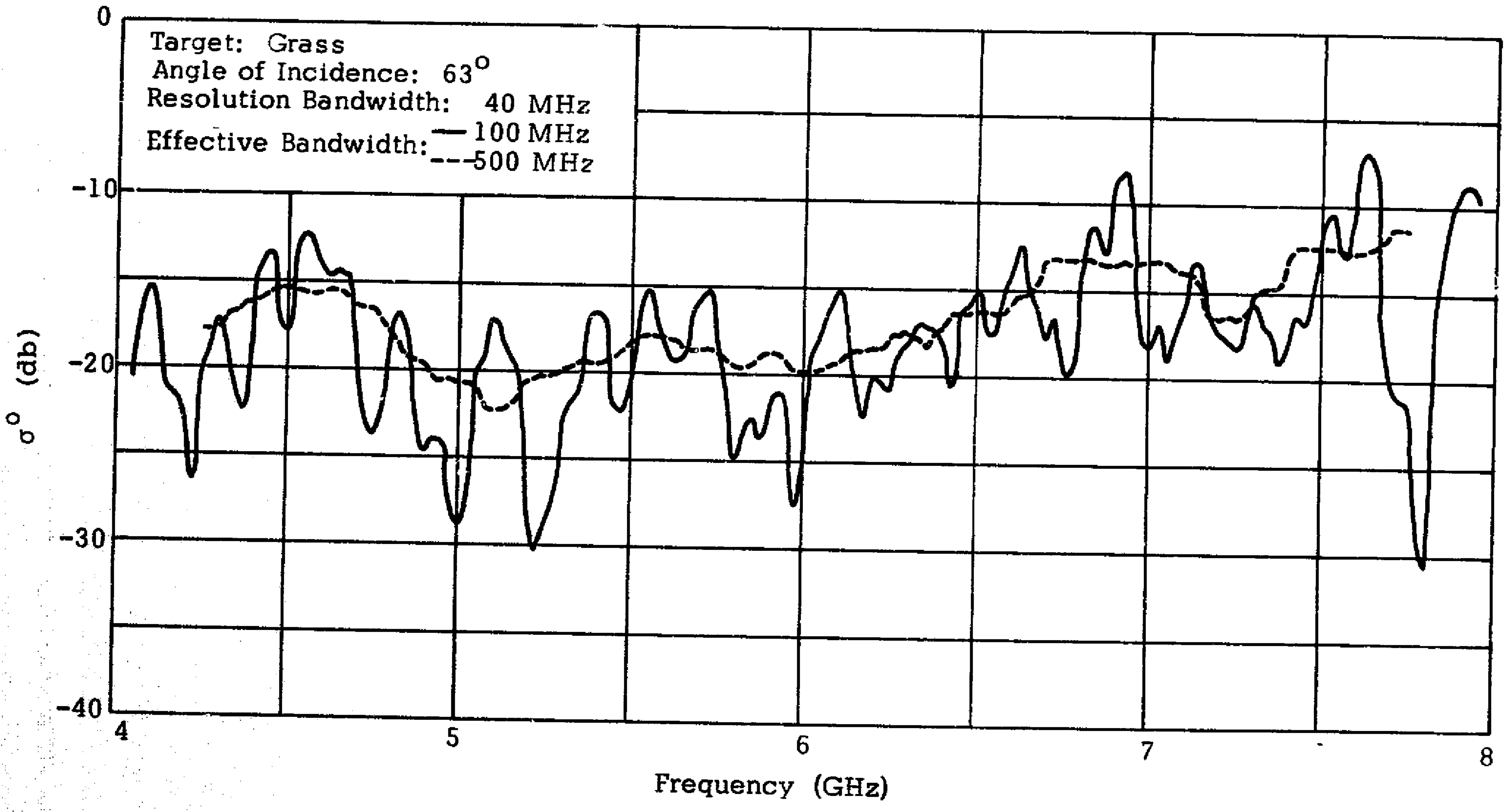

Figure 5.3 Spectral response curves for two different effective bandwidths.

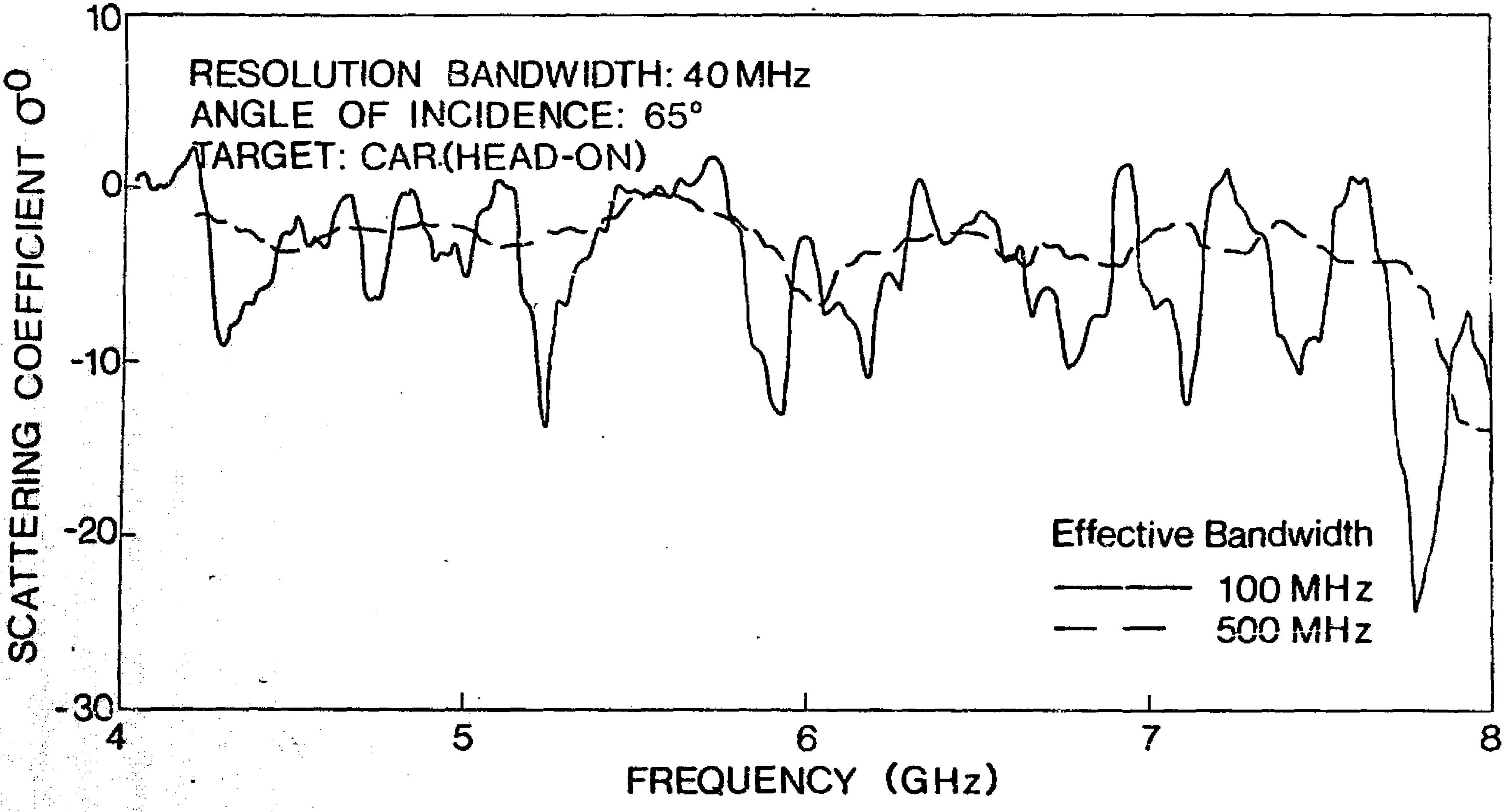

Figure 5.4 Spectral response curves for two different effective bandwidths.

the fading is caused by positional changes due to relative motion between radar and target. Averaging is performed in time with the assumption that during the averaging interval the surface being measured remains statistically homogeneous.

The system used here is stationary as are the targets, thus the only relative motion is that due to wind movement. For the cultural targets this motion is negligible at the wavelengths used for the measurements. The required averaging for these measurements must then be performed in the frequency domain.

The pulse widths used for these measurements are all in the range of 20 nsec. to 40 nsec. corresponding roughly to a resolution bandwidth range of 50 MHz to 25 MHz. As shown in Chapter 3, the reduction in variance by frequency averaging is approximately linear with multiples of the resolution bandwidth. Ten resolution bandwidths or 500 MHz was selected as the minimum effective bandwidth required to provide sufficient averaging of the data to remove fading effects and to permit viewing of the underlying spectral response.

Figures 5.5 through 5.11 show the spectral response characteristics of the seven targets described. If there is a single dominant characteristic of these data it is that, in general, the scattering coefficient increases with increasing frequency.

5.3 Discussion of Results

In this section an attempt is made to relate the experimental results with the theoretical predictions of Chapter 3. This, of course, applies only to the investigation of panchromatic illumination or the reduction of return variance with frequency averaging. No theory is put forth to explain the spectral response characteristic of such a diverse array of targets and indeed, it is doubtful that this is possible. The investigation of spectral response was rather an attempt to assay the potential value of polypanchromatic illumination, or the application of color techniques, to the microwave spectrum.

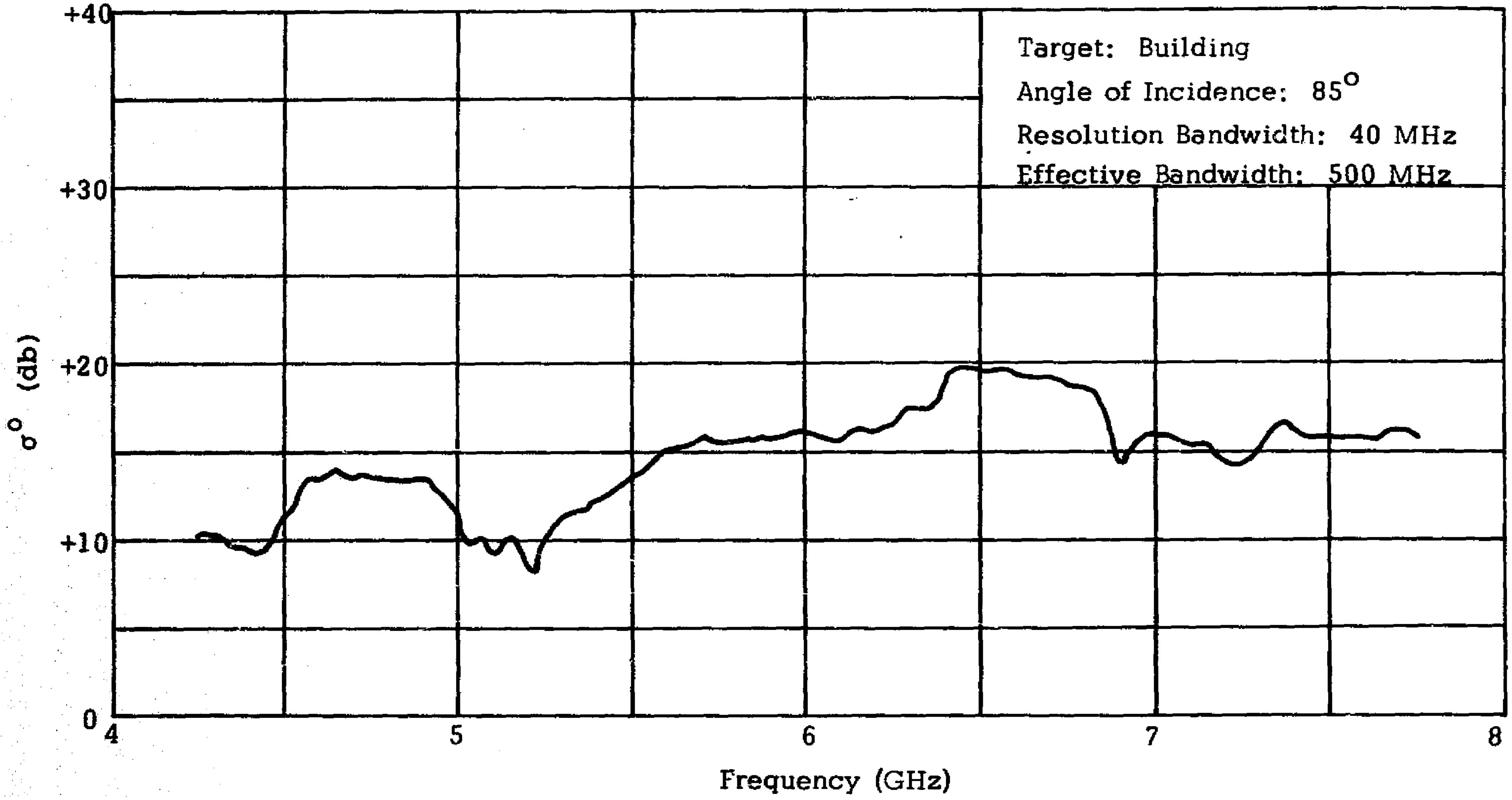

Figure 5.5 Spectral response of target 1.

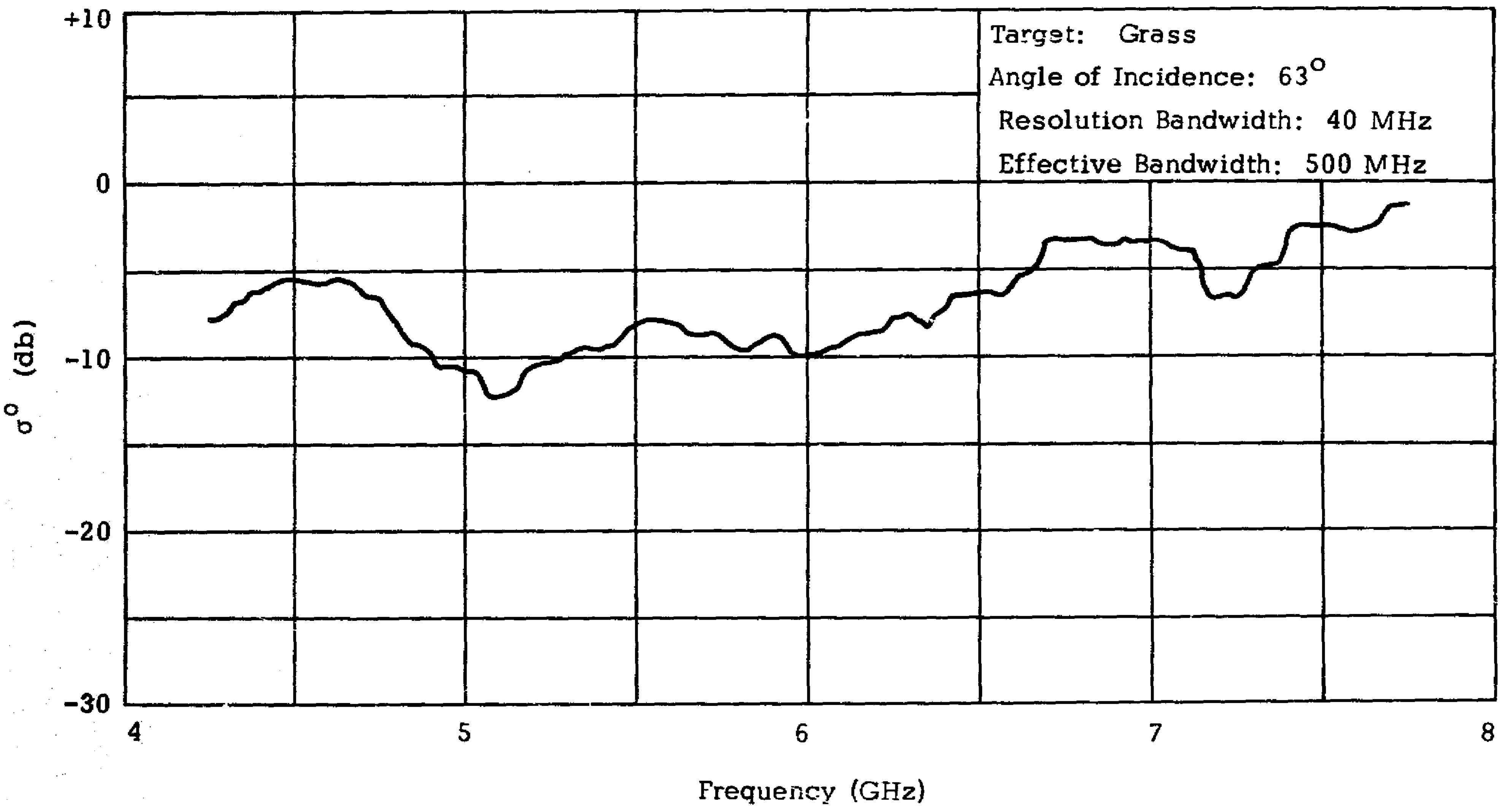

Figure 5.6 Spectral response of target 2.

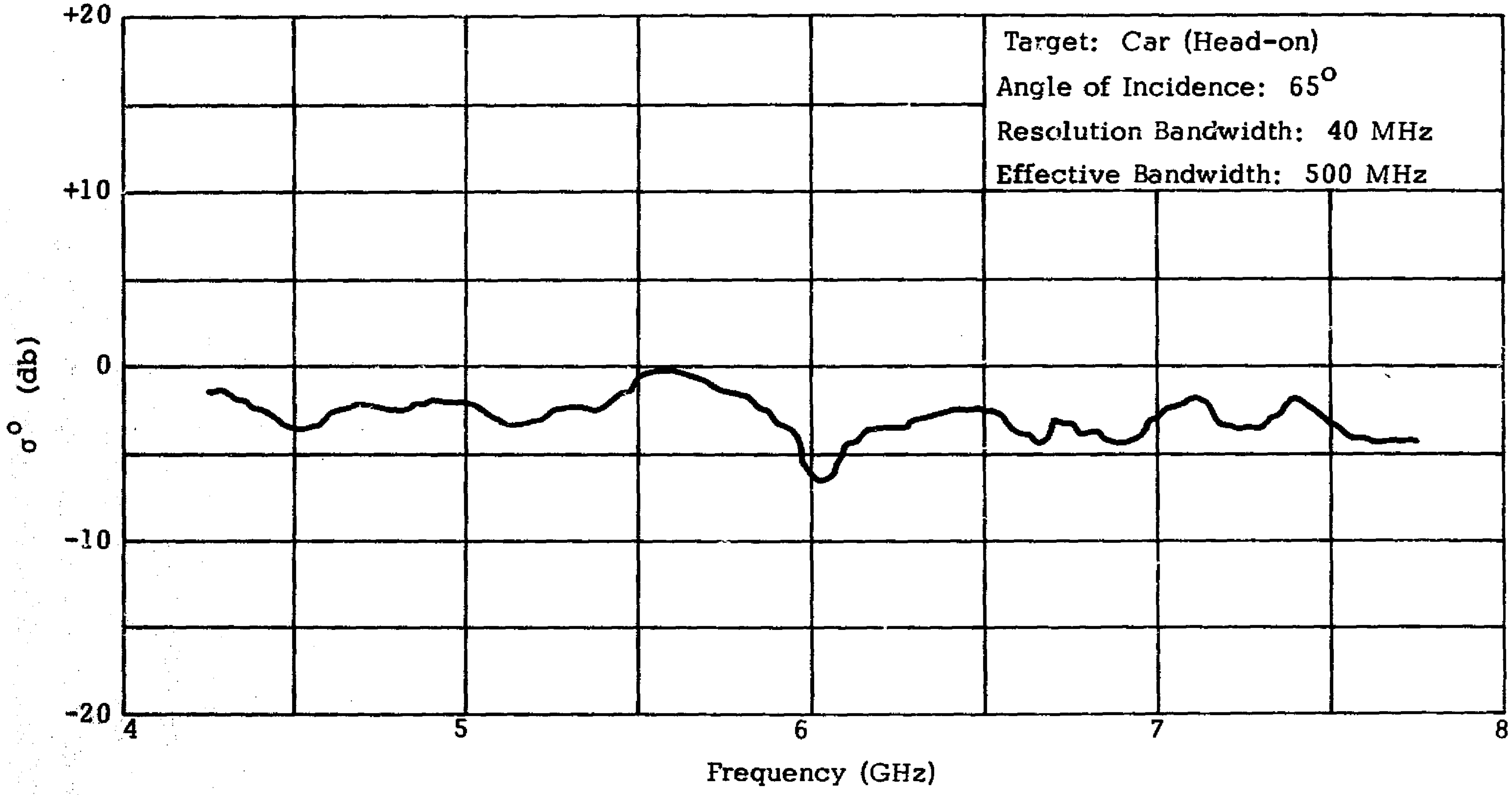

Figure 5.7 Spectral response of target 3.

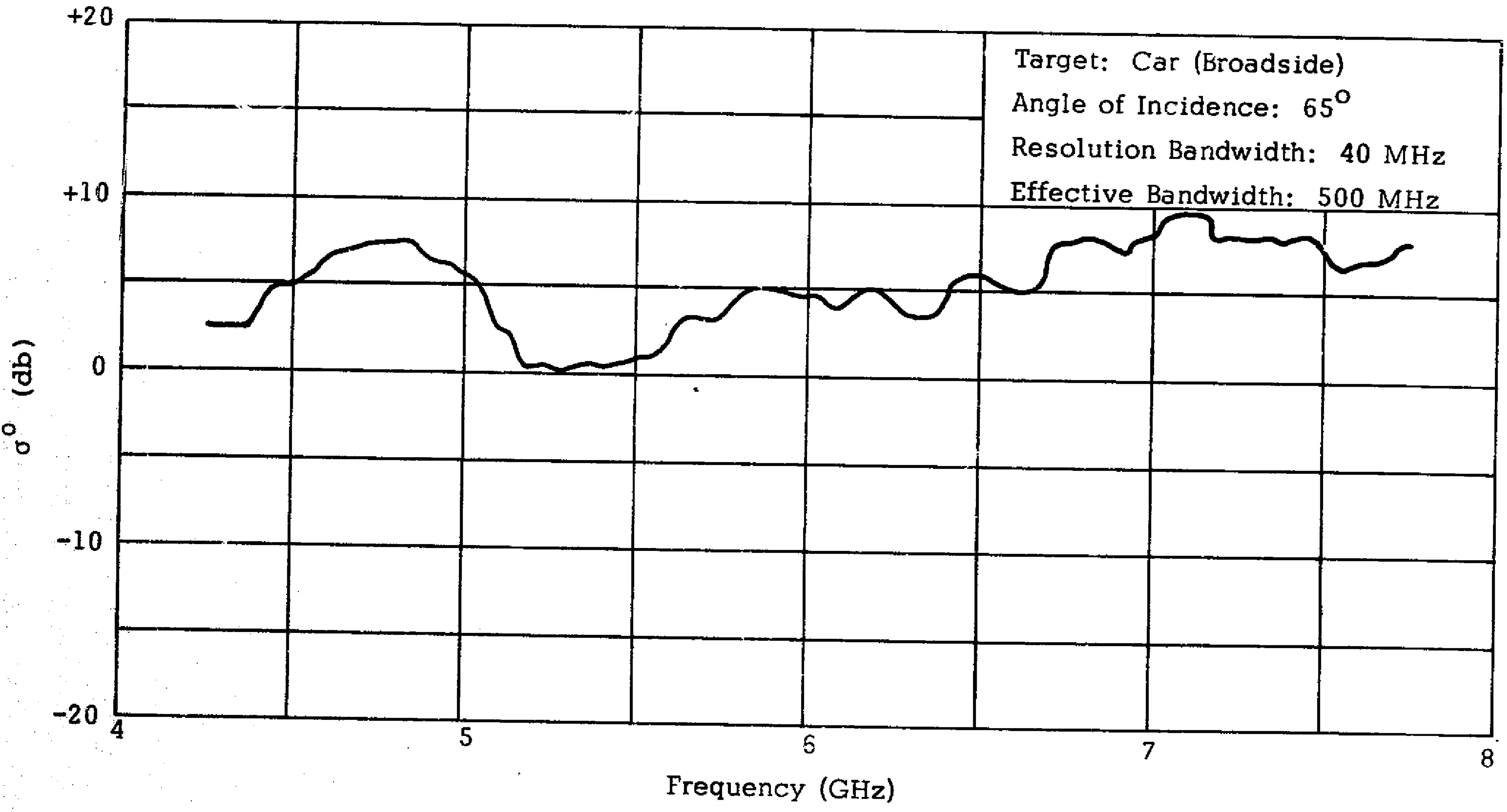

Figure 5.8 Spectral response of target 4

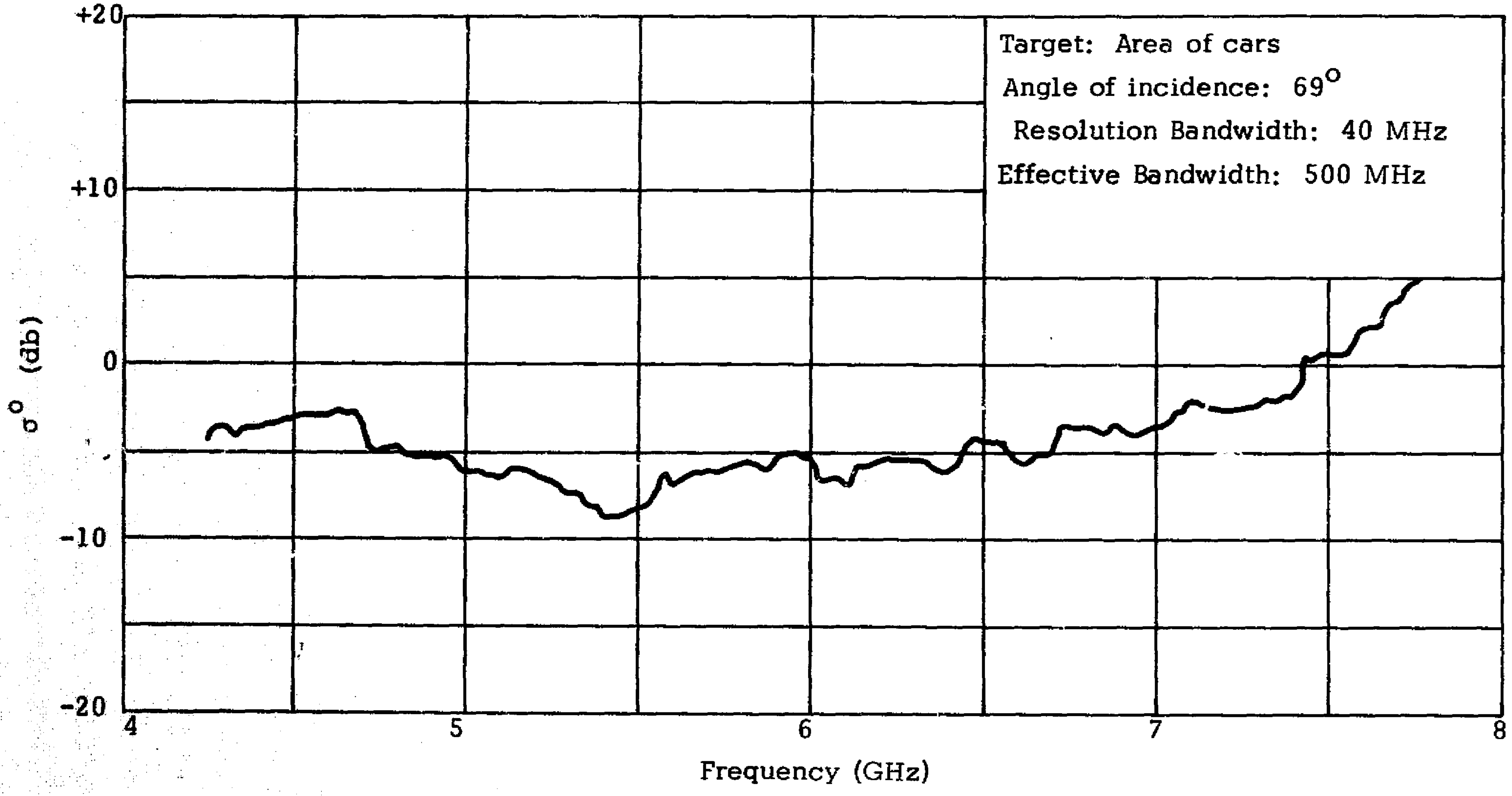

Figure 5.9 Spectral response of target 5.

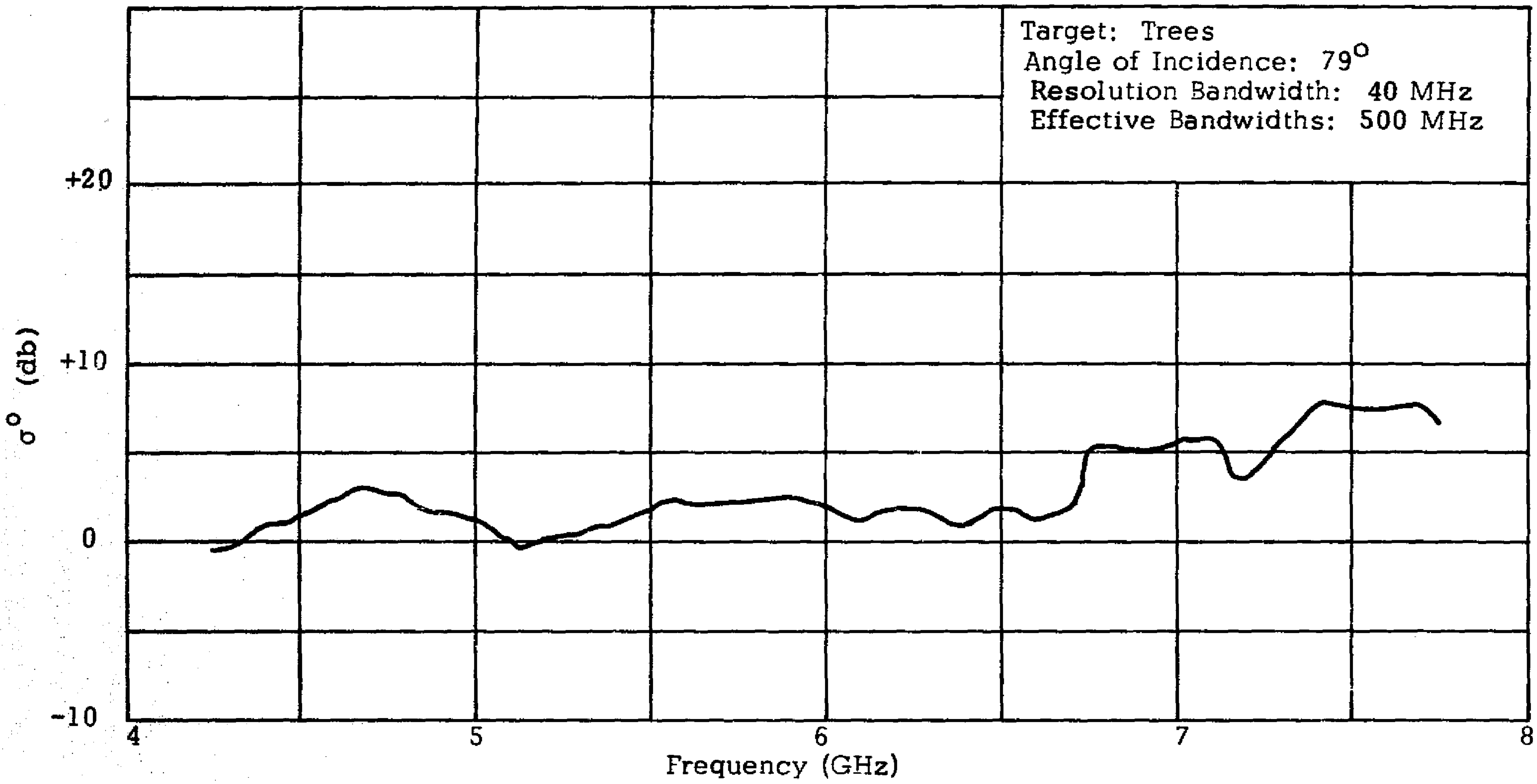

Figure 5.10 Spectral response of target 6.

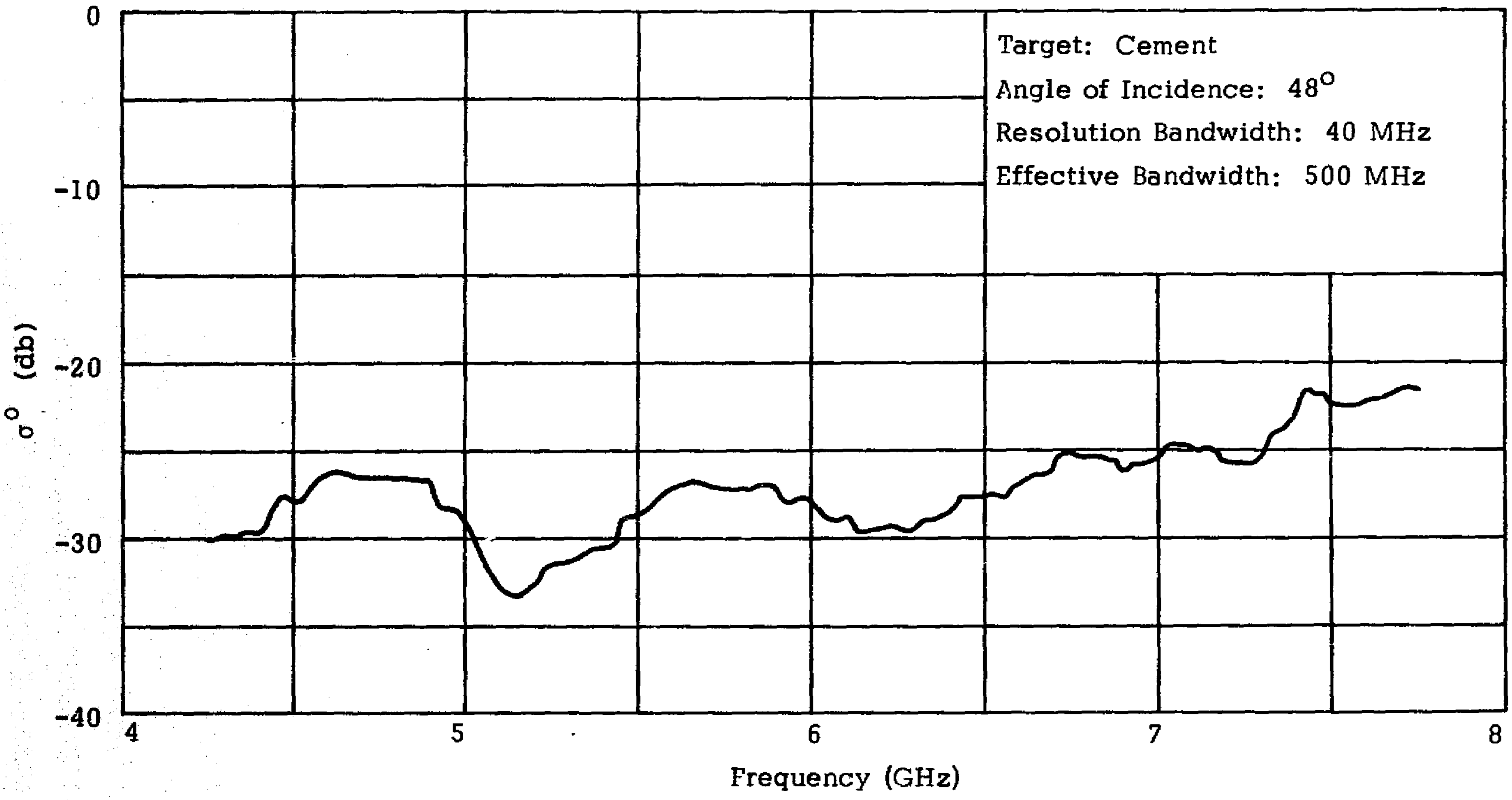

Figure 5.11 Spectral response of target 7.

5.3.1 Variance Reduction with Panchromatic Illumination

Frequency averaging will reduce the variance of the return signal, but the question remains: how much bandwidth is required for a given reduction of return variance and how well do the results and model of Chapter 3 predict the observed behavior?

The discrete scatterer model proposed in Chapter 3 was shown to give rise to a Rayleigh distributed return when monochromatically illuminated. The probability density functions shown in Figures 5.1 and 5.2 seem to indicate that the Rayleigh distribution is at least a reasonable approximation for the targets measured. However, the mean and variance figures shown in Table 5.1 seem to contradict this appearance for a Rayleigh power distribution has equal mean and variance. In addition, it was pointed out in Chapter 3 that a system with a resolving capability should actually have a ratio, $(\frac{\sigma}{\mu})^2$, of slightly less than one.

The answer to this contradiction lies in the frequency variation of the scattering cross-section noted in the spectral response curves. Figures 5.5 through 5.11. The calculations of mean and variance shown in Table 5.1 treat the data as a function of a single variable which is clearly not the case. Rather, the data represents at least a two-variable distribution where the variables are large and small scale variations of frequency. The distribution considered in Chapter 3 arises from relatively small changes in frequency which affect the relative phase between scattering centers in the resolution cell. However, no allowance was made for a change of scattering coefficient that may accompany frequency changes large enough to substantially alter the reradiation pattern and gain of the individual scattering elements.

To investigate the reduction of fading variance alone we must modify our calculation of variance to account for larger scale frequency variations. It would appear this might be done by fitting the data with a regression line and considering the variance about this regression line to represent the fading variation predicted by the theory of Chapter 3.

There still remains the choice of the type of regression analysis which should be used. From the spectral response curves it appears that at least two scales of variation are occurring above that of the fading. On a scale of a few hundred megahertz or less there appear to be appreciable resonance effects even with an effective bandwidth of 500 MHz. On an even broader frequency scale of at least a few gigahertz there appears a variation that might be attributed to the effective size of the scattering elements.

While a simple linear regression may suffice for those curves with no noticeable resonance effects, others will require a polynomial fit of the data. The selection of the degree of the polynomial is somewhat arbitrary and will directly affect the magnitude of the variance attributed to fading effects.

As an alternative to performing the regression analysis the variance was recalculated using an effective bandwidth curve of 1 GHz as an approximate regression line. The resulting mean, variance and their ratio are shown in Table 5.2.

The figures shown in Table 5.2 agree much better with those predicted by the analysis of Chapter 3. As expected, the greatest improvement is realized for those targets with the steepest slope in the spectral response characteristic. The ratios, $(\frac{\sigma}{\mu})^2$, are still somewhat larger than predicted; however, it is felt that this is due to differences between the resonance scale variation and the still larger scale approximately linear variation. The use of an effective bandwidth large enough to remove all resonance range effects gives approximately the same variance as the figures shown in Table 5.1. The use of a smaller effective bandwidth would undoubtedly yield better correlation for the figures of Table 5.2, however to go below 500 MHz would yield results of questionable validity as the approximate regression curve would actually be following to an extent the fading variations.

The improvement in return variance with increasing effective bandwidth is illustrated by the figures of Table 5.3. The figures shown are the predicted and measured improvement in $(\frac{\sigma}{\mu})^2$ between an effective bandwidth equal to the resolution bandwidth and the effective bandwidths shown.

TABLE 5.2
EXPERIMENTAL MEAN AND VARIANCE OF FADING DISTRIBUTION

Target	μ	σ	$(\frac{\sigma}{\mu})^2$
1	2.166	3.028	1.96
2	1.082	1.294	1.43
3	0.537	0.617	1.32
4	3.944	5.057	1.64
5	2.471	1.992	0.65
6	3.536	4.567	1.67
7	0.953	0.981	1.06

TABLE 5.3
MEASURED AND PREDICTED IMPROVEMENT IN VARIANCE AS A FUNCTION OF ILLUMINATION BANDWIDTH

	Eff. BW = 100 MHz		Eff. BW = 300 MHz		Eff. BW = 500 MHz	
	$(\frac{\sigma}{\mu})^2_{k=1}/(\frac{\sigma}{\mu})^2_k$		$(\frac{\sigma}{\mu})^2_{k=1}/(\frac{\sigma}{\mu})^2_k$		$(\frac{\sigma}{\mu})^2_{k=1}/(\frac{\sigma}{\mu})^2_k$	
Target	Predicted	Measured	Predicted	Measured	Predicted	Measured
1	2.0	1.5	5.3	3.9	8.8	6.1
2	2.0	2.4	5.3	6.4	8.8	9.2
3	2.0	2.3	5.3	5.5	8.8	6.9
4	2.0	2.0	5.3	5.0	8.8	6.5
5	2.0	2.4	5.3	4.9	8.8	7.9
6	2.0	1.9	5.3	3.9	8.8	5.3
7	2.0	2.0	5.3	4.6	8.8	6.3

While the agreement of the predicted and measured values is not precise it is reasonably close. This is to an extent to be expected since the analysis of Chapter 3 shows almost any averaging to follow an approximately linear decrease in $(\frac{\sigma}{\mu})^2$.

The results of the experiment conclusively show the benefit of panchromatic illumination. The agreement with the theory developed in Chapter 3 is not so apparent. This is felt to be a result of the additional frequency sensitivity ranges encountered rather than a deficiency of the model used to predict the fading variations. A truer test of both the value of panchromatic illumination and the applicability of the model would be provided with a system capable of absolute bandwidth variations over the range used and with the additional capability of positional averaging through relative movement. Such a system would be capable, at least for area extensive targets, of measuring an ensemble of homogeneous elements, thus reducing the resonance effects encountered here.

5.3.2 Spectral Response Curves

The investigation of the spectral response of radar target cross-section was undertaken in part to assay the potential signature content of such data. If recognition is to be attempted on the basis of these data the response must exhibit sufficient variation across the frequency range to discriminate between various targets. Examination of the spectral response curves of Figures 5.3 through 5.11 shows there to be distinct differences in the response characteristics of the different targets.

Let us for the moment ignore the differences in mean level between the curves and concentrate on the shape of the response characteristic. It appears that the variations shown occur on three different frequency scales. First is the very fine scale fading variation discussed in the previous section. This is seen to still be quite prevalent in the curves for 100 MHz effective bandwidth. In the curves for 500 MHz effective bandwidth we may assume that the fine scale fading variations have essentially been removed by the averaging. We note, however, that the variations remaining still have two distinct frequency scales. Apparently there are resonance effects that give pronounced variations on a scale of a few hundred megahertz. Superimposed on this resonance characteristic is still another variation on a scale of at least a few gigahertz. This latter trend was in the previous section attributed to the frequency sensitivity of the individual scattering elements.

To attempt recognition on a frequency scale that still contains appreciable fading variation appears to be a hopeless task. Either of the two broader scale variations might be used in an attempt to define spectral signatures. However, the resonance region variation, on a scale of a few hundred megahertz, would in all likelihood be overly sensitive to slight changes in target configuration or orientation. In addition, calibration of this range will be much more difficult than that of the broader scale.

It appears that recognition of spectral response characteristics would be both easier and more meaningful if the variations considered are on the scale of at least one gigahertz. To further investigate this scale of variation the spectral response curves of all targets were replotted with an effective bandwidth of 1 GHz. These curves are shown in Figures 5.12 and 5.13. Differences between the targets measured are still readily apparent on this scale.

Before proceeding further with possible recognition schemes for the spectral response characteristic let us review the most universal means of spectral response recognition, namely the perception of color in the visual region. The great variety of color as perceived by the human eye arises from spectral response variations across a region less than one octave wide. The receptor of this information is sensitive to a wavelength range of only 0.4 to 0.7 microns.

The instrument most often used to detect visual range response variations is the camera with color film. Colors are produced, in the case of film at least, by separating the response of the region into three response ranges which are appropriately dyed and weighted to produce a result

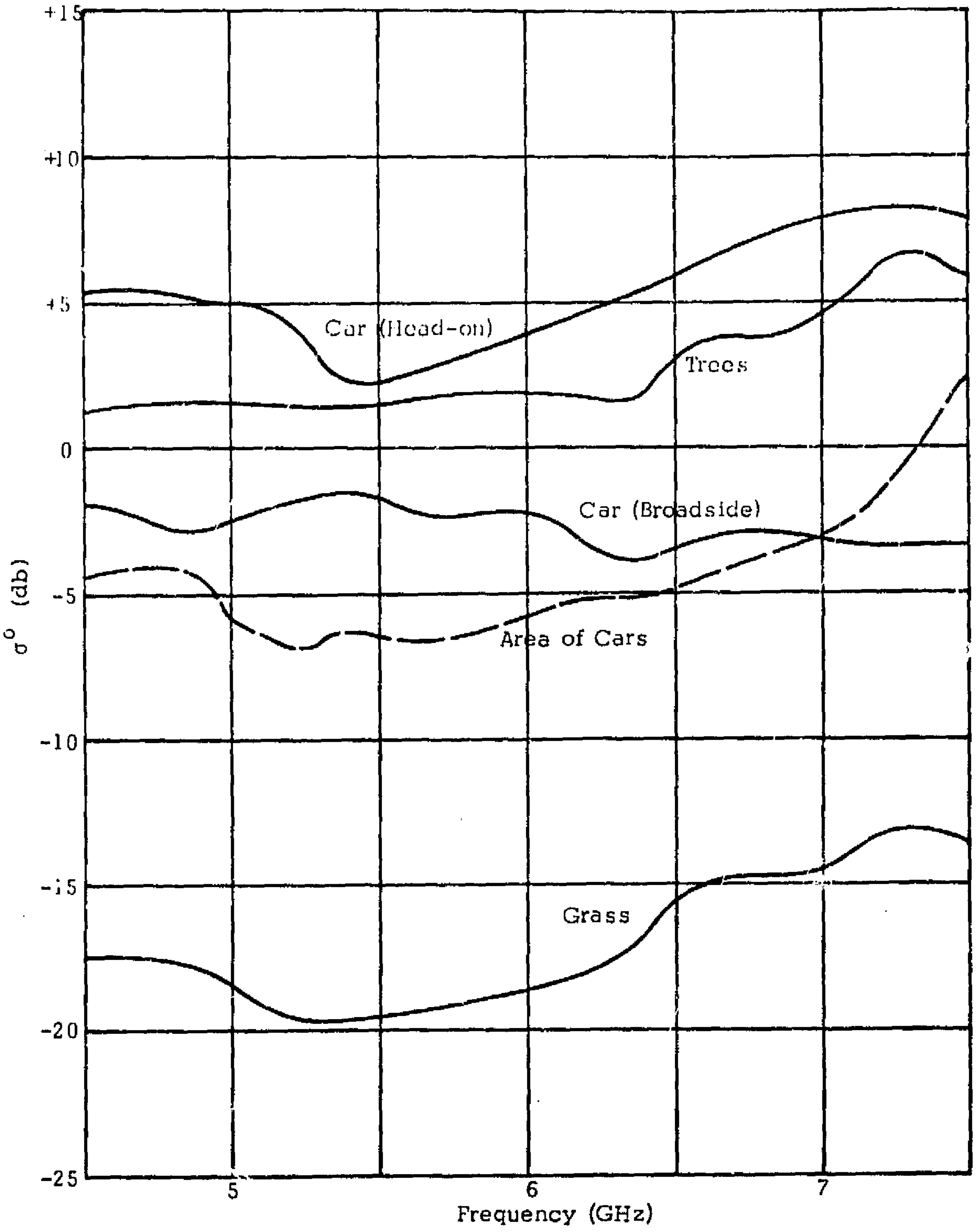

Figure 5.12 Spectral response with 1 GHz effective bandwidth.

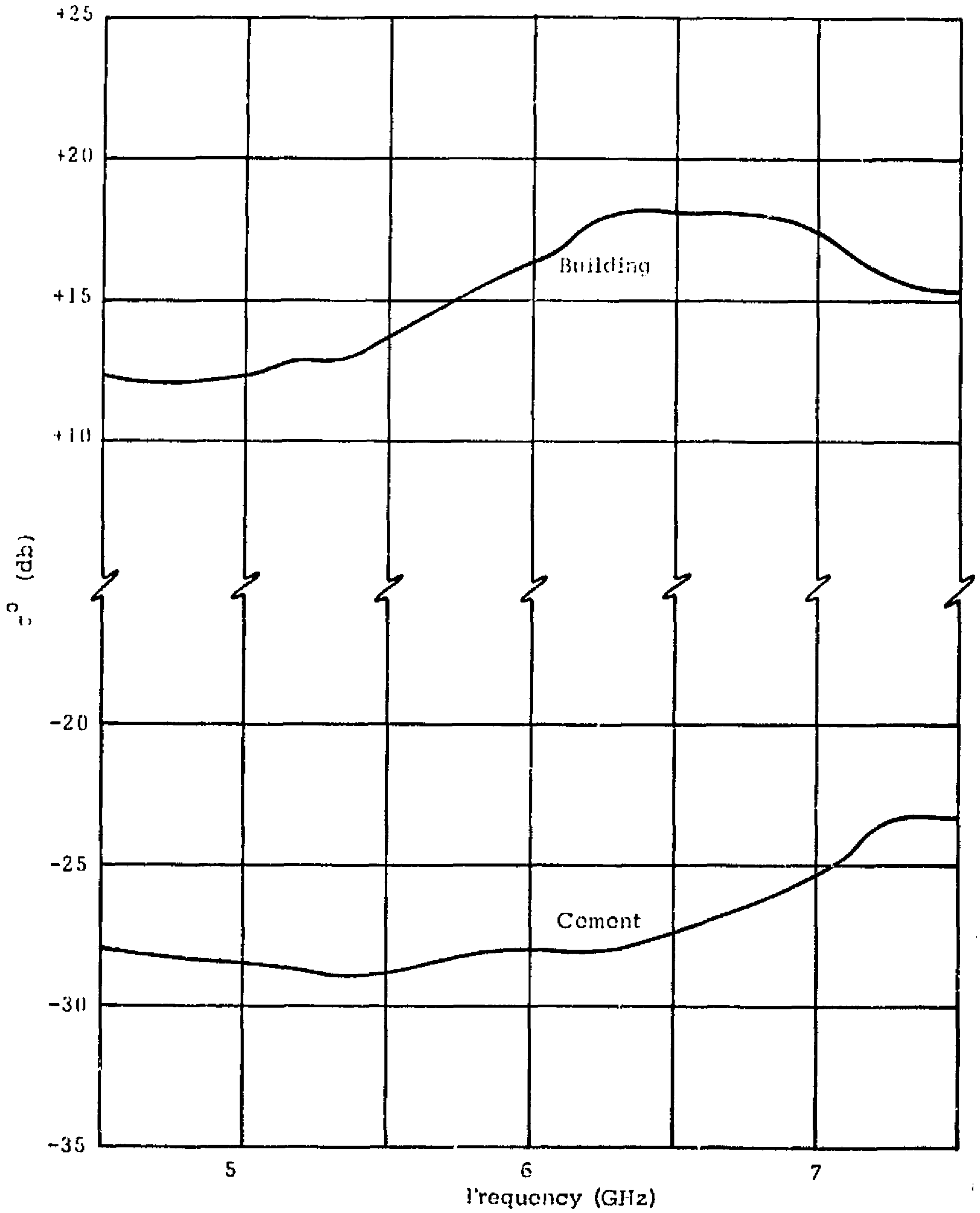

Figure 5.13 Spectral response with 1 GHz effective bandwidth.

equivalent to that perceived by the eye. Figure 5.14 illustrates the inherent color sensitivities of a three-layer film and the effective color separation of the emulsion layers (Sorem, 1967).

The type of response variation that is sensed by either film or eye is illustrated by the spectral reflectance curves of Figures 5.15 and 5.16 (Gates, 1970; Holmes, 1970). At first glance it may appear that these curves have significantly more variation than the curves shown for the microwave region of the spectrum. However, it may be shown that this is principally due to differences in the conventional means of presenting spectral reflectance and radar cross-section data. While reflectance is normally shown on a scale of 0 to 100 per cent, radar cross-section data is normally presented on a compressed logarithmic scale. The effect of this scale difference may be illustrated by replotting the radar cross-section data of Figures 5.12 and 5.13 in terms of normalized ratios similar to those shown for the visual region. These curves are shown in Figures 5.17 and 5.18. The normalization of each curve was with respect to its own mean value across the range; thus, the absolute values between curves do not correspond and the curves should be compared in functional form only similar to those of Holmes (1970), Figure 5.16.

From the above it may be seen that the potential variation in the microwave region is easily as great as that currently being exploited in the ultraviolet, visual and infrared ranges. This is apparent from an investigation of only a single octave of the microwave spectrum. One may only guess what the potential may be if greater use is made of the microwave region with a range of perhaps ten octaves. The techniques of recognition applied in the visual region may easily be adapted for use in the microwave region as will be demonstrated in Chapter 6.

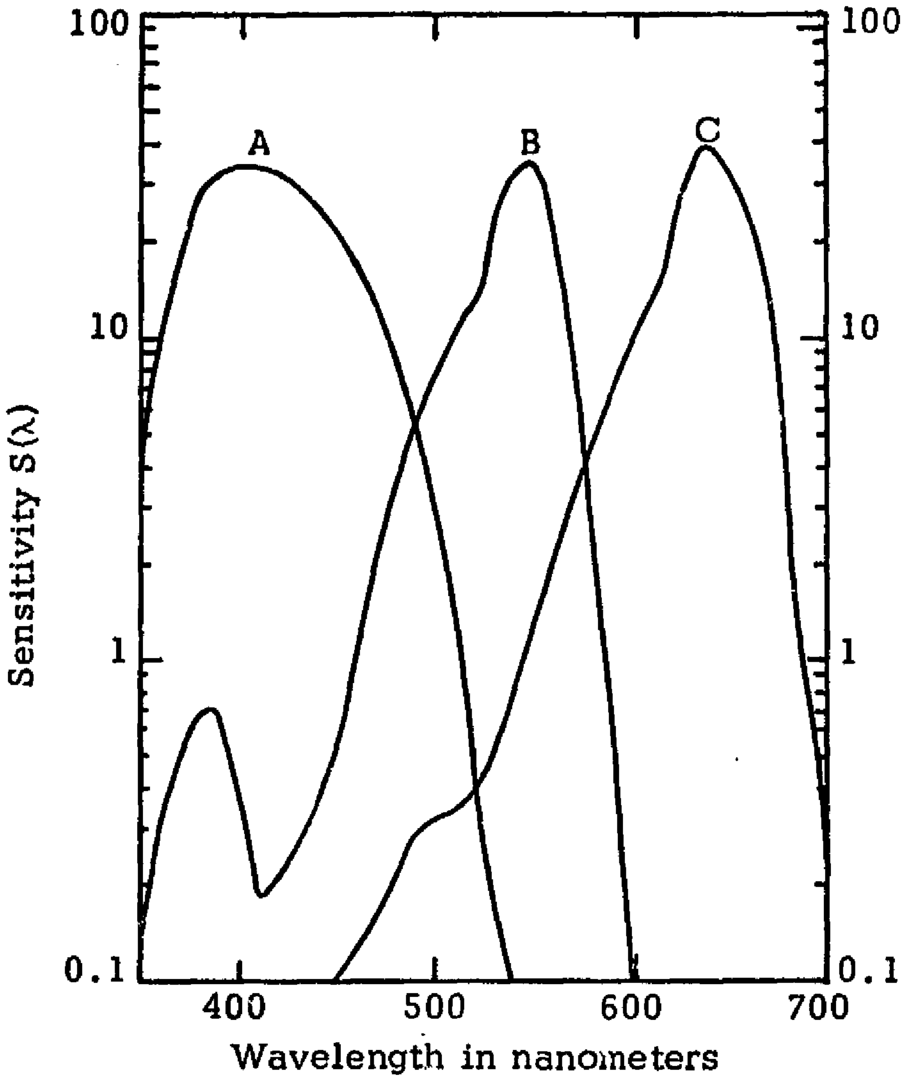

A - Yellow (blue producing dye)
B - Magenta (green producing dye)
C - Cyan (red producing dye)

Figure 5.14 Color film dye layer sensitivity ranges (from Sorem, 1967).

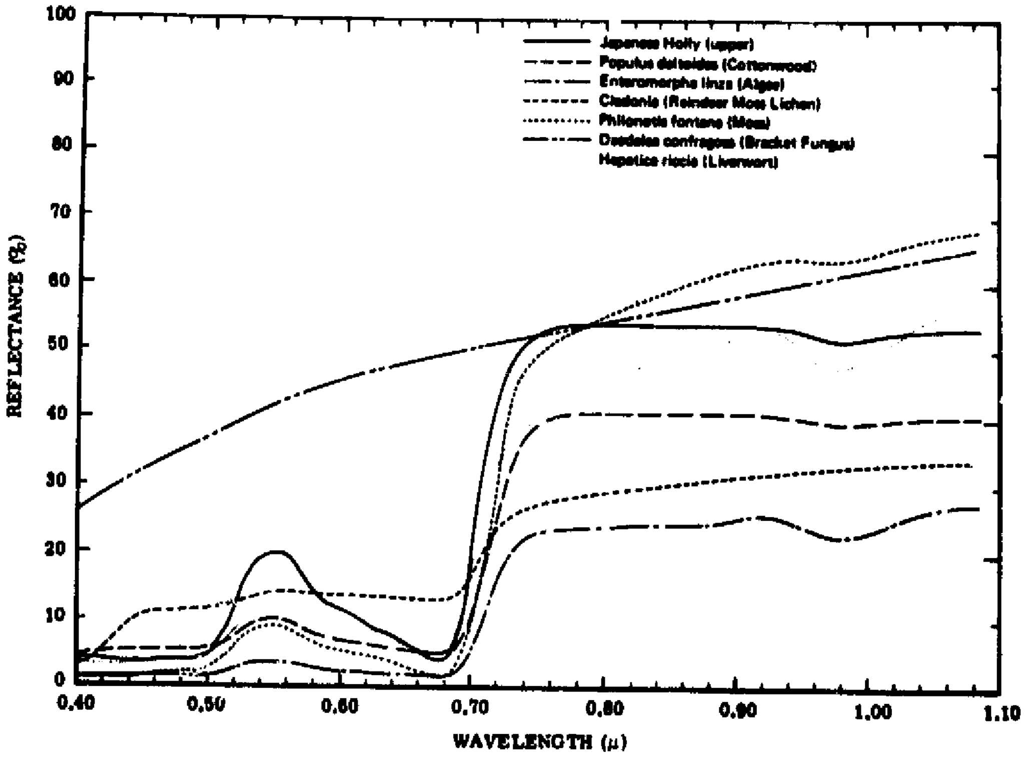

(a) Spectral reflectance of seven species of plants representing diverse groups.

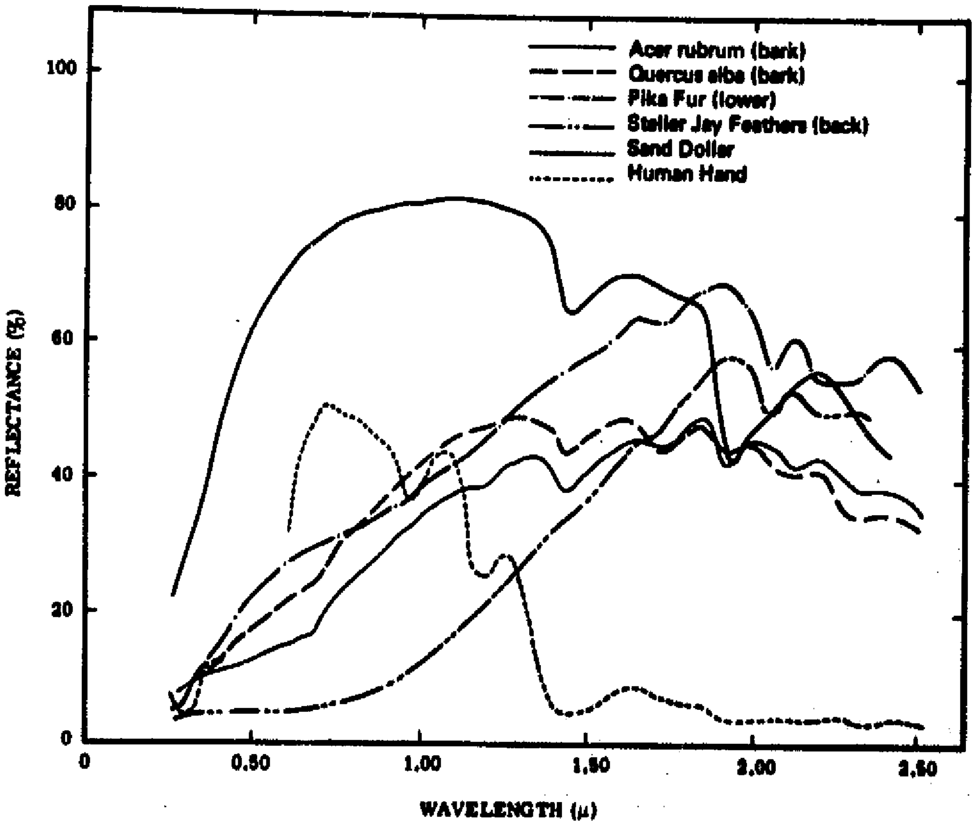

(b) Spectral reflectance of bark from two species of trees and parts of several animals.

Figure 5.15 Spectral response variations in the visual region (from Gates, 1970).

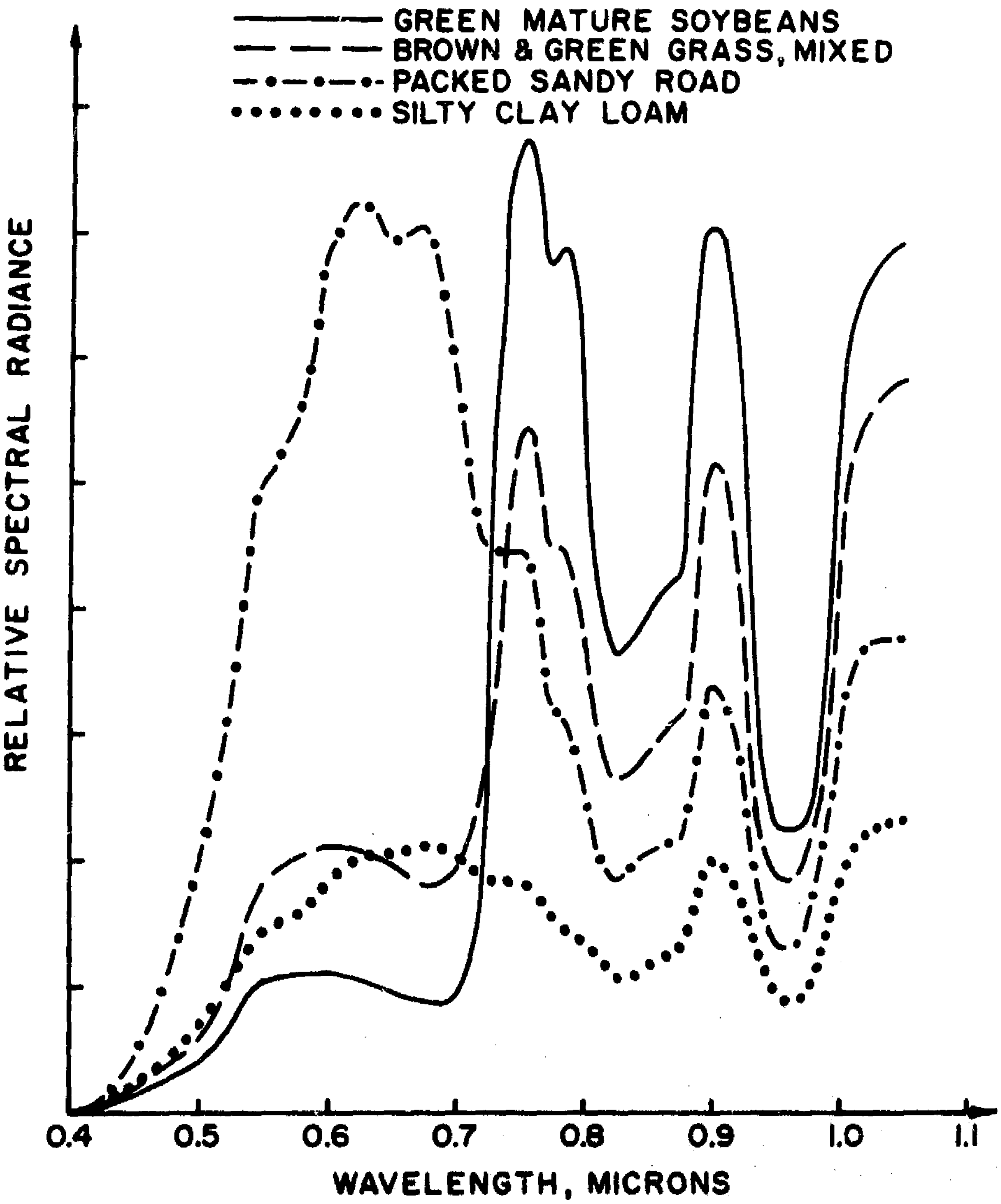

Figure 5.16 Relative spectral radiance spectra for agricultural scenes in the range of 0.4-1.05u, August 30, 1966, 11:50-11:56 a.m. Curves should be compared in functional form only; gain settings were changed between spectra (from Holmes, 1970).

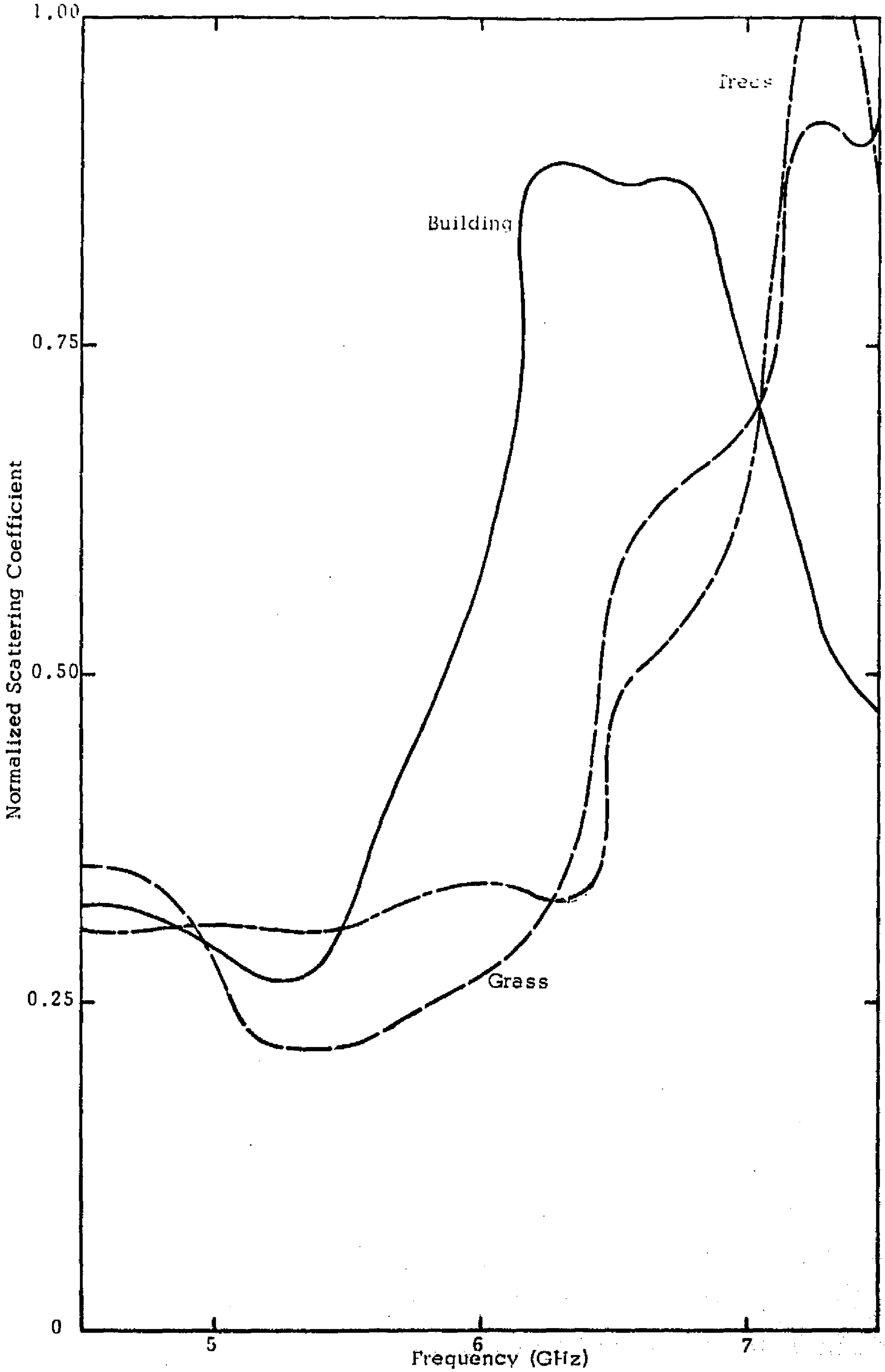

Figure 5.17 Normalized spectral response curves.

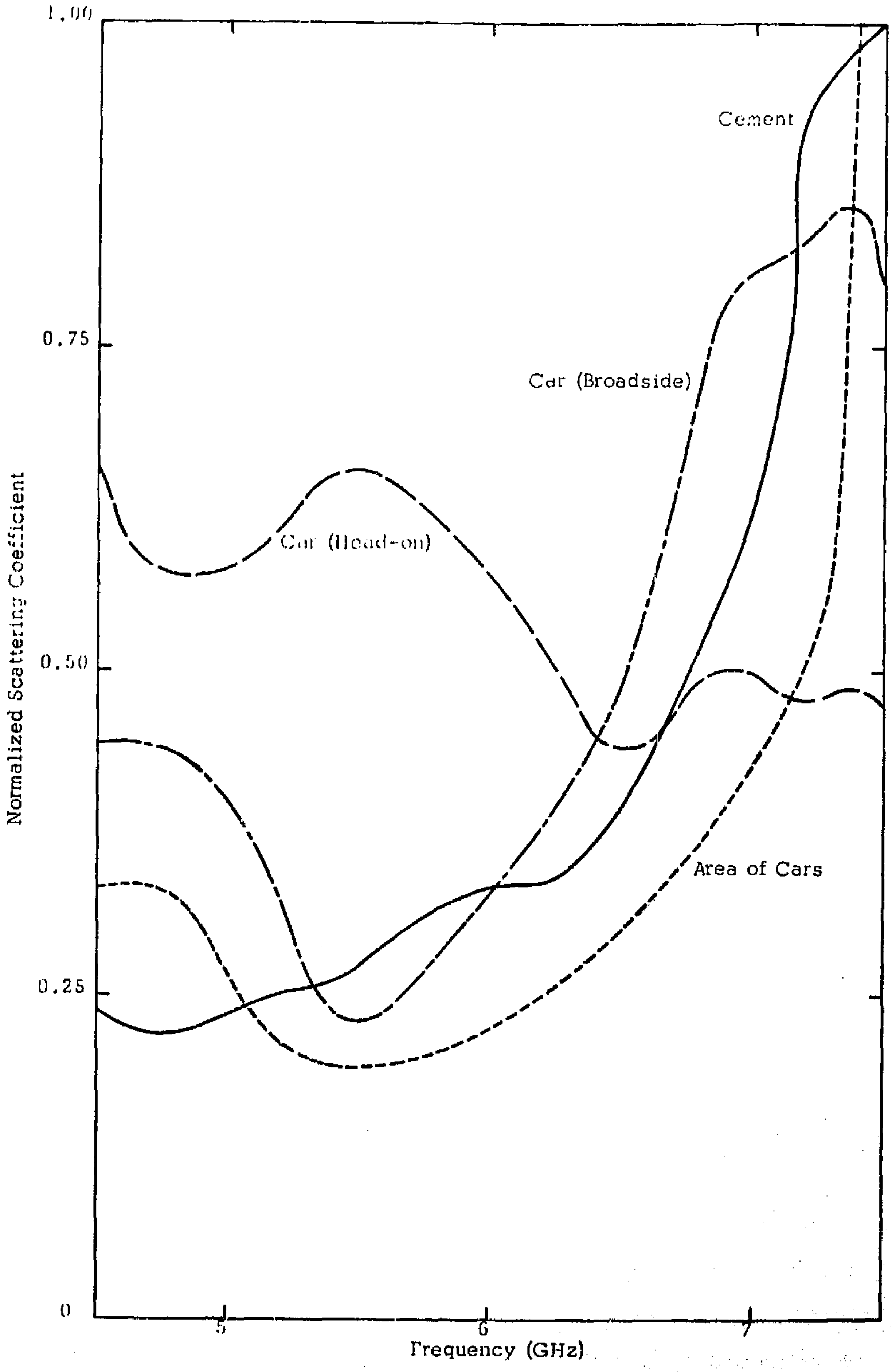

Figure 5.18 Normalized spectral response curves.

CHAPTER 6

IMAGING EXPERIMENT

The experimental results of Chapter 5 prove the original contention that frequency averaging may be used to reduce return variance and that spectral variations sufficient for recognition purposes are present in the microwave region. These results are not confined to any particular type of radar system and may find numerous applications. The application of these techniques to imaging radar systems was selected for demonstration as having great utility and giving a vivid and graphic presentation of the results.

In recent years the use of imaging radar systems for military reconnaissance and geoscience investigations has expanded rapidly (MacDonald, 1969; Wing, 1970). The imaging system provides an excellent example of the image improvement afforded by frequency averaging. A fully focused monochromatic synthetic aperture system obtains a single sample of the positional fading distribution. This gives rise to a large return variance which is most striking in the case of the "salt and pepper" effect noted in images taken by fully focused synthetic aperture systems. This effect seriously hampers the utility of such systems for applications such as change detection or the delineation of homogeneous area. The addition of panchromatic illumination, or excess range bandwidth, yields additional independent samples of the return distribution and thus reduces return variance and the scintillation noted in imagery of even homogeneous area extensive targets. Panchromatic illumination provides the radar imaging system designer another degree of freedom in his balancing of trade-offs between such parameters as swath width, power, resolution, image, quality, etc.

The interpreter of radar imagery is interested in the recognition or identification of objects portrayed on the image. Much has been written regarding the use of a possible multispectral signature for the purposes of this identification. In addition, a number of current programs are investigating partitioning of the spectrum in the infrared, visible and ultraviolet regions as a means of accomplishing such recognition. The experiment conducted here was designed to show that an equivalent amount of signature information resides in the microwave region and that identification techniques such as the use of false color imagery are applicable here as well.

6.1 Measurement Technique

The method of obtaining images was briefly described in Chapter 4. The return signal is detected, amplified with a broad-bandwidth oscilloscope and applied to the cathode of another broad-bandwidth oscilloscope. The imaging oscilloscope is modulated with a horizontal deflection voltage proportional to the angular position of the azimuth axis of the antenna positioner while the vertical axis is modulated with a ramp voltage proportional to the system range. The large difference in sweep times produces a raster display with many essentially vertical range lines for each horizontal azimuth line. Each return pulse intensity modulates a single vertical line. The result is a conventional B-scan display where an angular illuminated sector is presented in a rectangular display with azimuth as the abscissa and range the ordinate.

The PRF of the system is set at 100 kHz while the azimuth scan rate is approximately ten degrees per second. This large difference in rate gives a separation of the vertical range lines far below the resolution capability of the CRT or the recording film. This results in an effective integration of successive pulses on the CRT-film combination. When panchromatic illumination is desired the frequency is swept at a rate such that the entire sweep range is covered in less time than that required to traverse an azimuth resolution cell. The PRF of the system was held constant during the production of all images shown here, thus the sample rate and effective transmitted power were the same for monochromatic and panchromatic illumination.

A few limitations of the system imaging capability should be kept in mind when viewing the data. As mentioned previously, the presentation is a conventional B-scan which distorts an illuminated angular sector into a rectangular format. The range bandwidth of the system in imaging operation is constrained by the amplifying oscilloscope to approximately 25 MHz maximum. The combination of a relatively low system altitude and the use of a conical beam antenna prevents imaging of any appreciable range near grazing. At lower incidence angles the vertical beamwidth of the antenna confines the illuminated sector to a very narrow range dimension. With the above limitations on imaging operation it should be realized that the images shown here are not presented as a calibrated data format, but rather are intended merely to demonstrate the potential application of panchromatic and polypanchromatic illumination to airborne imaging systems.

The system was operated with a conical beam antenna of approximately 3.2° beamwidth at the center frequency. The pulse width was 25 nsec., however, the full resolution capability of this pulse was not realized due to the bandwidth limitation of the amplifying oscilloscope. The depression angle used was approximately 10° which gives sufficient range illumination to provide reasonably extensive image coverage.

The area imaged is that shown in Illustration 5.2. The angular coverage is approximately 90° with the near range of the image commencing approximately at the highway and the far range extending to the space sciences building.

6.2 Measurement Results

The results clearly indicate the improvement of image quality and definition obtained by the addition of frequency averaging or panchromatic illumination. Figure 6.1 shows successive monochromatic images of the area made with no change in system parameters. Close examination of these images indicates differences even though there is no relative motion between system and target other than the slight amount provided by the wind. For the purposes of orientation the bright line labeled "A" on the image is the far bank of the highway with the overpass visible in the near range. The target labeled "B" is the Space Sciences Building measured in Chapter 5. The differences shown here with such limited movement indicate the difficulty of performing change detection or recognition with a monochromatic system.

For the purposes of comparison, Figure 6.2 shows a sequence of monochromatic images taken with slight differences in frequency. The changes due to the relatively minor motion caused by wind are indistinguishable from those produced by small changes in frequency.

Figures 6.3 through 6.5 illustrate the improvement possible with panchromatic illumination. Each figure shows a monochromatic image and two panchromatic images with effective bandwidths of 0.5 GHz and 1.0 GHz. The improvement in image quality is so obvious as to hardly require comment. The images of Figure 6.3 are centered about 4.5 GHz while those of Figures 6.4 and 6.5 are centered at 6.0 GHz and 7.5 GHz, respectively.

The three 1 GHz bandwidth images may be considered the three components of a polypanchromatic system. As such it should be possible to combine the information on a single image and perceive differences due to variations in the spectral response of the various targets. While an effort has been made to compensate for variations of system response between the three bands, the images should not be considered as having an absolute reference of better than about 3 db.

Figure 6.6 shows a color combination of the three panchromatic images shown. While the calibration of this image is crude at best, the variation of colors noted is an indication of the response recognition possible with polypanchromatic illumination.

Figure 6.7 is a sketch of the area imaged showing the relative target locations for the distorted B-scan images.

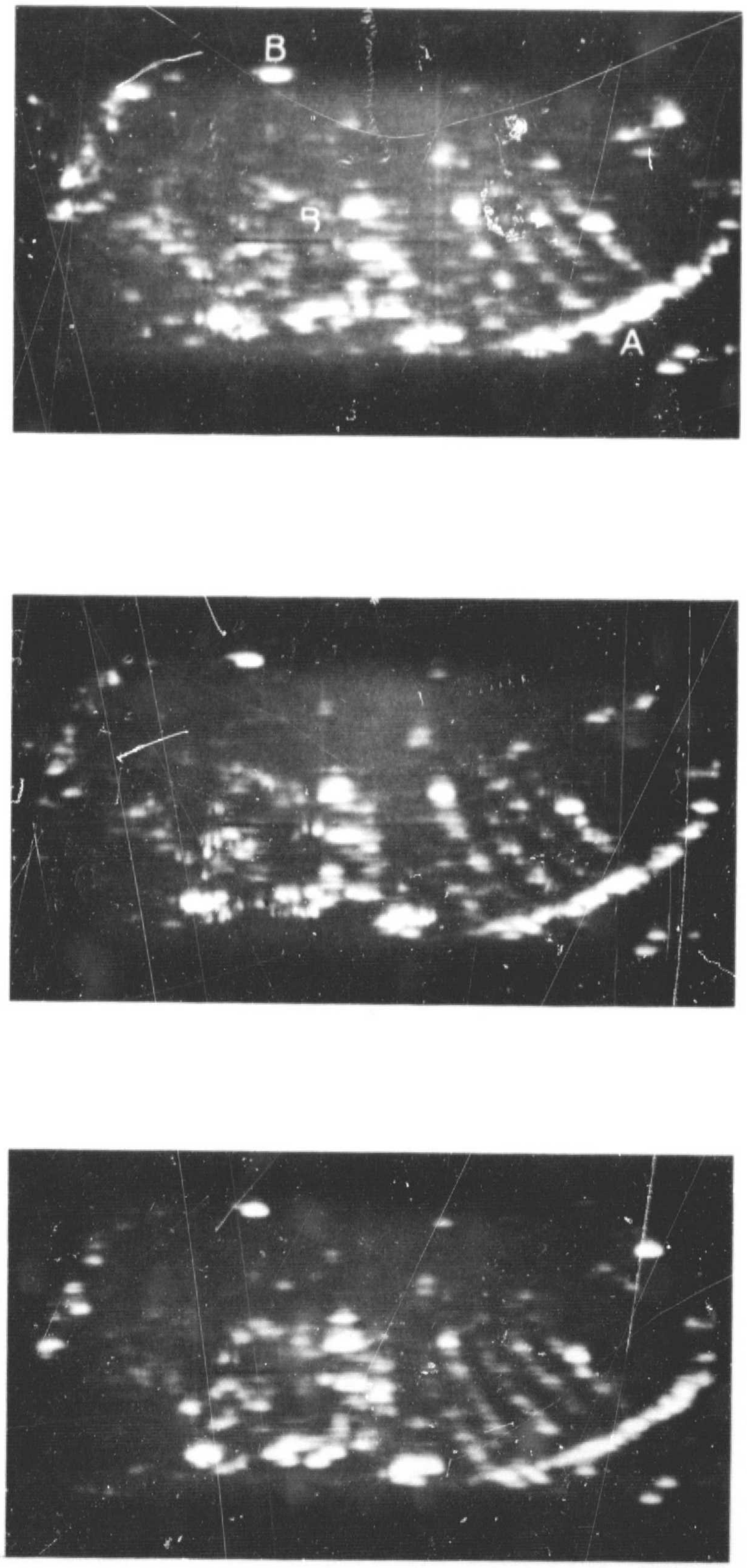

Figure 6.1 Successive monochromatic images made with no change in system parameters.

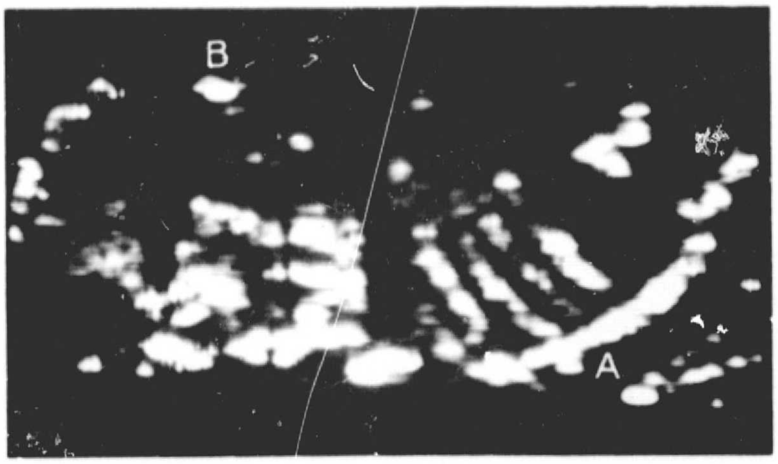

(a) f = 6.00 GHz.

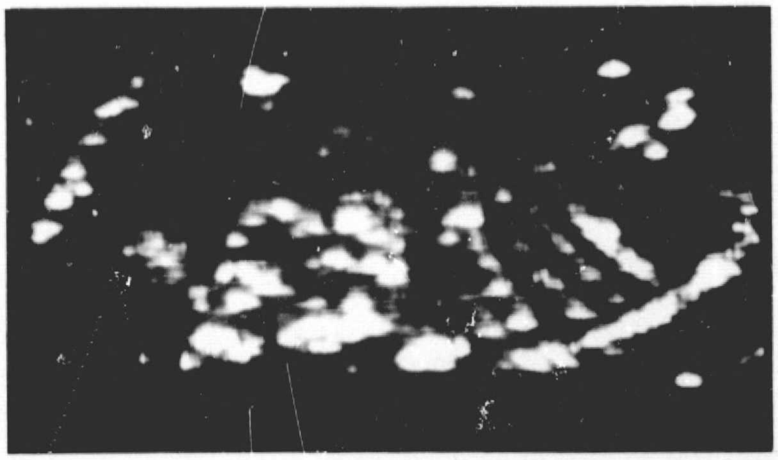

(b) f = 5.95 GHz.

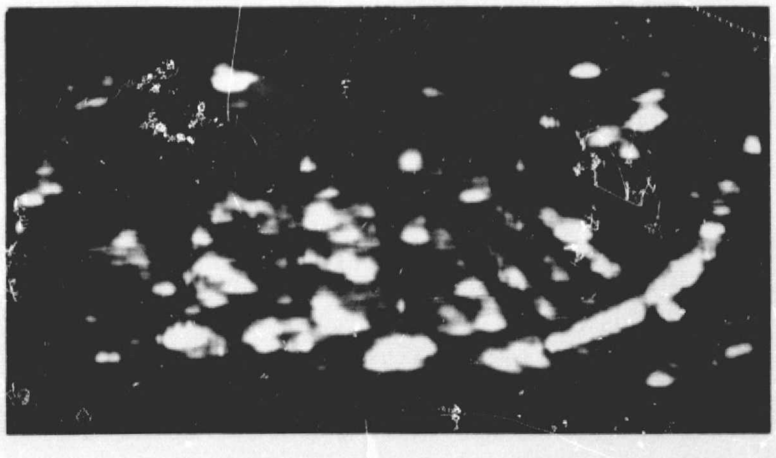

(c) f = 6.05 GHz.

Figure 6.2 Monochromatic images taken at slightly different frequencies.

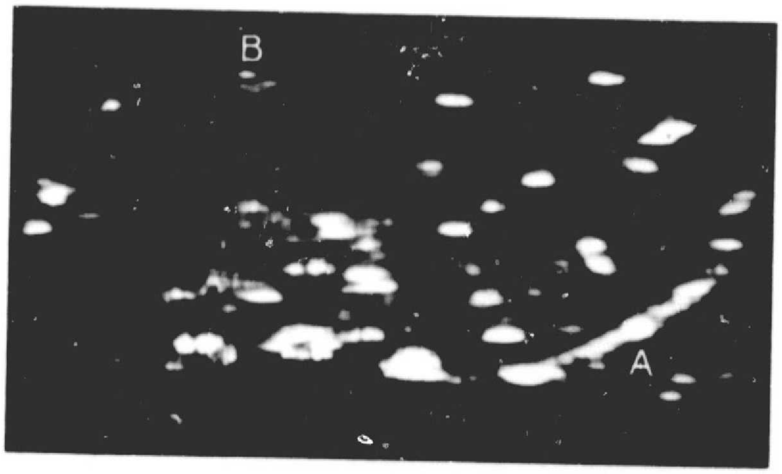

(a) Monochromatic f = 4.50 GHz.

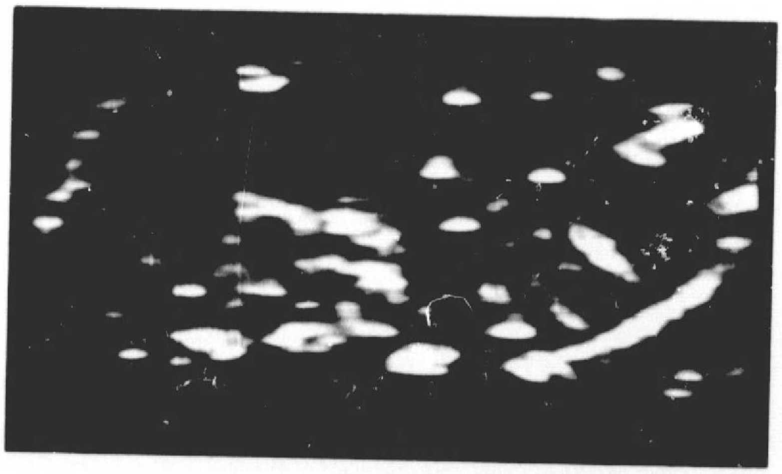

(b) Panchromatic f = 4.50 ± 0.25 GHz.

(c) Panchromatic f = 4.50 ± 0.50 GHz.

Figure 5.3 Comparison of monochromatic and panchromatic images.

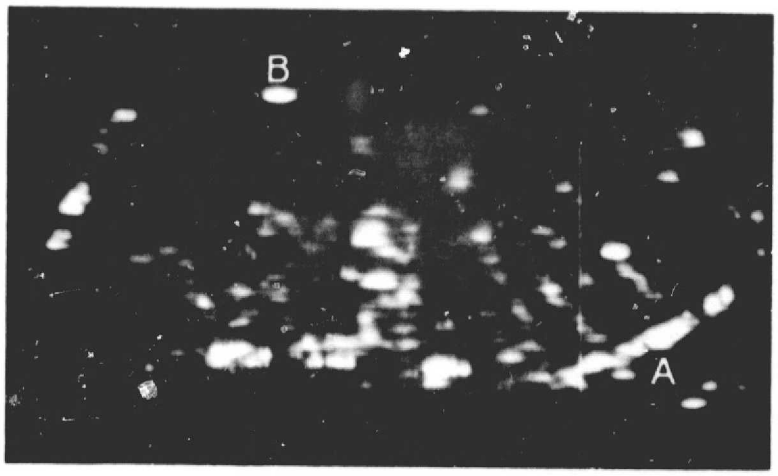

(a) Monochromatic f = 6.00 GHz.

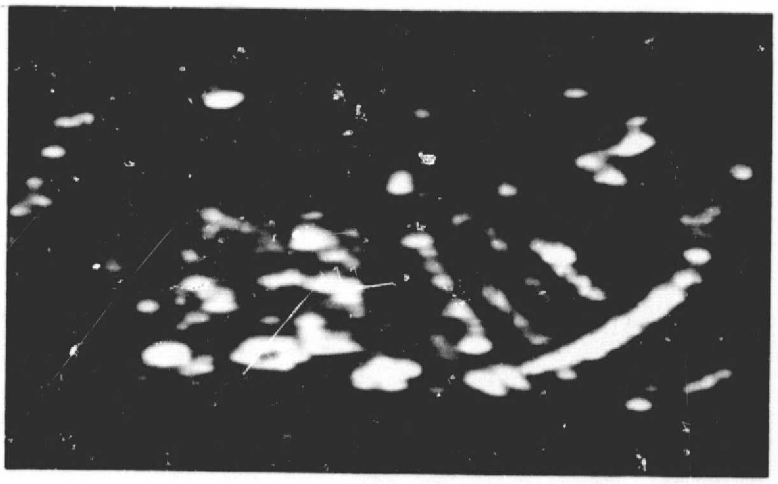

(b) Panchromatic f = 6.00 ± 0.25 GHz.

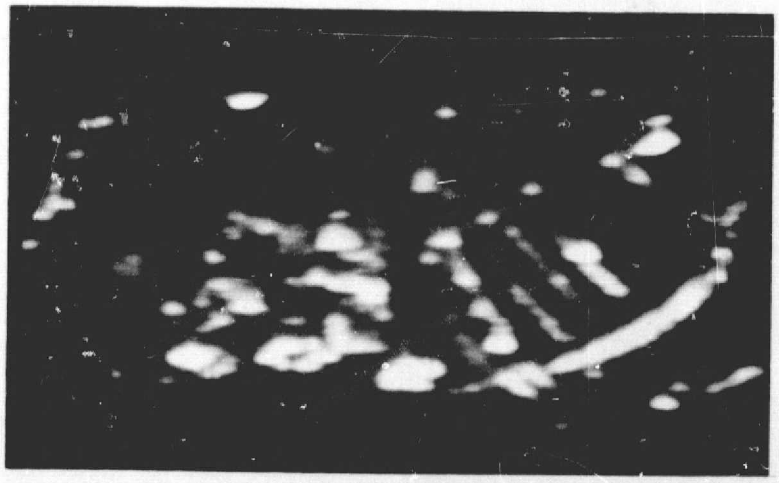

(c) Panchromatic f = 6.00 ± 0.50 GHz.

Figure 6.4 Comparison of monochromatic and panchromatic images.

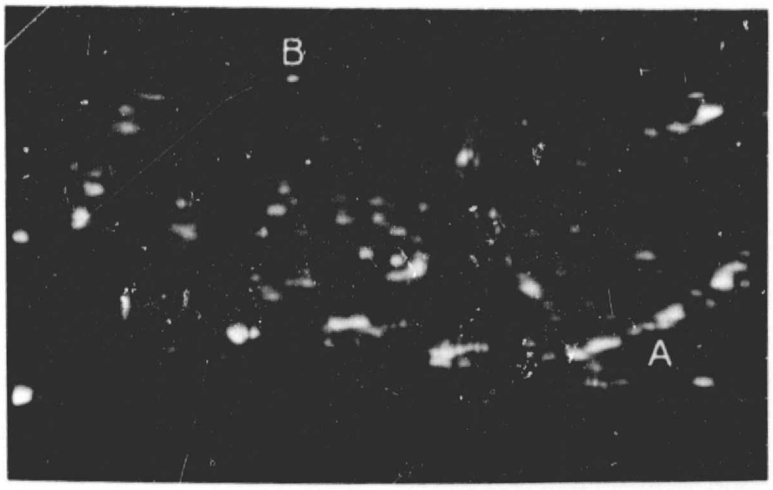

(a) Monochromatic f = 7.50 GHz.

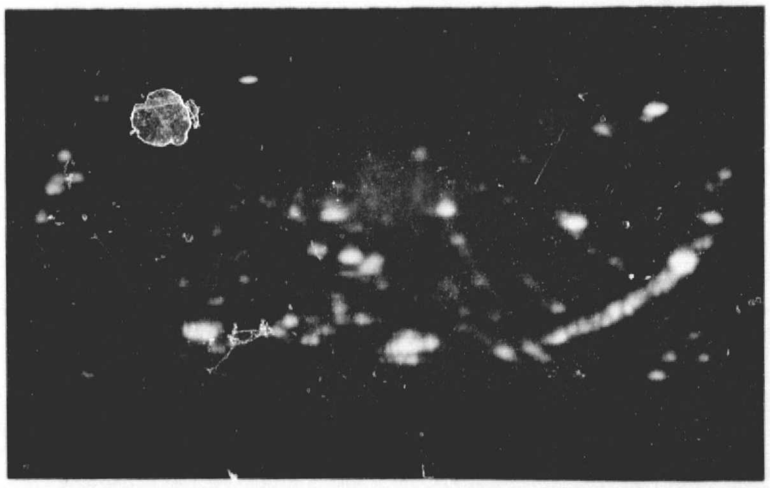

(b) Panchromatic f = 7.50 ± 0.25 GHz.

(c) Panchromatic f = 7.50 ± 0.50 GHz.

Figure 6.5 Comparison of monochromatic and panchromatic images.

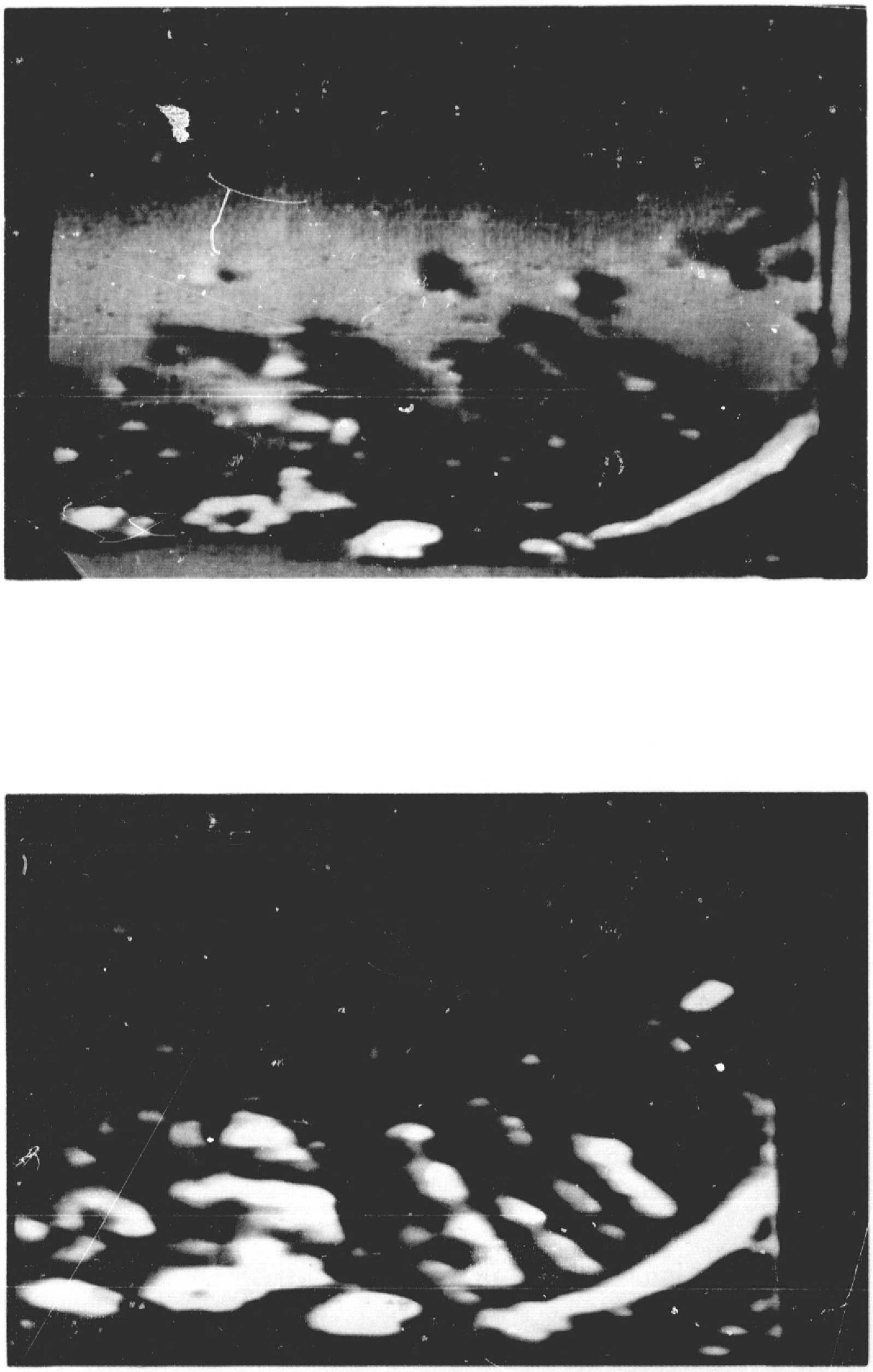

Figure 6.6 Polypanchromatic images.

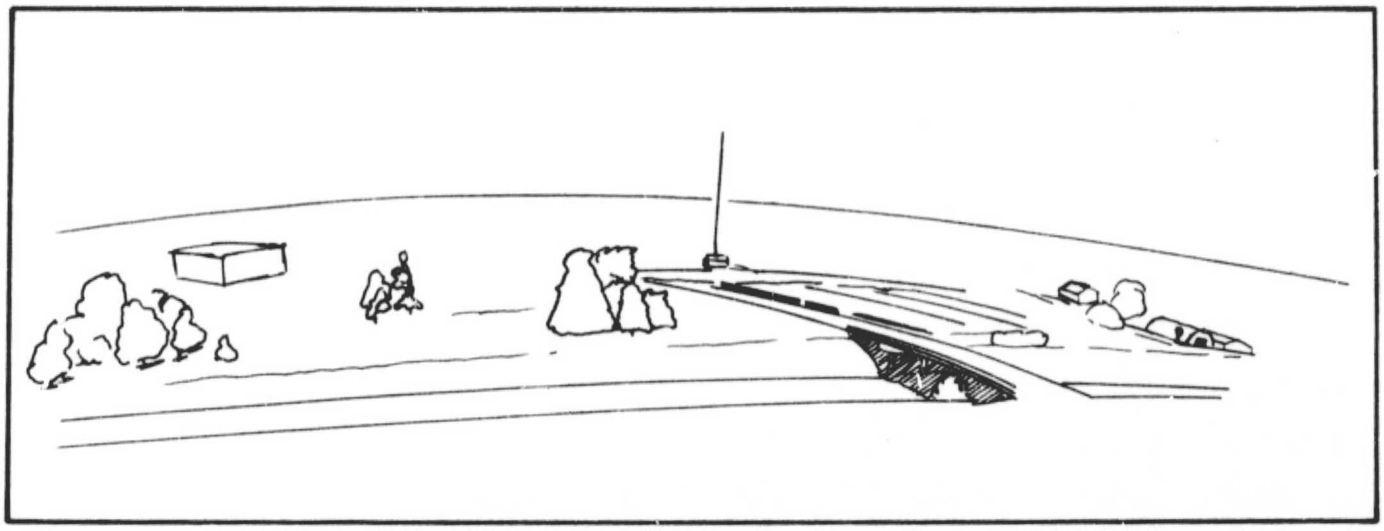

(a) Undistorted sketch of target area.

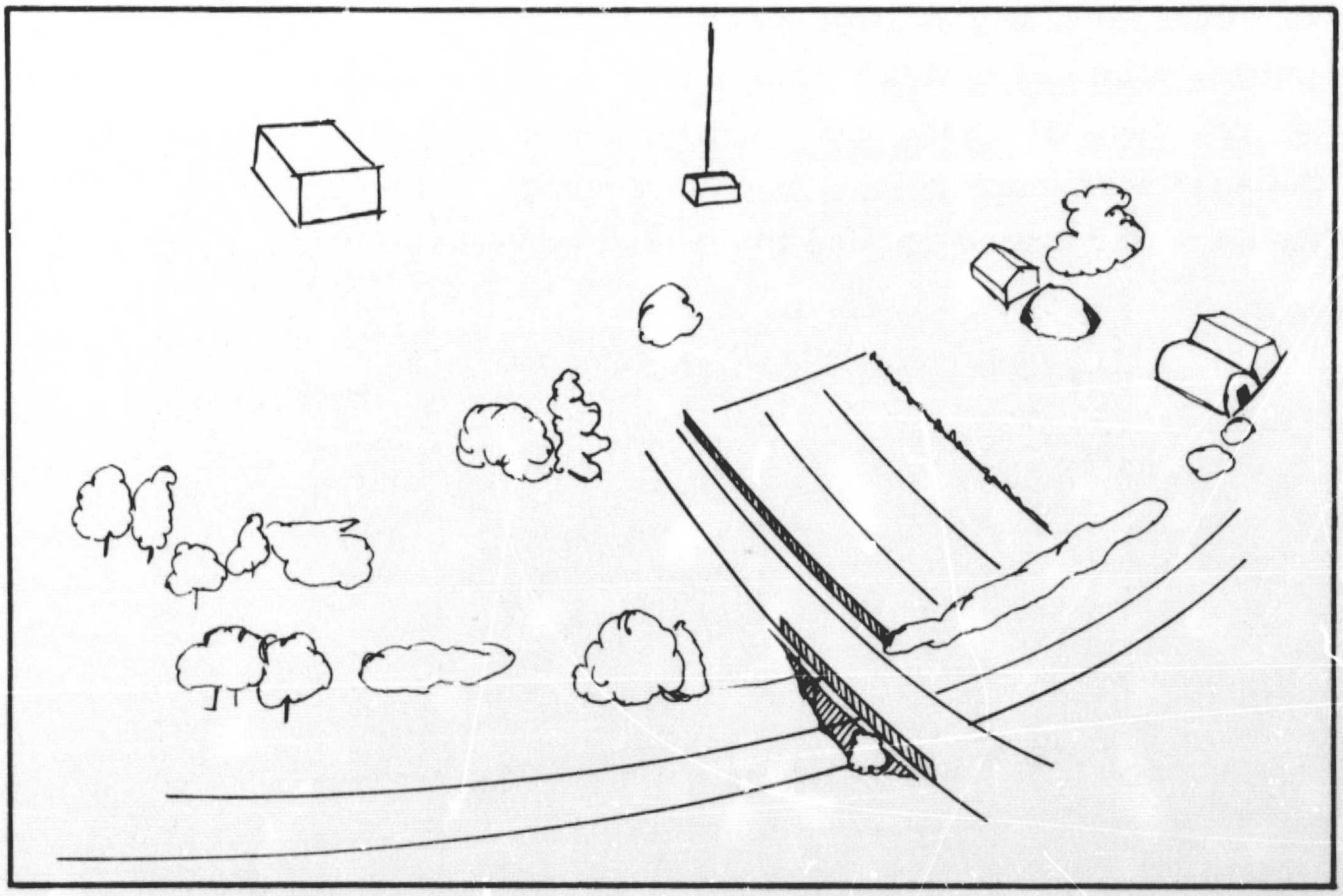

(b) Sketch of target area in B-scan geometry.

Figure 6.7 Relative target locations on B-scan imagery.

6.3 Discussion of Results

The results shown are largely self-explanatory. The images shown were obtained with far from optimum conditions. Namely, the resolution and dynamic range of the recording oscilloscope were marginal while the limited height of the system required operation over excessively high incidence angles. Despite these handicaps the improvement in image quality obtained with panchromatic illumination is quite striking. This is particularly evident in the recognition of linear features such as those shown in the parking lot just beyond the overpass. Additional increases of effective bandwidth are observed to improve the definition or fill, particularly of large complex targets.

The curves of spectral response variation shown in Chapter 5 illustrate the point that the variations encountered in the microwave spectrum are easily as large as those encountered in the visual spectrum. The potential use of this variation to produce color is at once immediate and obvious. The polypanchromatic color imagery shown demonstrates the ease with which color or any other recognition techniques used in the visual region may be applied to the microwave spectrum.

CHAPTER 7

CONCLUSIONS

The goal of this work was two-fold: first, to investigate the effects of frequency averaging upon the variance of the return signal; and second, to investigate the continuous spectral response of targets in the microwave portion of the spectrum and to compare this response with that observed in the visual region.

The frequency response of several targets was measured over a 4 GHz frequency range and with a sampling bandwidth of 40 MHz. The fine scale frequency variations (the frequency fading statistics) were measured and compared with those predicted by a theory based on a discrete isotropic scatterer model. The decrease of return variance with increasing illumination bandwidth was predicted quite well; however, the absolute value of the measured variance was higher than predicted for all targets. This discrepancy was attributed to additional resonance variations with broad scale frequency changes not taken into account by the theoretical model. The use of an approximate regression analysis for the calculation of the frequency fading variance substantially improved the agreement of measured and predicted absolute values.

The reduction in variance was shown to be essentially the same for a frequency averaging system and one operating at maximum resolution with post-detection integration. The advantage of the frequency averaging or panchromatic illumination is not in more efficient variance reduction but in possible decreased receiver and recording bandwidths.

The utility of frequency averaging was demonstrated by producing B-scan imagery of an area with both monochromatic and panchromatic illumination. The improvement in target and pattern definition obtained with the reduced-variance panchromatic illumination is obvious.

Examination of the spectral response characteristics led to the conclusions that at least three scales of variation with frequency were occurring: the fading variations predicted by the theory of a random scatterer model, a scale of a few hundred megahertz attributed to resonance phenomena, and a gigahertz scale variation attributed to changes of the reradiation pattern of the basic scattering elements.

Comparison of the observed microwave variations with those measured in the visual range revealed that the ranges of variations are comparable. The potential of color as a means of spectral response recognition is obvious. This is merely one example of a visual spectrum technique applied in the microwave region. The range of microwave variations shown indicate that virtually any multiparameter spectral recognition technique is applicable to the microwave spectrum.

The experiment performed resulted in defining a number of areas requiring further work. The most important of these are the following:

First and foremost is the need for additional continuous spectral response measurements in the microwave region. The measurement program should be expanded to cover a frequency range of at least 0.4 GHz to 35 GHz and must include a wide variety of target types.

Spectral response measurements over an ensemble of homogeneous target elements are needed to determine the effect upon the resonances noted. This will require a system with the additional capability of movement during measurement.

The application of panchromatic averaging to imaging radar systems will require further definition of the averaging means to take best advantage of the bandwidth compression to reduce system requirements and complexity.

APPENDIX A

DERIVATION OF AN IDENTITY

In equation (3.30) we encountered an expression of the form

$$E\left[|z_1|^2 |z_2|^2\right] \qquad (A.1)$$

where Z_1 and Z_2 are complex gaussian variables with zero means and uniform phase distributions.

By the use of the correlation coefficient, ρ, we may separate Z_2 into two orthogonal components.

$$z_2 = \rho z_1 + z_0$$

where

$$\rho = \frac{E[z_1 z_2^*]}{E[|z_1|^2]}$$

Since the process is gaussian, Z_1 and Z_2 are statistically independent. Thus we have

$$|z_1|^2 |z_2|^2 = |z_1|^2 |\rho z_1 + z_0|^2$$

$$= \rho^2 |z_1|^4 + |z_1|^2 |z_0|^2 + \rho |z_1|^2 z_1 z_0^* + \rho |z_1|^2 z_1^* z_0 \qquad (A.2)$$

and

$$E[|z_1|^2|z_2|^2] = \rho^2 E[|z_1|^4] + E[|z_1|^2]E[|z_0|^2]$$

$$+\rho E[|z_1|^2 z_1]E[z_0^*] + \rho E[|z_1|^2 z_1^*]E[z_0] \tag{A.3}$$

As the distribution has zero mean, the cross terms drop out leaving

$$E[|z_1|^2|z_2|^2] = \rho^2 E[|z_1|^4] + E[|z_1|^2]E[|z_0|^2] \tag{A.4}$$

It was shown in Chapter 3 that the envelope of a complex gaussian process with zero mean gave rise to the Rayleigh distribution function.

$$p(x) = \frac{x}{\alpha^2} e^{-x^2/2\alpha^2} \tag{A.5}$$

The fourth central moment of the Rayleigh distribution may be expressed as

$$E[x^4] = 2E^2[x^2] \tag{A.6}$$

Recall also that $z_0 = z_2 - \rho z_1$

We may now rewrite equation (A.4) as

$$E[|z_1|^2|z_2|^2] = 2\rho^2 E^2[|z_1|^2] + E[|z_1|^2]E[|z_2|^2] + \rho^2 E^2[|z_1|^2]$$

$$- E[z_1 z_2^*]\left\{E[z_1 z_2^*] + E[z_1^* z_2]\right\} \tag{A.7}$$

Recalling also that

$$\rho E[|z_1|^2] = E[z_1 z_2^*]$$

and that $E[z_1 z_2^*] = E[z_1^* z_2]$ we may write

$$E[|z_1|^2 |z_2|^2] = 3E^2[z_1 z_2^*] + E[|z_1|^2]\, E[|z_2|^2] \\ - 2E^2[z_1 z_2^*] \qquad \text{(A.8)}$$

and finally since $E[|z_1|^2] = E[|z_2|^2]$ we have

$$E[|z_1|^2 |z_2|^2] = E[z^2] + E^2[z_1 z_2^*] \qquad \text{(A.9)}$$

APPENDIX B

EVALUATION OF AN INTEGRAL

Equation (3.46) is given by

$$\sigma_{W_r}^2 = \frac{2\sigma_c^4}{\pi R}\int_0^{\pi R}\frac{\sin^2 x}{x^2}\left[1-\frac{x}{\pi R}\right]dx \tag{3.46}$$

Consider the integral

$$I = \frac{2}{\pi R}\int_0^{\pi R}\frac{\sin^2 x}{x^2}\left[1-\frac{x}{\pi R}\right]dx \tag{B.1}$$

Let

$$I = I_1 + I_2 = \frac{2}{\pi R}\int_0^{\pi R}\frac{\sin^2 x}{x^2}\,dx - \frac{2}{\pi^2 R^2}\int_0^{\pi R}\frac{\sin^2 x}{x}\,dx \tag{B.2}$$

Then

$$I_1 = \frac{2}{\pi R}\int_0^{\pi R}\frac{1-\cos 2x}{2x^2}\,dx \tag{B.3}$$

Integrate by parts letting

$$u = 1-\cos 2x \qquad du = 2\sin 2x$$

$$dv = \frac{1}{2x^2} \qquad v = -\frac{1}{2x}$$

$$I_1 = \frac{2}{\pi R}\left[\frac{\cos 2x - 1}{2x}\Big|^{\pi R} + 2\int_0^{\pi R}\frac{\sin 2x}{2x}\,dx \tag{B.4}$$

For I_2 we have

$$I_2 = \frac{2}{\pi^2 R^2} \int_0^{\pi R} \frac{\cos 2x - 1}{2x}\, dx \tag{B.5}$$

I is now

$$I = \frac{1}{\pi^2 R^2}\left[\cos 2\pi R - 1\right] + \frac{4}{\pi R}\int_0^{\pi R} \frac{\sin 2x}{2x}\, dx + \frac{2}{\pi^2 R^2}\int_0^{\pi R} \frac{\cos 2x - 1}{2x}\, dx \tag{B.6}$$

Let $\mu = 2x$ and $Q = 2\pi R$, then

$$I = \frac{4}{Q^2}\left[\cos Q - 1\right] + \frac{4}{Q}\int_0^{Q} \frac{\sin \mu}{\mu}\, d\mu + \frac{4}{Q^2}\int_0^{Q} \frac{\cos \mu - 1}{\mu}\, d\mu \tag{B.7}$$

Rational approximations are used for the sine and cosine integrals taken from National Bureau of Standards AMS 55, Handbook of Mathematical Functions with Formulas, Graphs, and Mathematical Tables. We have from here

$$Si(Q) = \int_0^{Q} \frac{\sin \mu}{\mu}\, d\mu = \frac{\pi}{2} - f(Q)\cos Q - g(Q)\sin Q \tag{B.8}$$

$$Ci(Q) = \gamma + \ln Q + \int_0^{Q} \frac{\cos \mu - 1}{\mu}\, d\mu = f(Q)\sin Q - g(Q)\cos Q \tag{B.9}$$

where $\gamma = 0.57721567$ and

$$f(Q) = \frac{1}{Q}\left[\frac{Q^4 + 7.241163\,Q^2 + 2.463936}{Q^4 + 9.068580\,Q^2 + 7.157433}\right] \doteq \frac{1}{Q}A \tag{B.10}$$

$$g(Q) = \frac{1}{Q^2}\left[\frac{Q^4 + 7.547478\,Q^2 + 1.564072}{Q^4 + 15.723606\,Q^2 + 12.723684}\right] \doteq \frac{1}{Q^2}B \tag{B.11}$$

We have finally for I

$$\begin{aligned} I &= \frac{4}{Q}\left\{ Si(Q) + \frac{1}{Q}\left[Ci(Q) - \gamma - \ln Q + \cos Q - 1 \right]\right. \\ &= \frac{4}{Q}\left\{ A\left[-\frac{1}{Q}\cos Q + \frac{1}{Q^2}\sin Q\right] - B\left[\frac{1}{Q^2}\sin Q + \frac{1}{Q^3}\cos Q\right]\right. \\ &\qquad \left. + \frac{1}{Q}\left[\cos Q - \ln Q - \gamma - 1\right] + \frac{\pi}{2}\right\} \end{aligned} \tag{B.12}$$

The program used to evaluate I for a range of values of R and Q is included.

```
      DIMENSION R(41)
      READ(5,1) (R(I),I=1,41)
    1 FORMAT(10(F.2))
      WRITE(6,3)
    3 FORMAT(1H1,8X,1HR,11X,1HQ,15X,3HSIQ,17X,3HCIO,18X,4HDARI)
      DO 10 K=1,41
      Q=R(K)*6.28318531
      A=((Q**4)+7.241163*(Q**2)+2.463936)/
     1((Q**4)+9.068580*(Q**2)+7.157443)
      B=((Q**4)+7.547478*(Q**2)+1.564072)/
     1((Q**4)+15.723606*(Q**2)+12.723684)
      SIQ-1.57079633-(A/Q)*COS(Q)-(B/Q**2)*SIN(Q)
      CIQ=(A/Q)*SIN(Q)-(B/Q**2)*COS(Q)
      DAIR=VARI(Q,A,B)
      WRITE(6,2)R(K),Q,SIQ,CIQ,DARI
    2 FORMAT(5X,F7.2,5X,F8.3,5X,E15.8,5X,E15.8,5X,E15.8)
   10 CONTINUE
      STOP
      END
```

```
      FUNCTION VARI(P,A,B)
      VARI=(4,O/P)*(1,57059633+A*((SIN(P))/(P**2)-(COS(P))/P)-B*((SIN(P)
     1)/(P**2)+(COS(P))/(P**3))+(1.0/P)*(COS(P)-1,57721567-ALOG(P)))
      RETURN
      END
```

BIBLIOGRAPHY

Ament, W. S., F. C. MacDonald, and R. D. Schewbridge, "Radar Terrain Reflections for Several Polarizations and Frequencies," Naval Research Laboratory, Unpublished Report, 1959.

Barrick, D. E., "Radar Signal Spectrum Distortions Produced by Volume and Surface Distributed Scatterers," Presented at USNC/URSI Spring Meeting, Washington, D. C., 1968.

Barton, D. K., Radar System Analysis, Prentice-Hall, New Jersey, 1964.

Beard, C. I. and I. Katz, "The Dependence of Microwave Radio Signal Spectra on Ocean Roughness and Wave Spectra," Trans. IRE AP-5, pp. 183-191, 1957.

Beasley, E. W., and H. R. Ward, "A Quantitative Analysis of Sea Clutter Decorrelation with Frequency Agility," Trans. IEEE AES-4, pp. 468-473, 1968.

Beckmann, P., "Scattering by Composite Rough Surfaces," Proc. IEEE 53, pp. 1012-1015, 1965.

Beckmann, P., "Shadowing of Random Rough Surfaces," Trans. IEEE AP-13, pp. 384-388, 1965.

Beckmann, P. and A. Spizzichino, The Scattering of Electromagnetic Waves from Rough Surfaces, The MacMillan Co., New York, 1963.

Birkemeier, W. P. and N. D. Wallace, "Radar Tracking Accuracy Improvement by Means of Pulse-to-Pulse Frequency Modulation," IEEE Trans. Comm. and Elec., pp. 571-575, Jan. 1963.

Blackman, R. B. and J. W. Tukey, The Measurement of Power Spectra, Dover Publications, Inc., New York, 1958.

Brekhovskikh, L. M., "The Diffraction of Waves by a Rough Surface," Part I, Zh. Eksper, i. Teor. Fiz. 23, pp. 275-289, 1952.

Chia, R. C., "The Theory of Radar Scatter from the Ocean," (Ph. D. Thesis) CRES Tech. Rept. No. 112-1, Univ. of Kansas, Lawrence, Kansas, 1968.

Cosgriff, R. L., W. H. Peake, and R. C. Taylor, "Terrain Scattering Properties for Sensor System Design," (Terrain Handbook II) The Ohio State University Engr. Exp. Sta. Bull. No. 181, Columbus, Ohio, 1960.

Dalke, G. W. and J. E. Estes, "Multi-Image Correlation Systems Study for MGI," CRES Tech. Rept. No. 122-4, University of Kansas, Lawrence, Kansas, 1968.

Davies, H., "The Reflection of Electromagnetic Waves from a Rough Surface," Proc. IEEE Pt. III 101, pp. 209-214, 1954.

Davies, H., "The Reflection of Electromagnetic Waves from a Rough Surface," Proc. IEEE Pt. III 102, p. 148, 1955.

Delano, R. H., "A Theory of Target Glint or Angular Scintillation in Radar Tracking, Proc. IRE 41, pp. 1778-1784, 1953.

Edison, A. R., R. K. Moore, and B. D. Warner, "Radar Terrain Return Measured at Near-Vertical Incidence," Trans. IRE AP-8, pp. 246-254, 1960.

Evans, J. V., "The Scattering of Radio Waves by the Moon," Proc. Phip. Soc. London 70, pp. 1105-1112, 1957.

Fung, A. K., "Scattering and Depolarization of Electromagnetic Waves by Rough Surfaces," (Ph. D. Thesis), CRES Tech. Rept. No. 48-5, University of Kansas, Lawrence, Kansas 1965.

Fung, A. K. and R. K. Moore, "The Correlation Function in Kirchoff's Method of Scattering of Waves from Statistically Rough Surfaces," J. Geophys. Res. 71, pp. 2939-2943, 1966.

Fung, A. K. and A. Leovaris, "Frequency Dependence of Ultrasonic Scatter from Statistically Known Rough Surfaces," WESCON Conv. Record, 1968.

Gates, D. M., Remote Sensing with Special Reference to Agriculture and Forestry, National Academy of Sciences, Washington, D. C. 1970.

Goldstein, H., "Frequency Dependence of the Properties of Sea Echo," Phy. Rev. 70, pp. 938-946, 1946.

Grant, C. R. and B. S. Yaplee, "Back Scattering from Water and Land at Centimeter and Millimeter Wavelengths," Proc. IRE 45, pp. 976-982, 1957.

Gustafson, B. G. and B. O. Ås, "System Properties of Jumping-Frequency Radars," Phillips Telecom. Rev. 25, pp. 70-76, 1964.

Hagfors, T., "Relationship of Geometric Optics and Autocorrelation Approaches to the Analysis of Lunar and Planetary Radar," J. Geophys. Res. 71, pp. 379-383, 1966.

Hansen, V. G., "A Sequential Logic for Improving Signal Detectability in Frequency-Agile Search Radar," Trans. IEEE AES-4, pp. 763-773, Sept. 1968.

Hayre, H. S., "Statistical Radar Estimate of the Lunar Surface Roughness," J. Franklin Inst. 277, pp. 197-205, 1964.

Hayre, H. S. and R. K. Moore, "Theoretical Scattering Coefficient for Near Vertical Incidence from Contour Maps," J. Res. NBS 65-D, pp. 427-432, 1961.

Holmes, R. A., "Remote Sensing with Special Reference to Agriculture and Forestry," National Academy of Sciences, Washington, D. C., 1970.

Katz, I., "Radar Reflectivity of the Earth's Surface," APL Technical Digest, Jan.-Feb. 1963.

Katz, I. and L. M. Spetner, "Polarization and Depression-Angle Dependence of Radar Terrain Return," J. Res. NBS-64D, 1960.

Katz, I. and L. M. Spetner, "A Polychromatic Radar," CF 2898, Appl. Phys. Lab., The Johns Hopkins University, 1960.

Kerr, D. E., Propagation of Short Radio Waves, MIT Radiation Laboratory Series (McGraw-Hill, New York), 1951.

Kosowsky, L. H., S. S. Brody, L. Chanzit, and S. Saslovsky, "The Reduction of Angle-of-Arrival Scintillation by a Frequency Shifting Technique," presented at the 1963 Natl. Elec. Conf., New York.

Lind, G., "Reduction of Radar Tracking Errors with Frequency Agility," Trans. IEEE AES-4, pp. 410-416, 1968.

Lundien, J. R., "Terrain Analysis by Electromagnetic Means," U. S. Army Engineer Waterways Experiment Station, Tech. Rept. No. 3-693, 1966.

Lyon, R. J. P. and R. S. Vickers, "Remote Sensing: Vision Beyond Sight," Stanford Today, Series I, No. 17, October 1966.

Marcum, J. I., "A Statistical Theory of Target Detection by Pulsed Radar," Trans. IRE IT-6, pp. 59-267, 1960.

Micronotes, vol. 5, no. 1, Publ. by Microwave Associates, Burlington, Mass., 1967.

Moore, R. K., "Radar as a Remote Sensor," CRES Tech. Rept. No. 61-7, University of Kansas, Lawrence, Kansas, 1966.

Moore, R. K., "Heights from Simultaneous Radar and Infrared," Photogrammetric Eng., pp. 649-651, July 1969.

Moore, R. K. and W. P. Waite, "Radar Scatterometry," CRES Tech. Rept. No. 118-15, University of Kansas, Lawrence, Kansas, 1969.

Moore, R. K., W. P. Waite, and J. W. Rouse, Jr., "Panchromatic and Polychromatic Radar," Proc. IEEE 57, pp. 590-593, 1969.

Muchmore, R. B., "Aircraft Scintillation Spectra," Trans. IRE AP-8, pp. 201-212, 1960.

National Bureau of Standards AMS 55, "Handbook of Mathematical Functions with Formulas, Graphs, and Mathematical Tables," Edited by M. Abramowitz and I. A. Stegun, U. S. Dept. of Commerce, NBS, 1964.

Pardoe, G. K. C., "Earth Resource Satellites," Science J. 5, pp. 58-67, 1969.

Parker, D. C. and M. F. Wolff, "Remote Sensing," Int. Sci. and Tech. 45, pp. 20-31, 1965.

Parkins, B. E., "The Omnidirectional Scattering of Acoustic Waves from Rough Surfaces with Application to Electromagnetic Scattering," (Ph. D. Thesis), University of Kansas, CRES Report 48-4, 1966.

Peake, W. H., "Theory of Radar Return from Terrain," IRE National Convention Record, Pt. 1, on Antennas and Propagation, 1959.

Peake, W. H., "Interaction of Electromagnetic Waves with Some Natural Surfaces," Trans. IRE AP-7 (Special Supplement), pp. 5324-5329, 1959.

Pierson, W. J., B. B. Scheps, and D. S. Simonett, "Some Applications of Radar Return Data to the Study of Terrestrial and Oceanic Phenomena," (CRES Tech. Rept. 61-3, University of Kansas, Lawrence, Kansas) Proc. of the Third Goddard Mem. Symp. on Scientific Exp. for Manned Orbital Flights, March 1965, Washington, D. C.

Ray, H. K., "Improving Radar Range and Angle Detection with Frequency Agility," Microwave J., pp. 63-68, May 1966.

Rayleigh, L. D., The Theory of Sound, 3rd Ed., MacMillan London, 1896.

Rheinstein, J., "Tables of the Amplitude and Phase of the Backscatter from a Conducting Sphere," MIT Lincoln Lab., Rept. No. 22G-16, June 1963.

Rice, S. O., "Reflection of Electromagnetic Wave from Slightly Rough Surfaces," Comm. and Appl. Math 4, pp. 351-378, 1951.

Sorem, A. L. (1967) Principles of Aerial Color Photography, Photogrammetric Engineering 33(9), pp. 1009-1018.

Rouse, J. W., "The Frequency Dependence of Backscatter from Rough Surfaces," (Ph. D. Thesis) CRES Tech. Rept. No. 133-4, University of Kansas, Lawrence, Kansas 1968.

Rouse, J. W., W. P. Waite, and R. L. Walters, "Use of Orbital Radars for Geoscience Investigations," Proc. of the Third Space Congress, Cocoa Beach, Fla., March 1966.

Skolnik, M. I., Introduction to Radar Systems, McGraw-Hill, New York, 1962.

Spetner, L. M. and I. Katz, "Two Statistical Models for Radar Terrain Return," Trans. IRE AP-8, pp. 242-246, 1960.

Swerling, P., "Probability of Detection for Fluctuating Targets," Trans. IRE IT-6, pp. 269-308, 1960.

Wiltse, J. C., S. P. Schlisinger, and C. M. Johnson, "Backscattering Characteristics of the Sea in the Region from 10 to 50 K mc/s," Proc. IRE 45, pp. 220-228, 1957.

UNCLASSIFIED
Security Classification

DOCUMENT CONTROL DATA - R & D

(Security classification of title, body of abstract and indexing annotation must be entered when the overall report is classified)

1. ORIGINATING ACTIVITY *(Corporate author)* Center for Research, Inc. University of Kansas Lawrence, Kansas 66044	**2a. REPORT SECURITY CLASSIFICATION** Unclassified **2b. GROUP**

3. REPORT TITLE

Broad-Spectrum Electromagnetic Backscatter

4. DESCRIPTIVE NOTES *(Type of report and inclusive dates)*

5. AUTHOR(S) *(First name, middle initial, last name)*

William P. Waite

6. REPORT DATE August, 1970	**7a. TOTAL NO. OF PAGES** 172	**7b. NO. OF REFS** 64

8a. CONTRACT OR GRANT NO. DAAK02-68-C-0089	**9a. ORIGINATOR'S REPORT NUMBER(S)** 133-17
b. PROJECT NO.	
c.	**9b. OTHER REPORT NO(S)** *(Any other numbers that may be assigned this report)*
d.	

10. DISTRIBUTION STATEMENT

Each transmittal of this document outside the agencies of the U. S. Government must have prior approval of the Commanding Officer, U.S. Army Engineer Topographic Laboratories, Ft. Belvoir, Virginia.

11. SUPPLEMENTARY NOTES Department of the Army Corps of Engineers	**12. SPONSORING MILITARY ACTIVITY** US Army Engineer Topographic Laboratory Geographic Information Systems Branch Geographic System Division Ft. Belvoir, Virginia

13. ABSTRACT

An experimental investigation of broad-spectrum electromagnetic backscatter was performed. Continuous spectral responses of natural and manmade targets and surfaces were measured to examine the fine grain and gross variations with frequency of the backscattered return. The frequency variation of a discrete scatterer model was examined for a variety of illuminating conditions. Experimental measurements of return variance for several effective bandwidths were compared with the predictions of the theoretical model. The spectral response variations remaining after the removal of fading affects were normalized and compared with similar response characteristics from the visual and infrared regions. Monochromatic and panchromatic images were produced to illustrate the improvement obtainable with frequency averaging.

The results of this experiment graphically illustrate the improvement in return variance possible with panchromatic illumination. In addition, the spectral response variations remaining after the removal of fading effects were shown to be comparable to the variations encountered in the visual and infrared regions.

DD FORM 1 NOV 65 **1473** REPLACES DD FORM 1473, 1 JAN 64, WHICH IS OBSOLETE FOR ARMY USE.

UNCLASSIFIED
Security Classification